5-2018

How Heat Affects Human Hair: Thermal Characterization and Predictive Modeling of Flat Ironing Effects

Jaesik Hahn
Purdue University

HOW HEAT AFFECTS HUMAN HAIR: THERMAL CHARACTERIZATION AND PREDICTIVE MODELING OF FLAT IRONING RESULTS

A Dissertation

Submitted to the Faculty

of

Purdue University

by

Jaesik Hahn

In Partial Fulfillment of the

Requirements for the Degree

of

Doctor of Philosophy

May 2018

Purdue University

West Lafayette, Indiana

THE PURDUE UNIVERSITY GRADUATE SCHOOL
STATEMENT OF DISSERTATION APPROVAL

Dr. Tahira N. Reid, Co-Chair

School of Mechanical Engineering

Dr. Amy M. Marconnet, Co-Chair

School of Mechanical Engineering

Dr. Marisol Koslowski

School of Mechanical Engineering

Dr. Lia A. Stanciu

School of Materials Engineering

Approved by:

Dr. Jay P. Gore

Associate Head for Graduate Studies

To everyone who longs for unrestrained expression of creativity and personality through hair

ACKNOWLEDGMENTS

Had I not reached out to Prof. Reid and joined her lab, I would have never been able to work on such a unique and inspiring project. I thank God for granting me the precious opportunity. Next to it, I appreciate Prof. Reid's genuine care, embracing patience, and perspicacious insights that guided me along this extended academic journey. The encounter with her and the research was truly a life-changing moment that continues to shape my life even still. Equally important was Prof. Marconnet's guidance. Without her help, I would not have been able to delve as deeply into the fundamentals of heat transfer. I appreciate her unceasing and dedicated support in every aspect of the work.

Collaboration with Procter and Gamble deserves equally great significance. Intellectual support from Principle Scientists Mike Vatter and Tim Felts enabled steady progress in the work and guided it in the right direction. Financial support facilitated by David Salloum enabled initiation and completion of the work at the current state of rigor and sophistication. It is truly an indispensable element in the work that I could find nowhere.

I would like to acknowledge faculty and students who directly and indirectly helped me achieve my research goals. Prof. Starkey, Prof. Meckl, and Prof. Shelton in the School of Mechanical Engineering offered insights into improving the design of the automated flat ironing mechanism, and Steven Florence assisted me with design and fabrication of a humidity chamber; Prof. Rochet and Prof. Rossie in the Department of Biochemistry and Prof. Stanciu, Prof. Youngblood, and Prof. Howarter in the School of Materials Engineering guided me through answering inquiries related to their respective background with alacrity; Prof. Craig and Evidence Matangi in the Department of Statistics helped the design of experiments and statistical analysis of the data through the Statistical Consulting Services. Dr. Gilpin in the College of Agriculture conducted SEM/EDX analysis of hair surfaces; Priya Seshadri contributed to the initial design of the automated flat ironing mechanism and compiled specifications of multiple flat irons with Tikyna Dandridge. Jiahong Fu introduced me to Angstrom's method with his initial design of the technique which further inspired me to develop the current state of the technique as presented in this work. Yuqiang Zeng offered his expertise in heat transfer simulation to help identify the sources of errors in the technique and facilitate its improvement. I thank my lab mates from the REID lab, Youyi Bi, Wan-Lin Hu, and Joran Booth, all of whom hold a doctorate now, for being there to walk the academic journey together and often offering helping hands as seniors. I also extend my gratitude to the lab mates from the MTEC lab, Aalok Gaitonde, Collier Miers, Rajath Kantharaj, Albraa Alsaati, David Cuadrado, and Aaditya Candadai, for being always resourceful and willing to offer help when I was in need. Also, I would like to express gratitude to all those who participated in an interview and donated their hair.

Finally, I want to express gratitude to the unconditional love and emotional support I received from my family and friends. Above all, I cherish the commitment and faith that Kyoyoon Koo, the most reinvigorating source of energy despite the physical distance, has shown for the past seven years.

TABLE OF CONTENTS

LIST OF TABLES

LIST OF FIGURES

Figure Page

Figure Page

ABSTRACT

Hahn, Jaesik PhD, Purdue University, May 2018. How Heat Affects Human Hair: Thermal Characterization and Predictive Modeling of Flat Ironing Results. Major Professors: Tahira Reid, Amy Marconnet, School of Mechanical Engineering.

Many people with curly hair experience heat damage —loss of curls and structural degradation of hair — after repetitive use of flat irons. While an array of relevant studies provide insight into thermochemical processes behind the phenomenon, practical tools for flat iron users are unavailable. As a result, people shun heat for fear of unpredictable amount of heat damage while adopting other laborious methods to satisfy a persevering need for temporary hair straightening. Thus three overarching research projects emerge to address the problem. In Part 1, I develop an empirical approach to mathematically correlate four flat ironing parameters (a temperature setting, gliding speed, the number of passes, and exposure time) with three metrics of flat ironing results (reduction in fatigue strength, straightening efficacy, and permanent curl loss). The objective is to establish user-friendly predictive models for flat ironing results to help users make informed decisions. Hair samples are exposed to various flat ironing conditions to evaluate the impact of each parameter thereby formulating predictive models. In the subsequent study, the impact of heat protectants on the flat ironing results is exclusively investigated to provide insight into better utilizing the widely marketed products for protecting hair from heat damage. In Part 2, thermal characterization of human hair and heat transfer modeling serve as a practical tool for predicting the amount of heat damage due to flat ironing in conjunction with the previously developed predictive models. To measure thermal diffusivity of hair, I develop and validate a non-contact infrared thermography measurement technique based on the Angstrom Method. Then, these properties are integrated into a 2D heat transfer model of the thermal transport between a hair bundle and flat iron utilizing the finite difference method. Experimental validation of the model follows to complete the overarching goal of providing practical tools for decision making before flat ironing. This work provides a practical tool that assists flat iron users in making decisions regarding the use of flat irons. It also introduces novel empirical and modeling approaches for understanding the effects of flat ironing. Furthermore, it presents a novel measurement technique for thermal characterization of polymer fibers.

1. INTRODUCTION

The objective of this research is to better understand the effects of flat ironing conditions on hair straightening results and to develop a practical tool that can help flat iron users' decision making processes and hair scientists' endeavor to develop related products. It was motivated by the observation of heat damage which flat iron users often experience with repetitive heat straightening. Such damage usually includes increased proneness to breakage, dryness, and loss of curls [1–9].

For such a widely used appliance as a flat iron, the mechanism of its work is surprisingly little understood. This is evident from the much expressed frustration by flat iron users regarding the heat damage. The best advice even the most experienced stylists can give is to minimize the use of heat. The manufacturers of the device do no better. They recommend specific temperature ranges for different types of hair, but the descriptions of hair types and corresponding temperature ranges are inconsistent across manufacturers and confound the uncertainty [10].

Addressing this topic is important because many people's lives hinge on the concerns about hair. Satisfactory hair care results can lead to increased positivity in the mood [11]; a concern for maintaining hair styles could hinder participation in physical activities, which leads to an increased rate of obesity [12,13]; even though heat is a well-known and persistent cause of many hair and scalp disorders [14–17], a great number of people continue to depend on heat appliances for styling their hair. In fact, observation of an online natural hair community naturallycurly.com identified a persistent need for temporary straightening of hair. However, people try to minimize the use of heat for fear that it will damage their hair to a larger degree than they are willing to sustain. This fear leads customers to explore alternative methods that involve wetting hair and air drying it in a straight form [10]. These methods eliminate the risk of heat damage at the expense of higher time and energy required to achieve inferior and unsatisfactory results compared with heat straightening.

The investigation of the hair care community identified the lack of knowledge in heat straightening as the underlying problem. While the existing studies on heat straightening made efforts to understand the thermochemical process through which hair is damaged, they provide little practical knowledge that can assist flat irons users' decision making.

1.1 Past Efforts to Understand How Heat Affects Hair

There are a number of studies that investigated the effects of heat appliances such as a flat iron and curling iron [2–9, 18–21]. Even though they offer a variety of ideas for quantifying hair damage and great insight into the phenomena, they fall short of providing practical knowledge that flat iron users can readily utilize. Moreover, African hair simply characterized the denaturation temperature of hair [9], which is the temperature at which the keratin protein (comprises 80% of hair [22]) starts disintegrating. The absence of African hair in the scope of the studies is surprising given the widespread usage of flat irons and the particular interest in hair straightening in this population. However, it is understandable given the difficulty in obtaining samples of African hair.

In addition, there is a collection of studies that offers invaluable insight into thermochemical processes behind hair straightening and resultsant degradation of internal structure [1, 23–30]. However, they fail to translate the data into the practical knowledge from which ordinary flat iron users can benefit.

1.2 Past Efforts to Mitigate Heat Damage

There are three broad approaches employed to mitigate the heat damage to hair: using alternative straightening methods, enhancing the performance of flat irons, and protecting the hair fibers subjected to heat.

Alternatives to heat straightening includes a use of reduced heat by stretching hair while blow drying and use of water set principle such as banding, threading and wrapping methods [31–33]. However, these methods require more time and energy yet yield inferior results compared with simple flat ironing.

Performance of flat irons have been improved mainly by replacing the material of the heating plates [34, 35]. Most popular materials are tourmaline and ceramic. The cited patents claim that these materials generate far infrared and negative ions that increase the smoothness of hair fibers and their structural integrity. However, such effects have not been well verified.

Various forms of heat protectants, whether it be cream or spray, dry or wet, synthetic or natural, are used to protect hair from heat. While lots of anecdotal evidence about their effectiveness exists, some studies suggest that they are only effective if used out of the typical use context (e.g. repeatedly applying products without washing hair in between) [8, 9].

1.3 Research Questions

Having identified clear gaps in addressing the problems flat iron users face, I formulated two research questions to fill the gaps.

(1) What is the effect of flat ironing under various conditions?

(2) How is the behavior of heat in human hair related to the flat ironing conditions?

The first question focuses on the relationships between flat ironing conditions (i.e., things that the user can control) and flat ironing results. Identification of these relationships would enable development of a decision making tool for flat ironing. Then, a subsequent question arises: how does the behavior of heat differ according to flat ironing conditions and how is this related to the flat ironing results? Answering this question will bring a better understanding of heat transfer through human hair and its effect on the structure of hair, which will benefit both flat iron usage and development of related products or technologies alike.

The dissertation is divided into two parts to answer each question. Before addressing each question in a separate part, reviews of background literature precedes to lay the foundation for mutual understanding of the concepts to appear throughout the whole study. This includes basic anatomy of human hair, differences among hair types, and existing studies on the effects of heat appliances and heat on human hair. It will also elaborate on the existing gaps in academia, industry, and a community of consumers, which were briefly touched upon in the previous section of this chapter.

In Part 1, I evaluate the impact of flat ironing conditions on the results to address the first question. To do so, first, I discuss selection of relevant flat ironing parameters and quantifiable flat ironing results. Next, a description of the experimental equipment, design, and procedures follows. Then, mathematical correlations between the flat ironing parameters and results are established using a statistical tool to account for the inherent variability in the individual hair. Part 1 will also contain an empirical study on the effects of heat protectants which are often marketed to protect hair from heat damage. The results of these investigations will offer a practical decision making tool that flat iron users can utilize to improve their overall experience with flat ironing. Also, they contribute to the community of hair scientists by providing novel metrics to assess flat ironing performance and ways to utilize the experimental results through statistical analyses.

In Part 2, I construct a heat transfer model which explains the exchange and flow of heat energy between a bundle of hair and a flat iron. The prerequisite of modeling is accurate knowledge of thermal properties of hair; thus, a discussion on the development of a measurement technique and the measured properties appears first. Following this is the development of the heat transfer model, supplemented by discussions on the modeling technique and justification of the assumptions made. The model will be compared with experimental results to test its accuracy, and a discussion on the limitations and possible improvements will follow. The results of the work will contribute to the body of knowledge by offering a novel measurement technique for thermal diffusivity of polymer monofilaments and a modeling technique for heat transfer through a bundle of fibers, which is broadly applicable beyond hair to fabrics and composites.

2. BACKGROUND

While heat damage is experienced by most people using heat appliances, the adverse effects are more conspicuous and noted among those with curly hair due to gradual loss of curls and inherently fragile hair. Nevertheless, surprisingly little is known about how curly hair responds to flat ironing despite the more prevalent usage of flat irons among the population with curly hair. In this chapter, I will briefly cover the most relevant information about basic hair structure to discuss the differences among hair types and to subsequently discuss the gaps in the current studies regarding the use of flat iron and its impact.

2.1 Hair Fundamentals: Morphology and Chemical Composition

2.1.1 Basic Hair Anatomy

A human hair fiber can be dissected into three major parts: the cuticle, cortex, and medulla [36, 37]. The exterior shell of the hair, called the cuticle, is composed of transparent and overlapping, scale-like cells. Inside this outer layer is the cortex, which is the structure that accounts for most of hair weight, volume, and mechanical strength. Finally, the inner core is called the medulla.

Cuticle: The cuticle is the outermost layer of hair fiber that protects the internal structures from mechanical impacts and other external sources of damage [36]. It is composed of multiple layers of overlapping individual cuticle cells, which resemble the structure of shingles on a roof. On average, 6-8 cuticles form a cuticle layer at thickness of approximately 0.45m [38]. It is high in cysteine content with contributions from high sulfur and ultra high sulfur proteins [39] but comprises only about 10% of total hair weight [40]. The thickness of cuticle layer is similar regardless of overall hair fiber diameter [41], which makes a thin hair fiber stiffer than a thicker one due to its higher cuticle to whole fiber ratio. The cuticle composes about 10% of overall fiber weight [40]. In terms of mechanical properties, the cuticle is considered to contribute to torsional properties with 3.5 times more rigidity [42], and has insignificant contribution to tensile properties [43].

Cortex: The cortex, which makes up about 60-90% of fiber bulk [41], accounts for most of hair fibers weight and tensile strength [44]. Therefore, it is the structural component that most frequently investigated by researchers.

Morphologically, it is composed of elongated, spindle-like cortical cells aligned with the central axis through the fiber [44] with cell membrane complexes (CMC) in between that glue them together [45]. Cortical cells can be divided into three types: paracortical, mesocortical, and orthocortical cells [37]. The distinction between them is how the materials inside are organized. More detailed discussion about how they differ from one another will be covered later along with the discussion on the difference among hair types (2.2).

Inside each cortical cell are macrofibrils, which comprises approximately 50-60% of cortexs mass [36], and inter-macrofibrillar material; inside each macrofibril are microfibrils, which are also called intermediate filaments, and inter-microfibrillar matrices also called keratin associated proteins [37]. Each intermediate filament is composed of several protofibrils which are formed by two coiled dimers in an anti-parallel manner, which are again comprised of Type I and Type II keratin polypeptide chains that form a coiled coil [37].

The most widely adopted model of hair treats a hair fiber as a mixture of water-impenetrable, crystalline fibrous proteins (intermediate filaments) and water-penetrable, amorphous matrix substances [46]. It can be imagined as highly structured, elastic ropes immersed in a viscous material, which resembles a damped spring model in its macroscopic stress-strain characteristics [47].

Medulla: The medulla is a small tubular portion in the center of the hair fiber. In animal hairs, it takes up significant amount of the total volume [48]; however, in human hair, it only accounts for a small portion and may be discontinuous and sometimes even absent [49]. It contributes to the stiffness of hair fiber to a certain degree but due to its small volume, the contribution is insignificant. It is considered to play little to no role in hair cosmetics and have little physicochemical significance [44, 50, 51].

Chemical Composition of Hair: Human hair contains approximately 65-95% by weight proteins [49], and 80% of hair by weight is a protein called keratin [22]. Other constituents include water, lipids, pigments, and trace elements [49]. Keratin is composed of 18 amino acids, and hair fiber's exceptional strength and, structural and thermal stability are often attributed to its high cystine content, which provides strong covalent bonds originating from a disulfide bond.

The majority of keratin is located in the cortex which comprises approximately 85 wt% of total protein contents. 50 wt% of the total protein is low-sulfur proteins, which are considered to be intermediate filaments. 25 wt% of the total proteins is high-sulfur proteins also called keratin associated proteins, 10 wt% is high glycine and tyrosine (HGT) proteins, and 15 wt% is other low- and high-sulfur proteins located in the cuticle layer [37]. The overall structural stability and strength of hair come from the combination of intermediate filaments and matrix substances. intermediate filaments, which are formed by multiple coiled α-keratins that exhibit a characteristic α-helical structure, are responsible for hair fibers' elasticity coming from intra-chain hydrogen bonds, while matrix substances, which are rich in sulfur contents, are responsible for structural stability [49].

Cortical cells are usually classified according to how the macrofibrils and matrix substances are distributed and organized inside it. A paracortical cell contains loosely packed macrofibrils which are filled with intermediate filaments relatively parallel in their orientation [52]. Thus, it contains a relatively large amount of matrix substances and sulfur. A mesocortical cell is intermediate in sulfur content and the degree of density. An orthocortical cell has more densely packed macrofibrils with whorl-like intermediate filaments in them, and due to the dense pack, contains less sulfur [53].

2.2 Differences among Hair Types

The most distinctive difference among hair types is the curls of varying degree. Thus, the discussion will start from the origin of curls. Then, the discussion on the chemical composition and mechanical properties of different types of hair will follow.

The origin of human hair curvature has long been attributed to peculiar cross-sectional shapes among hairs of different races [54, 55]. For instance, Asian hair can be characterized with a circular cross-section, Caucasian with an ovoid cross-section, and African with a flat cross-section. However, it was later proposed that the curvature in human hair originates from different shapes of hair follicles, which tend to be relatively symmetrical in Asian and Caucasian population but asymmetrical in African population [54–56]. A recent study proposed that there may be differential mechanical stresses generated on each side of follicle that would cause difference in the rate at which hair fiber is extracted and hence a consequential asymmetrical structure that leads to a curled shape [57].

Not only the exterior, but also the interior morphology of the hair fiber appears to correlate with hair curvature. It is a well-known fact among textile researchers that the crimp in wool fiber originates from the bilateral structure of fiber interior, which can be divided in half with orthocortical cells on a convex side and paracortical cells on a concave side [58]. The similar disposition to a bilateral structure was found in human hair and was proposed to be the morphological characteristic of human hair that contributes to curvature [45, 59]. For instance, one study found that African hair had a bilateral structure between orthocortical and paracortical cells, while Caucasian hair was composed mainly of paracortical cells [60]. It was also discovered that hair of varying curvatures among Japanese hair exhibited distinct disposition of cortical cells [45, 61].

Past studies had given human cortical cells of different morphologies names such as orthocortical, paracortical, and mesocortical cells following the convention used in studies of wool fiber. However, more recent studies pointed out that human cortical cells are strictly different from those of wool fiber, and classified each cortical cell into four groups from Type A to Type D [45]. However, the precise relationship between the degree of disposition to a bilateral structure in cortical cells and the degree of hair curvature requires further investigation.

Another interesting proposed factor responsible for hair curvature is the ratio between fibrous protein and matrix substance [62]. Though expressed in a different way, the fibrous protein to matrix substance ratio is highly probably directly related to the disposition of cortical cells, because each cortical cell is composed of macrofibrils and inter-macrofibrillar material which in turn are composed of fibrous protein and matrix substance [36, 37]. African hair exhibited the lowest fibrous protein to matrix substance ratio, while Asian hair exhibited the highest ratio; the increase in curvature negatively correlates with the ratio. Since a curved hair fiber with bilateral structure contains more orthocortical cells than a straighter fiber, it is most likely contains less matrix substances. Thus, one can easily infer that higher curvature is directly related to lower content of matrix substance, which consequently leads to higher fibrous protein to matrix substance ratio.

Different types of hair exhibit varying degrees of tensile properties [36, 49, 63, 64]. African hair with a highly irregular cross-sectional profile along its fiber axis tends to have lower tensile properties compared with Asian and Caucasian hair. This tendency in lower mechanical strength for African hair is consistent with the results on fatigue strength of hair where an individual fiber is subjected to cyclical loading well below its break strength. African hair had a significantly lower fatigue strength compared with Asian and Caucasian hair [65].

The differences metioned above are not only present among geo-racial hair types but also among the hairs in the same geo-racial hair type. Segmentation Tree Analysis Method (STAM), a curl classification method strictly based on geometric features of hair such as a curl index, curl diameter, and the number of waves, classified African hair of into five curl classes and clearly demonstrated the presence of such differences [66]. The suggested method was applied to more than 2,400 subjects and Robbins [49] confirmed in the book its robustness for classifying hair types. Each curl class between Type IV and Type VIII has surprisingly high negative and positive correlations with a cross-sectional area ($R^2 = 0.98$) and ellipticity ($R^2 = 0.95$) of hair respectively [67]. The curl class also had relatively high negative correlations with Young's modulus ($R^2 = 0.79$) and breaking strength ($R^2 = 0.66$). The study also found differences in thermal stability among the hair of different ethnicities by statistically significant differences in denaturation temperature and denaturation enthalpy. However, the difference is very small, and it is unclear if it will significantly impact response to heat.

Despite the observed differences in morphological disposition and clear distinction in mechanical properties, variations in the chemical composition of hair has been reported to be insignificant across hair types [36, 50].

2.3 Effect of Heat Appliances on Human Hair

A review of the exiting literature revealed the gaps in the current studies. First, it was noticeable how all the studies were based on Caucasian hair alone , if not Asian hair in a few occasions [3–8, 21]. It was peculiar to witness such propensity, considering the fact that African-American women are having particularly many issues related to flat irons that often receive academic attention [12, 15, 68–70]. The paper that talks about "progressive straightening" exhibits such a bias more prominently [9]. It depicts gradual loss of curl as a favorable phenomenon, proposing it as an alternative method of permanent hair straightening except for the damage introduced to hair that makes it more fragile. In fact, loss of natural curls is one of the worst things that can happen in African-American community; thus, the paper clearly does not consider the need of this community. Furthermore, in the same study, African hair was used for characterization thermal stability of human hair but disregarded for the investigation into gradual curl loss with repeated heat treatments which is a more coveted issue to be considered by this population.

Second, most of the studies relied on manual application of heat which is more susceptible to experimental errors by introducing more variability to how heat is applied [3–8]. Only two studies [9, 21] can exonerate themselves from this criticism.

Third, the evaluations of the product performance conducted by the previous studies seem inadequate for correctly reflecting what customers expect from heat styling. To discuss this point, the metrics used to gauge hair damage in each study needs to be examined first.

McMullen and Jachowicz's [3,4] work on thermal degradation of hair with a curling iron is the most frequently cited work among the literature that directly addresses the use of heat appliances on human hair . The first work confirmed the detrimental effect of heat applied continuously for a long period and intermittently for a short period in metrics of hair chromophore (Trp) decomposition, color change, and surface damage. The result indicated that the intermittent and short term heat application was more destructive, which may be attributed to the rinsing and towel drying that occurred between each cycle of heat application. The second work examined the effectiveness of protective agents such as copolymer, surfactant and hydrolyzed protein against the heat using Trp decomposition, surface damage, and stiffness as metrics. The results revealed that all the agents decreased the decomposition rate of Trp by 10%-20% while only copolymer and surfactant were effective at reducing surface damage, and none of them made significant difference to stiffness except for copolymer making hair fiber stiffer at a high temperature, which can be eliminated by shampooing.

Ruetsch and Kamath [5] studied the possible damages caused by a curling iron used in ways that violate the specification: use on wet hair, excessive pull on hair, and prolonged time of use. The study confirmed that the hair treated under wet condition and tension experienced the most severe damage. Also, changes in tensile properties such as slight increase in break strength, reduction in extension to break, and large increase in post-yield modulus were observed. Interestingly, fatigue resistance of hair pre-treated with a conditioner increased, which led to higher characteristic life.

Zhou et al. [7] investigated the effects of pretreatments with various metrics such as hair keratin denaturation, molecular modification of keratin, surface damage, change in sorption/desorption rate of water vapor, thermal imaging of hair cross section, hair temperature during flat ironing, and hair breakage with combing. The results reconfirmed the protein denaturation and reduction in the amount of overall protein content with heat. The heat-induced cuticular damage was again observed. They also observed sorption and desorption rate of water vapor into and out of hair fiber finding that water regain and retention both reduced. However, selected pretreatments were able to mitigate the effect of heat and reduce the change in sorption/desorption rates. Cuticular damage and hair temperature during flat iron also decreased with the pretreatments.

Harper et al. [6] presented an interesting work, investigating the efficacy of thermal styling. Along with checking heat damage done to hair with some of the classic metrics associated with mechanical properties of hair fiber, they looked at the efficacy which is defined as how well and long the thermal styling retains the desired hair shape. In conclusion, they suggested that increasing the temperature of appliance beyond 150°C made no significant difference to the effectiveness of hair styling, which poses an important question as to how manufacturers of heat appliances came up with the specific temperature ranges for hair textures. However, certainly, the work in the study needs to be expanded more to assess the validity of market claims.

Christian et al. [8] examined the effect of a heat protectant spray as well as the difference in the effect between dry and wet ones. They utilized Trp decomposition, structural damage and change in tensile properties to assess the amount of damage. As a result of the experiment, they discovered that the use of heat protectant did not yield any significant improvement in protecting hair from heat damage unless they build up enough to form a thick layer over time. Furthermore, they discovered that the water-based wet heat protectant had more adverse effect to structural integrity compared to the dry one. It was the first paper that, at least among the studies researched in this work, explicitly sought for addressing the needs for the appropriate methods of using heat appliances to minimize the damage.

The work proposed by Dussaud et al. [9] investigated the effect of repeated heat application with a flat iron to human hair, which they referred to as "progressive straightening". Even though it described the gradual loss of curl as a favorable phenomenon that can substitute for the chemical hair straightening, it was most closely related to what this research intends to address. In addition to change in curliness, they also measured the damage to hair using metrics such as shift in denaturation temperature, change in wet Young's modulus, and degree of disorganization in the microfilament organization which is supposed to be related to the denaturation of proteins. They concluded that the repeated application of heat removes natural curls from hair and decreases denaturation temperature, Young's modulus and microfilament organization. They also discovered that the silicone-based heat protectant did not mitigate the effect of heat damage except for enhancing the fiber alignment.

Wortmann et al. [21] proposed a first-order kinetic models to describe the relationship between the duration of flat ironing and denatruation temperature and enthalpy. Assuming the two-phase model, the content of α-helix is expected to reduce to zero with an extended period of flat ironing while denaturation temperature will converge to a finite value.

All these studies offer invaluable insights into thermal degradation of hair by either a flat iron or a curling iron. They provide many quantifiable metrics that are direct consequences of using heat. However, the connection between some of the metrics and the perceived amount of damage that flat iron users experience is not well defined. For instance, keratin denaturation or Young's modulus exhibits only partial information about the structural integrity of hair; it is unclear how much of it will translate into a palpable degree of reduction in hair strength that customers experience during their daily grooming activities.

Fourth, the reviews of the existing studies above clearly show that the studies focused mainly on the effects of heat on hair strength and neglected other effects.

In particular, when it comes to heat styling that involves flat ironing, the results of straightening and the resultant loss in curls also become the center of concerns. Depending on individual's unique hair care needs, one or both of these concerns may compromise the concern for hair strength to a certain degree. Thus, the performance of flat ironing should consider more relevant metrics that reflect the concerns of flat iron users such as reduction in hair strength, effectiveness of straightening, and permanent loss of curls.

Lastly, there is a case of inconsistency between studies about the effects of heat, which could confound flat iron users in utilizing the tool. For example, even though in most cases heat reduces the overall mechanical properties of hair, under specific conditions it can improve the mechanical properties [5,6]. Therefore, evaluation of flat ironing results under various conditions is necessary to assist flat iron users in better utilizing the tool.

In addition to the gaps identified in the academic works, there are gaps in the guidelines on the flat iron usage suggested by flat iron manufacturers. Comparison of usage guidelines for five select flat irons exposes its lack of consistency and little knowledge in guiding flat iron users (Table 2.1). First, the guidelines are provided for a certain best result defined by manufacturers, which may not align with what flat iron users want. arbitrarily define the best result for the users and fail to provide multiple usage scenarios for different styling goals. The best results and styling goals for the users can vary from gently stretched-out hair with remaining waves to completely straightened hair. Second, the classification of a hair type is highly subjective and nebulous. Qualitative descriptions of hair types such as wavy, curly and frizzy could differ from person to person. Third, the classification of hair types and the corresponding ranges of recommended temperature are inconsistent across manufacturers. Fourth, manufacturers only consider a temperature setting as a factor and neglect other factors such as flat ironing speed and the number of passes which are likely to have an impact on the results.

Table 2.1. Comparison of guidelines on flat iron usage provided by 5 select manufacturers (Adopted from [10]).

Manufacturer	Flat Iron Type	Pricing*	Hair Type	Temperature Setting (°F)	Notes
1	Ceramic	High	thin/fragile	300-350	-No frequency recommendation -Hair care product recommendation -Detailed instructions -Mentions that hair should be fully dried -Electrical and burn warnings
			fine	350-390	
			normal	375-400	
			wavy/ curly/ permed	385-400	
			kinky/ coarse/ thick	400-420	
2	Titanium	Medium	fragile	240-265	-No frequency recommendation -Hair care product recommendation -Electrical and burn warnings
			thin	265-305	
			normal	305-350	
			wavy	350-370	
			coarse	390-450	
3	Argan ceramic	Medium	fragile	225-275	-No frequency recommendation -No hair care product recommendation -Electrical and burn warnings
			thin	275-315	
			normal	315-345	
			wavy	375-415	
			coarse	415-450	
4	Ceramic	Low	thin	low	-No frequency recommendation -No hair care product recommendation -Limited instructions -Electrical and burn warnings
			normal	medium	
			thick	high	
5	Argan oil infused ceramic	Low	thin/delicate/ easy to straighten hair	low	-Limited instructions -No mentioning of hair care products -No frequency recommendation -Electrical and burn warnings
			average to thick/treated hair	medium	
			thick or wavy hair	medium-high	
			hard to straighten hair	high	
			very resistant hair	maximum	

*Pricing: Low (less than $50), Medium ($50-149.99), High (more than $150)

2.4 Relevant Effect of Heat on Human Hair

A lot of studies regarding the effects of heat on human hair focus on thermal analysis. It is a technique widely employed by researchers for studying various phases hair goes through, in which its chemical composition and structure experience remarkable change. The primary method for performing such investigation is called Differential Scanning Calorimetry (DSC). In this method, a sample of interest is heated up at a slow rate (usually around 5 K/min to 10 K/min in the papers reviewed) while change in energy intake and output during endothermic and exothermic processes are recorded. These various processes, which are commonly summarized in terms of enthalpy and characteristic peak temperature, are directly related to chemical and structural change of samples. Thus, researchers widely use this method as a means to thermally characterize the state of hair structure and its response to heat.

While these papers are not directly related to thermal degradation caused by heat appliances, they offer compelling models of chemical changes inside hair fibers that cause change to its mechanical properties and geometry by heat insult. The knowledge they offer will play a significant role in interpreting the empirical results to be presented. Therefore, a brief overview of the studies will be provided in this section.

Milczareck et al. [24] studied the thermal transitions in keratin as it relates to loss of water and toughening process. By observing a DSC curve, they proposed that water is removed through three stages: first, weakly bound water (50 °C to 75 °C), more strongly bound water (90 °C to 120 °C), and the most strongly bound water (90 °C to 120 °C). At around 155 °C, they observed toughening transition which seems to increase the crystallinity of α-keratin and stiffens hair fiber. α-crystallites finally denatured or melted at around 233 °C. To investigate the role of water in the toughening process, they annealed hair at different temperatures and observed shift in denaturation temperature. Hair annealed for 30 min at temperature ranging from 70 °C to 180 °C experienced shift of denaturation temperature to higher value, but beyond 180 degreeCelsius, denaturation temperature started to decrease again. They discovered that the increase in crystalline peak area (stability of crystalline structure) by annealing at low temperatures (at 80 °C and 110 °C), which only removes weakly bound water, is reversible upon introduction of humidity while annealing at high temperatures (at 150 °C and 180 °C), which removes strongly bound water, is irreversible.

Cao [25] suggested that DSC measurement without a sealed pan leads to thermal degradation/pyrolysis of hair, which underestimates enthalpy required for denatruation of α-form crystallites. He compared the results among the conditions with a sealed pan which are without a medium, with water and with silicone oil. By examining the DCS curves obtained, he concluded that silicone oil is the best medium to accurately and consistently measure enthalpy for denaturation and hence the estimation of α-crystalline content of hair fibers. He used his finding in the later work with Leroy [71] to investigate the effect of water content on shift of denaturation temperature (or melting peak as they call it). They discovered that the plot of water content and melting temperature can be fitted with a slightly parabolic line, where higher water content shifts the melting temperature to a lower value. They concluded that α-form crystallites share characteristics in common with a crystal, and therefore, defined the endothermic peak as melting rather than denaturation of the crystallites.

Wortmann and Deutz [72] obtained DSC curves of various keratin base materials ranging from a Rhinocerous horn to human hair to observe their thermal transition through different phases. The results showed a denaturation range of 20 °C to 30 °C with peak temperature at around 140 °C regardless of material. In contrast to Cao, Wortmann specifically made a comment that the transition of α-helix during endothermic peak will be referred to as denaturation rather than melting. They tried to incur partial denaturation in African hair, which led to permanent straightening. According to them, it is a consequence of supercontraction suggesting a close relationship between keratin denaturation and gradual loss of curls. In another work, Wortmann et al. [73] looked at the effect of water on glass transition of hair. They observed shift of glass transition temperature to higher value with less water content. Also, they compared DSC curves of untreated hair and hair with denatured α-helical material and confirmed that crystallinity has no relationship with water sorption and glass transition of hair. One aspect of his work worth mentioning is his long-standing favor in the two-phase model of a hair structure first proposed by Feughelman [46]. In this model, crystalline intermediate filaments are embedded in amorphous matrix substances, which is analogous to springs immersed inside a dampening fluid. He proposed from the observation of DSC curves that matrix substance kinetically impedes α-helices from unfolding, which plasticizes with the introduction of water and yields lower denaturation temperature as a consequence. Wortmann et al. [29] discovered that denaturation enthalpy of dry hair shows significant dependency on a heating rate. This seemed to be due to the kinetics of pyrolysis of cortex. On the other hand, there was no correlation when hair in water was used. From the observation of heat capacity dependent on a heating rate, they suggested that a higher heating rate transforms α-helices to random coils, which increases heat capacity whereas a lower heating rate transforms the helices into more organized β-domains with reduced heat capacity. This heating rate dependency also appears in denaturation temperature; an increase in a heating rate increases the denaturation temperature. The authors conclude their work by suggesting that the denaturation occurs through more complex stages than the one step transition authors proposed before.

Istrate et al. [74] proposed a three-phase model in which additional scaffolds between intermediate filaments and matrix substances exist in the form of disulfide bond. In the subsequent work, Istrate et al. [30] investigated the effect of pH on thermal stability of human hair and discovered that denaturation peak can be shifted higher for previously oxidated hair if treated with low pH solution. This cannot be due to increased crystallinity because a decrease in enthalpy and denaturation temperature indicates irreversible damage of α-helices. Furthermore, there was no difference in tensile strength between the damaged hair and the hair treated with low pH solution, which further excludes participation of crytalline structure in the phenomenon. Thus, authors suggested that the interface phase, which can be characterized as ligands, between crystalline and amorphous phase binds the two phases upon the introduction of low pH and hence increases denaturation enthalpy and temperature. This study set a strong case for the three-phase model Istrate has been promoting.

In addition, Rebenfeld et al. [1] investigated the effect of heat on tensile properties of hair. Monteiro et al. [27] utilized thermal analysis as means to observe how the change in keratin structure is induced by bleaching and chlorinating agents. Humphries et al. [23] investigated the potential of commercially available thermomechanical analyses for detecting the damage and chemical changes to hair by various treatments.

While the literature reviewed above offers useful models for explicating thermal transition of hair and implication for the change in its geometry and properties, one should be careful when applying them. DSC requires cutting hair into small pieces and could differ from an intact hair fiber responding to heat. Moreover, DSC employs a very slow heating rate compared to flat ironing. The range is usually around 10 K/min and 20 K/min at most; however, flat ironing instantaneously exposes hair to temperature typically around 200 °C. Given the dependency of thermal transition on a heating rate [29] it is highly likely that thermal transition during the flat ironing will occur differently from what has been observed.

Part 1: Emprical Investigation of Flat Ironing Results and Predictive Modeling

Part 1 consists of experimental investigation of flat ironing results. In the first half, metrics of the flat ironing results are defined and experiments are conducted using flat ironing parameters such as a temperature setting, gliding speed, and the number of passes. In the second half, the performance of commercially available heat protectants is examined using the newly proposed metrics of flat ironing results.

3. PREDICTIVE MODELING OF FLAT IRONING RESULTS

To address the gaps identified in the previous chapter, I propose predictive modeling to help flat iron users. A predictive model which can forecast how much damage one should expect can be a powerful tool for decision making. A better informed decision can improve the overall hair care experience and results of heat straightening by saving one from frustration and use of excessive amount of time, money and energy to recover from or avoid the heat damage.

There have been several attempts to model cosmetically meaningful hair assembly characteristics by measurable parameters of hair properties. Robbins and Scott proposed an idea for predicting the hair assembly (tresses or heads) characteristics closely related to cosmetic procedures with single fiber properties [75]. They suggested that the hair assembly characteristics such as manageability, combing ease, style retention, flyaway and body can be predicted with single fiber properties such as stiffness, static charge, weight, diameter, curvature, and friction. 8 years later, Robbins and Reich implemented the idea and established a predictive model for combing ease [76]. They discovered that the curvature has the largest impact on combing ease and that the effect gets more dominant as one's hair becomes curlier. There have been a few follow-up studies to further refine the idea. Robbins, Reich and Clarke more rigorously defined the definition of manageability, utilizing surveys from users, to further enhance the effectiveness of addressing user needs [77]. Later on they collaborated again to successfully correlate hair volume and texture to the body by using an image analysis [78]. Also, Rennie et al. [79] attempted to model hair shine based on a spatial arrangement of hair fibers. However, none other significant modeling attempt for cosmetic characteristics of hair is known, let alone the effort to model the effect of flat ironing on hair.

In this chapter, quantifiable metrics for flat ironing results and relevant flat ironing parameters to be considered are discussed. The effort put into the development of an automated flat ironing mechanism to minimize the experimental error is elaborated, and experimental procedures and results follow.

3.1 Metrics for Flat Ironing Results

Four metrics (fatigue strength, straightening efficacy, long-term straightening efficacy, and permanent curl loss) serve to quantify the effects of flat ironing. These metrics were carefully chosen to reflect both desirable and undesirable consequences of flat ironing that flat iron users constantly grapple with.

Past studies measured tensile properties to assess the reduction in hair strength [1, 5, 6, 8, 9]. Even though it is an excellent measure of hair strength, the measured quantity is far from suitably reflecting the long-term strength and resilience of hair at a moderate stress level, which hair is more likely to experience during the daily grooming practices. Evans and Park [80] argued and demonstrated that it captures the mechanical strength of hair against daily grooming practices better than the traditional break strength measurement. Fatiguing is one mode of failure in which initially formed superficial cracks and/or internal pores in a material propagate under cyclical loading to subsequently cause breakage. The fatigue strength is measured by applying stress that is sufficiently lower than the break strength of the material which induces breakage by a single application of force. Fatigue testing quantitatively captures this structural failure by counting the number of cyclical loading required to induce such a result. Thus, the number of cycles to failure will be presented as a metric of hair strength throughout the rest of this work.

Straightening efficacy is an obvious measure of the desirable effect, which assesses the effectiveness of straightening. To quantify straightening efficacy, a familiar concept of a curl index was utilized. A curl index (CI) is one way of quantifying the curliness of hair by taking the ratio between a natural length (L_n) and an extended length (L_e) defined as below.

$$CI = \frac{L_e}{L_n} \tag{3.1}$$

A natural length is defined as the distance between any two farthest points on a single strand of hair and an extended length a stretched length of the same strand (Figure 3.1).

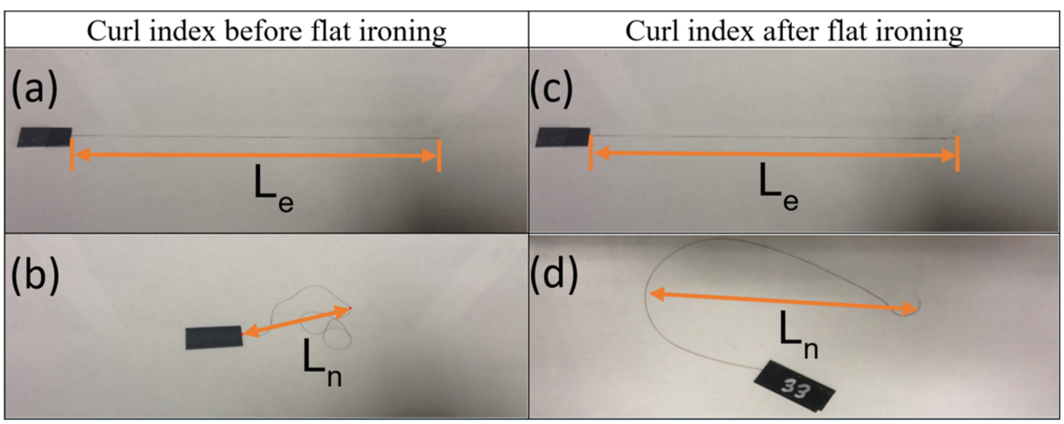

Figure 3.1. (a) Measurement of an extended length L_e and (b) natural length L_n before flat ironing. (c) Measurement of extended length and (d) natural length immediately after flat ironing. L_e is measured by stretching the strand and taping both ends with a tape on a piece of paper. L_n is measured by placing the strand between two glass plates and measuring the distance between the two farthest points.

Straightening efficacy (SE) calculates the percent change in a curl index before and immediately after flat ironing as shown below.

$$SE = \frac{CI_{immediatelyafterflatironing} - CI_{beforeflatironing}}{CI_{beforeflatironing}} \tag{3.2}$$

Similarly, the long-term straightening efficacy measures the retention of straightness after 24 hours of exposure to an ambient environment at 21 °C to 22 °C and 48 %RH to 52 %RH. The corresponding equation for calculating the percent change is as follows.

$$LTSE = \frac{CI_{24hoursafterflatironing} - CI_{beforeflatironing}}{CI_{beforeflatironing}} \tag{3.3}$$

Finally, permanent curl loss assesses how much curl is permanently lost as a result of flat ironing under each condition. A curl index was again used to quantify the change in curliness. However, a previous experience indicates that a curl index can be poor at fully reflecting the change in curliness unless the change is drastic as between before and after flat ironing. The permanent curl loss is measured after washing hair, which removes the effect of heat straightening and the difference in curliness less obvious. Thus, instead of solely relying on the curl index, an additional metric that measures the change in the diameter of the largest curls in a strand was used to quantify the permanent loss in curls. The CI and a largest curl diameter (CD) was measured from an intact strand, then from the same strand after drying in the air overnight after washing that immediately followed flat ironing; a template of multiple concentric circles of known diameters shown in Figure 3.2 was utilized for the measurement. The measurement was taken in these two states because permanent change in curls rather than temporary change was of interest. The percent change between the two states quantifies permanent curl loss in two ways: permanent curl loss by CI (PCLCI) and permanent curl loss by CD (PCLCD).

$$PCLCI = \frac{CI_{afterwashing} - CI_{beforeflatironing}}{CI_{beforeflatironing}} \tag{3.4}$$

$$PCLCD = \frac{CD_{afterwashing} - CD_{beforeflatironing}}{CD_{beforeflatironing}} \tag{3.5}$$

Figure 3.2. A curl diameter of a hair strand is measured by utilizing a template of multiple concentric circles of known diameters.

3.2 Selection of Flat Ironing Parameters

The most obvious parameter to consider is a temperature of a flat iron. There are numerous reports on the dominantly detrimental effects of temperature [1–9, 21]. Another intuitive and repeately reported factor to consider is the period of exposure to heat [9, 21]. It is easy to derive three most intuitive and certain parameters related to heat damage: a temperature setting, gliding speed, and the number of passes.

Water content in hair is another important factor. Water can substantially influence Youngs modulus of hair [8, 49, 81]. Hair flat ironed in a wet state receive an amplified amount of damage due to evaporating water creating pores [82, 83] and pressure created by a differential expansion rate between the cortex and cuticle leading to crack formation on the cuticle [2]. Moreover, water acts as a plasticizer that accelerates keratin denaturation under high heat [29, 71]. Thus, careful control of water content in hair is important to conduct well-controlled experiments. This parameter has been traditionally controlled in the means of equilibrating hair fiber under certain relative humidity (%RH).

Because of the large influence of temperature and water content on mechanical strength of hair, tension in hair during flat ironing needs close attention. For example, tension at one temperature level might be within the Hookean region and have not significant impact on the change in mechanical strength, but at a higher temperature, it might substantially deforms the shape of hair and diminishes its mechanical strength.

It is intuitive to assume that accumulating heat energy will be directly proportional to the amount of damage. However, intermittent cooling between each pass of flat ironing may have unknown effect. For example, a cyclical heat treatment with overnight restoration of a water content in hair mitigated the surface temperature when compared with omitting the water restoration in-between [7]. Therefore, careful control of a cooling period between strokes of flat ironing needs consideration.

Density in which a bundle of hair is configured, which is a characteristic of hair assembly rather than a single fiber, affects the interaction with heat. A rate of heat dissipation through hair can differ with the varying degree of bundle density [84].

Some other potential factors to consider include age, nutrition and light. Hair characteristics can vary along with age [49]. The nutrition condition is also an important factor to consider since hair that grows anew will certainly be affected by how one is nourished [49]. Finally light, more specifically ultraviolet radiation, can affect hair structure [85,86]. A sufficiently long period of exposure to sun light, for example, can weaken CMC between cuticles or cortical cells and cause step-like fractures.

Additionally, I hypothesize that the exposure time defined as the amount of time a segment of hair is above a certain critical temperature is an effective single metric for quantitatively assessing the thermal history. The critical temperature was set to be 100°C for the following reasons. First, a recent study to assess the styling efficacy of curling irons determined the efficacy increased up to approximately 100°C and stalled, or adversely impacted the hair, near 200°C [6]. Secondly, 100°C is the boiling point of water, and it is well known that rapidly evaporating water can form small pores as it exits the hair [82, 83] or form cracks due to rapid contraction of cuticle layer pressing against the cortex lagging in the drying process [2].

After careful consideration, the parameters are divided into two groups: one of variable parameters and the other of fixed parameters. A temperature setting, gliding speed, and the number of passes were selected as variable parameters. The exposure time is contingent on the three variable flat ironing parameters: a temperature setting, gliding speed and number of passes. Therefore, it may be able to capture the collective impact of the three parameters better than the addition of individual contribution from each parameter. On the other hand, the water content, tension, duration of cooling, and density will remain at fixed values. The rest of the factors age, nutrition, and light are difficult to control and remain to be parts of an uncontrollable environmental factor. The decision was made based on the feasibility of accurately varying the parameters at the current state of technology and availability of equipment or facilities.

The following equation illustrates how the predictive model would be constructed as a function of the aforementioned variables that outputs change in the four flat ironing metrics.

$$\Delta M = f(T_{iron}, V, N, E) \tag{3.6}$$

where:

ΔM = change in one of the four metrics

T_{iron} = temperature setting on a flat iron

V = gliding speed of a flat iron

N = number of passes

E = Exposure time above 100°C

3.3 Automated Flat Ironing Mechanism

As was pointed out in the previous chapter, most studies on the use of heat appliances used the appliances manually, which could cause variability in the effects due to uncontrolled variables such as duration of heat application [2–8, 18–20]. Furthermore, the heat application was done statically (i.e. appliance did not translate along the length of hair), which is far from realistic usage of flat irons.

There were two exceptional cases where an automated flat ironing system was employed. One of the studies utilized a linear stage to provide constant speed at which a flat iron grazes a hair sample [9]. The mechanism as well as hair samples were vertically oriented. The hair samples were secured at the top with the low end freely hanging. In this set-up the mechanism can utilize a Dia-Stron tensile tester to monitor the tension on hair. The other study employed Instron's tensile tester to draw out hair through flat iron in a contrlled manner [21]; however, it did not detail the descriptions of the mechanism.

The first system has several limitations for performing a controlled experiment. First of all, instead of maintaining the pulling force, which is highly likely an influential factor in flat ironing, constant, it only monitored its variation during the process. Also, it seems that the failure to secure the other end of hair hindered working with African hair samples. This is a mere inference based on that fact that even though they had an African hair sample, they did not perform the experiment for progressive straightening with it and used it instead for thermal characterization of human hair. Finally, their mechanism did not allow the flat iron to automatically open and close. It prevented them from doing experiments with multiple passes, which is another important factor to include and a practice that frequently appears among flat iron users.

In this section, an effort to address the shortcomings of the previous studies by designing a fully automated flat ironing mechanism is elaborated. The mechanism consists of two parts: a sample stage and clamp mechanism. The sample stage consists of a linear stage to enable a lateral motion and a tension mechanism to control the tension on hair samples. The clamp mechanism consists of a linear stage to engage/disengage the flat iron and a motor-driven system to open and close the flat iron.

3.3.1 Design Requirements

As a first step to designing a flat ironing mechanism, design requirements were established. They were created by carefully observing YouTube videos of people flat ironing to closely emulate the flat ironing process. The requirements were divided into two sets, each corresponding to the sample stage and clamp mechanism, for the convenience of description.

Requirements for The Sample Stage:

- Accommodate various lengths of hair samples (3 in - 6 in)
- Easy to mount/demount hair samples
- Apply tensile force between 0 g and 25 g
- Apply tensile force with the resolution of 0.1 g
- Apply/cease tension on hair samples for each pass

- Move laterally at between 1 cm/s and 5 cm/s
- Hold up to 850 g of load

The minimum hair length the sample stage should accommodate was established by considering the typical width of flat irons. It is typically between 1 in and 1.5 in. At the same time, it was assumed that the flat iron should be able to travel at least the width of itself to yield meaningful results for the experiment. Therefore, the minimum length of hair samples should be 3 in.

According to the available data from literature, the break force of a single fiber of curly hair can range from 31.06 g to 68.89 g [67]. However, this range was achieved at a very slow rate of stretching. Furthermore, since curly hair is more prone to breakage [50, 64, 87, 88], tension applied needs to be well below the lower bound to safely apply tension across all hair types. A simple experiment using a spring force gauge suggested that the break force of the hair samples at possession could vary between approximately 10 g and 150 g depending on the hair type. Thus, the tension mechanism should be able to apply tension at least up to 10 g, which is well below the lower bound calculated from the available data. Also, to be able to apply accurate tension to the sample, the resolution should be at least 0.1 g. Based on the observation made on the video clips, flat iron users stretch their hair either by using hand or pulling with flat irons as they apply heat. To simulate this practice as well as to measure the effect of tension on hair straightening, the mechanism should be able to pull and loosen hair samples at the beginning and the end of each cycle.

Each bound of required speed was estimated by observing videos. The typical speed at which the flat iron would travel when gliding on hair and going back to roots for a subsequent pass was estimated. Finally, the capacity of the linear stage was estimated by calculating the weight of the whole structure to be mounted on by using SolidWorks since the fabrication of all the parts was not completed at the moment.

Requirements for The Clamp Mechanism:

- Secure a commercial flat iron
- Open and close a flat iron
- Adjust the speed of opening/closing a flat iron
- Exert constant pressure on hair samples
- Align the surface of plates on a flat iron in parallel with hair samples
- Deploy/retract a flat iron at the rate of 5 cm/s or faster
- Hold up to 3.7 kg of load

The clamp mechanism has to be able to securely hold a flat iron. It should be able to actuate opening and closing of the flat iron automatically. In addition, the speed of closing should be moderate to prevent the ceramic plates on the flat iron from being damaged. The pressure exerted on hair by the flat iron should be constant across all hair types. Even though the friction between the hair fiber and ceramic plates is expected to be quite low, it is better to be cautious and avoid introduction of any additional friction which might add to the tension in hair, and hinder the control of this parameter. The plane in the center of the flat iron in a vertical direction should align with the plane on which the hair sample is. In other words, as the flat iron opens/closes and moves along the hair sample, it should not affect the height of the sample. Any change in the height will extend the hair fiber and result in an undesirable increase in tension. Finally, the whole clamp mechanism should have a way to engage and retract the flat iron on and from the hair sample so that the flat iron does not hinder mounting and demounting of the hair sample. This will also allow the flat iron for time to heat up without affecting hair samples before it is deployed. Moreover, this will enable more accurate simulation of a flat ironing procedure which involves users' taking a flat iron away from hair after each pass.

Overall, each mechanism should be well secured to each other and work autonomously to minimize both the time spent for each experiment and experimental errors.

3.3.2 Final Concept

Figure 3.3 shows the final concept of the flat ironing mechanism. The sample stage consists of a linear stage that provides a lateral motion (Figure 3.4) and the tension mechanism which secures a hair sample and applies tension to it (Figure 3.5). The tension mechanism is actuated by a DC motor to avoid affecting the reading on a load cell with vibration. The motor drives a threaded rod which in turn moves a slider back and forth. Mounted on this slider is a thin beam load cell. It measures the tension in hair. To do so, it is also connected to a 3D printed clamp that secures the distal end of a hair fiber. On the other side of the extruded frame is a binder clip that secures the other end of the hair sample, which is going to be wrapped with an electrical tape. Also, as a safety measure, limit switches were installed to prevent linear stage from operating past each end of the hair sample and damaging hair samples or other parts.

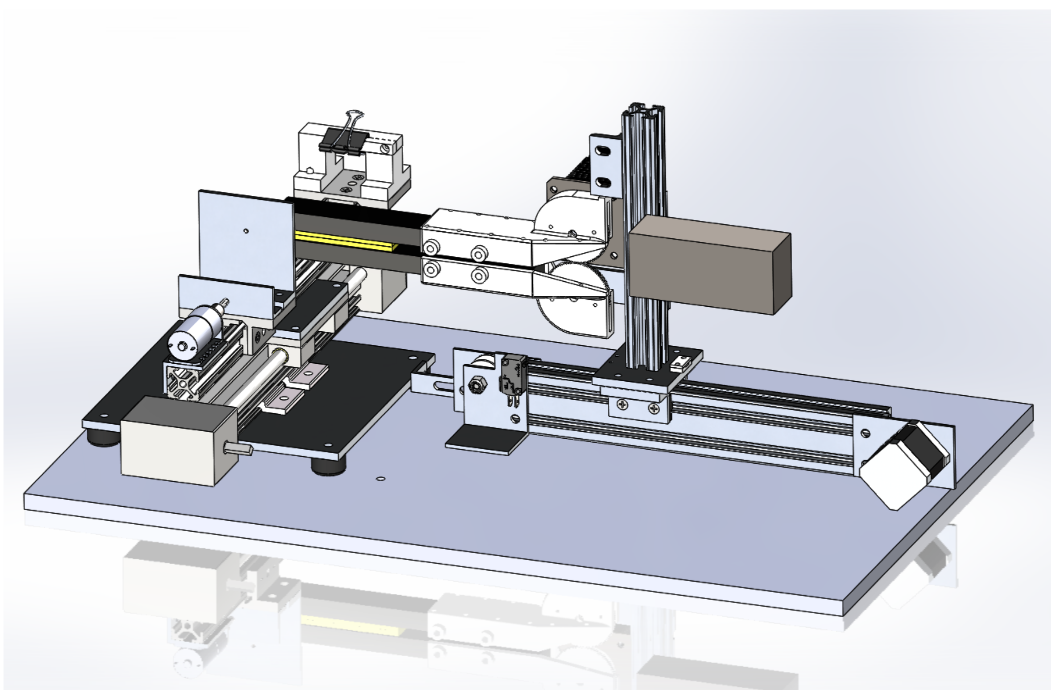

Figure 3.3. CAD model of the final concept.

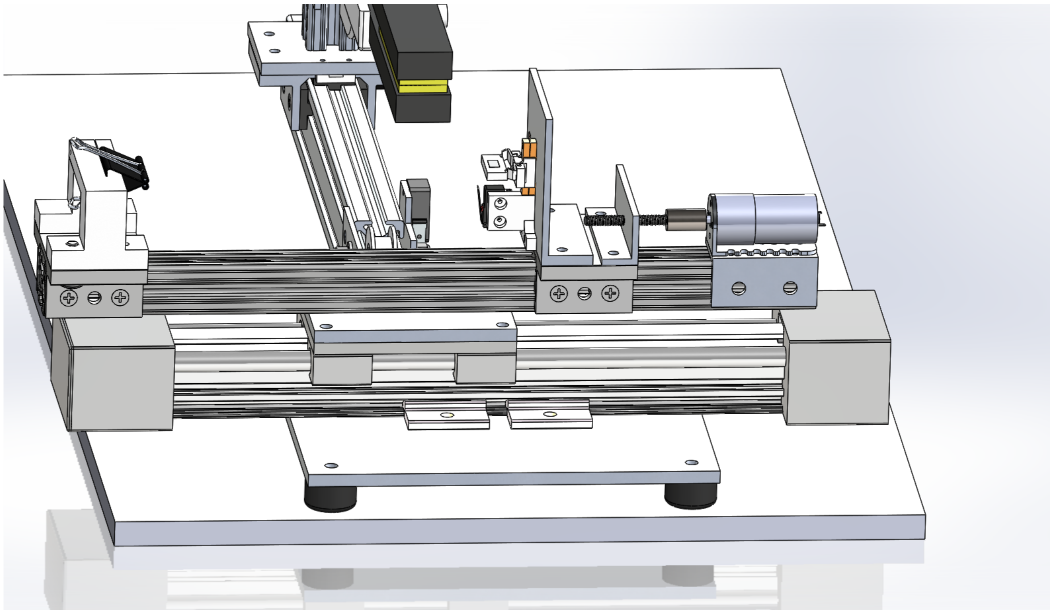

Figure 3.4. CAD model of the linear stage.

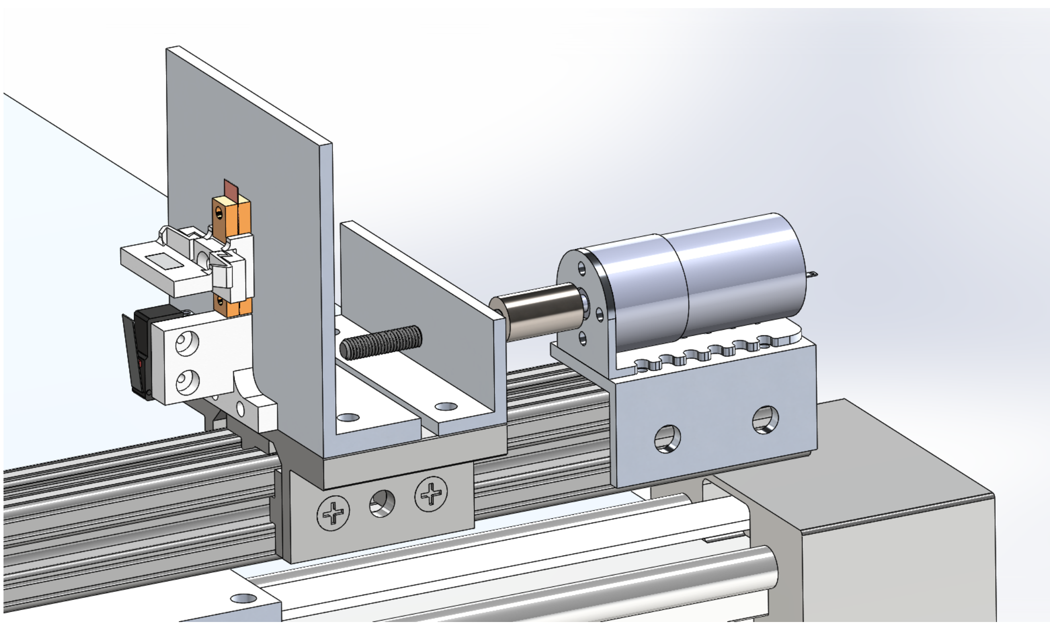

Figure 3.5. CAD model of the tension mechanism.

The clamp mechanism consists of a linear stage that engages and disengages the flat iron and 3D printed clamps in which the flat iron is installed (Figure 3.6). The clamps utilize thumb screws on its sides to secure the flat iron. A stepper motor actuates the upper clamp which subsequently drives the lower clamp via attached plastic gears. This mode of actuation is convenient for exerting constant pressure on hair samples.

A belt-driven linear stage operated by a stepper motor enables deployment and withdrawal of the mechanism as shown in Fig 3.7. The rest of the parts are simply supporting structures that ensure the planes on which the hair sample and flat iron plates coincide.

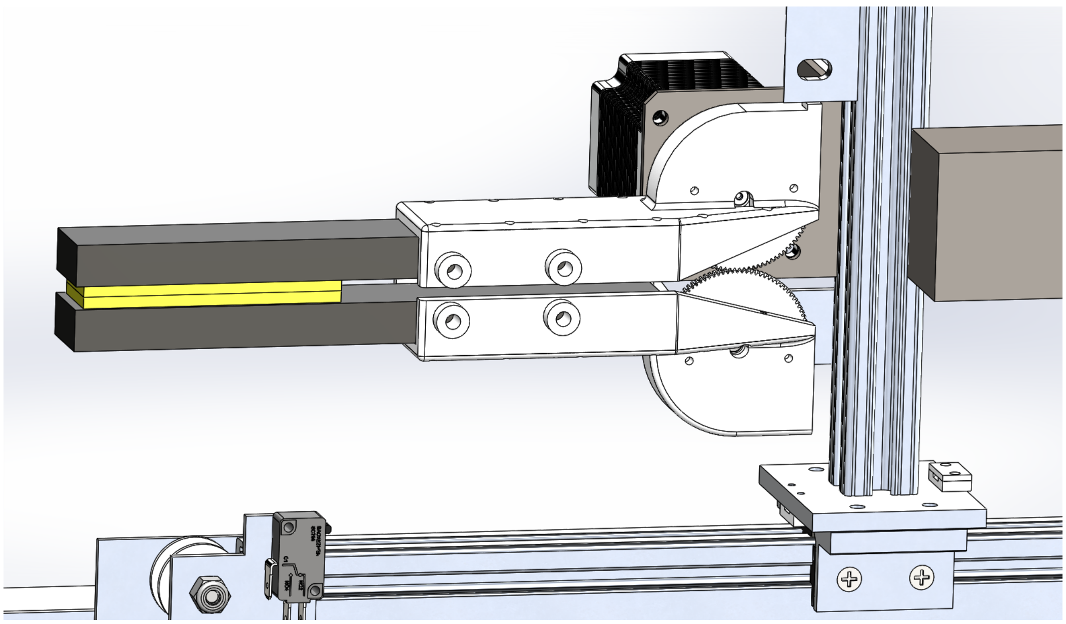

Figure 3.6. CAD model of the clamp mechanism.

3.3.3 Analyses for Motor Selection

The design requires no parts where structural rigidity is crucial. Thus, no structural analysis was performed. Instead, analyses were performed to select appropriate motors to drive all the parts. The sample linear stage requires no analysis as an appropriate motor that meets design criteria was provided by Igus. For the flat iron

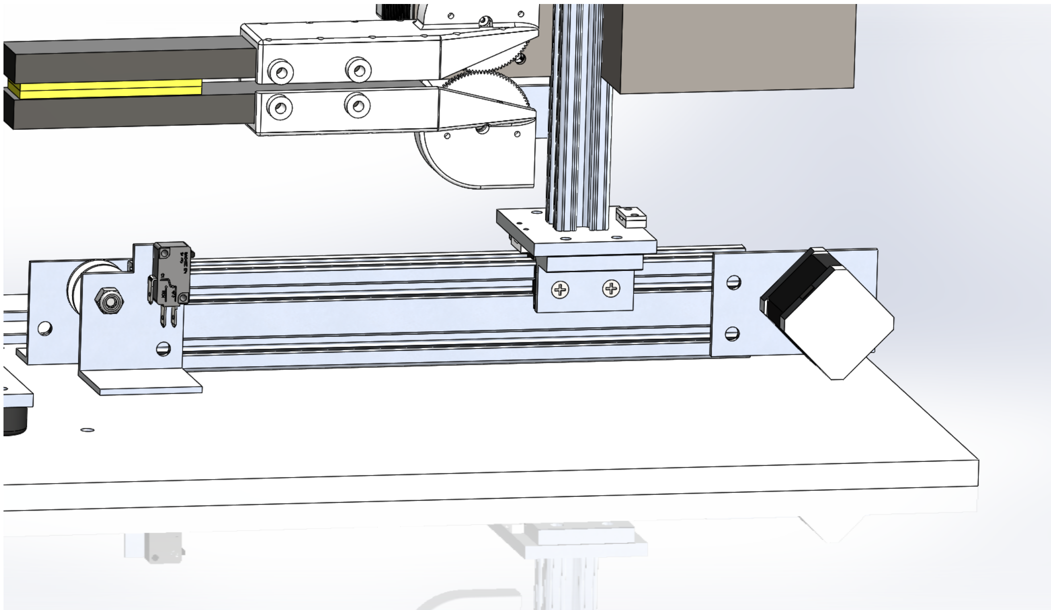

Figure 3.7. CAD model of the linear stage for the clamp mechanism.

linear stage, required torque was calculated by measuring the friction between the slotted frame and linear bearing (Free body diagram shown in Figure 3.8).

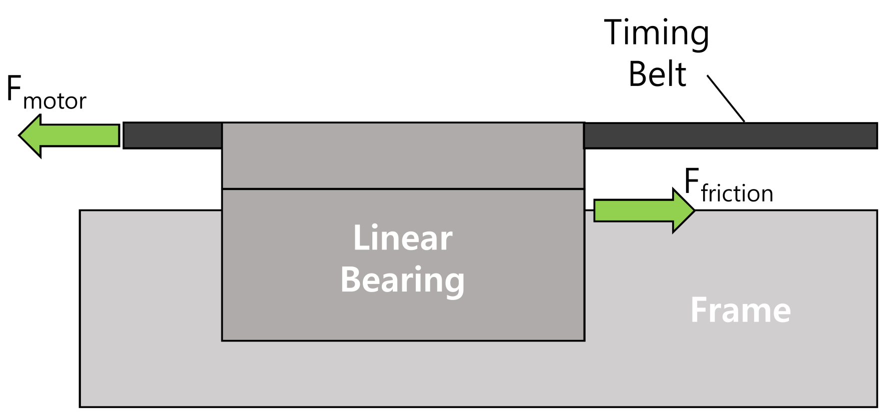

Figure 3.8. Free body diagram of flat iron linear stage.

Required torque for the clamp mechanism was calculated by treating the clamps as beams (Figure 3.9). For the tension mechanism, the friction between the frame and linear bearing was used (Figure 3.10) along with an equation for a lead screw (Equation (3.7)) to calculate the necessary torque.

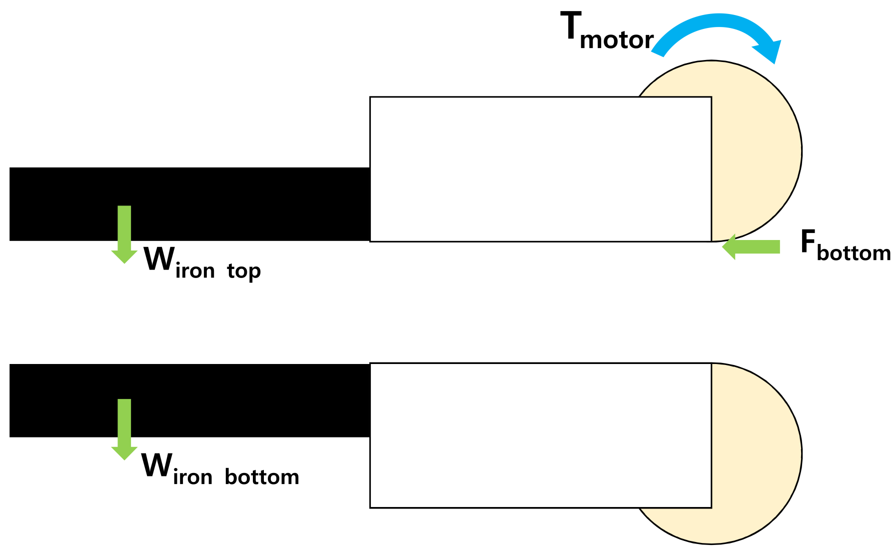

Figure 3.9. Free-body diagram of clamp mechanism.

$$T_{motor} = \frac{F_{friction} d_m}{2} \left(\frac{l + \pi f d_m \sec \alpha}{\pi d_m - f l \sec \alpha} \right) \tag{3.7}$$

3.3.4 Selection of Electronic Components

There are three main electronic components involved in the design: motor drivers, Arduino microcontrollers and Arduino shield for stepper motors. A motor driver is a breakout board specifically designed to control a motor. Three stepper motor drivers control the sample and flat iron linear stage and the clamp, and a DC motor driver controls the tension mechanism. Arduino microcontrollers were used to accept input variables for the experiment and coordinate the movement of each component of the

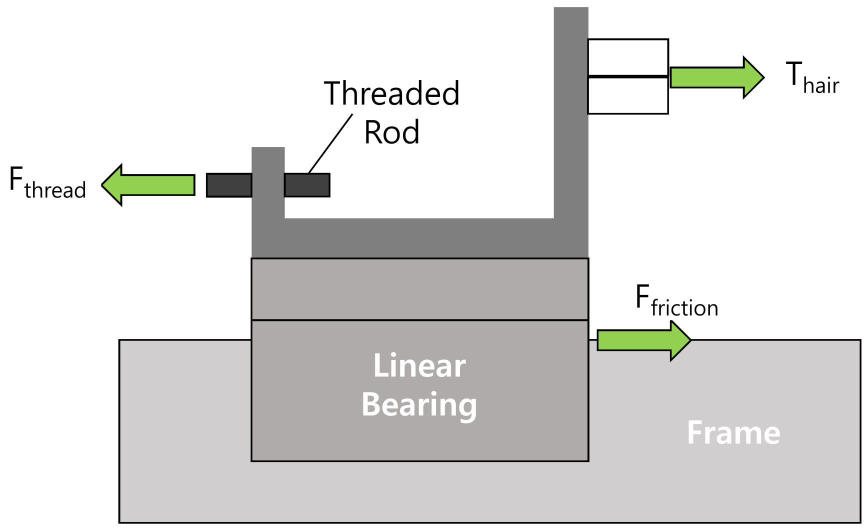

Figure 3.10. Free body diagram of tension mechanism.

system to simulate a flat ironing process. In total, three Arduino controllers were used. One Arduino Uno receives and feeds signal from a load cell to main controller, and each of the two Arduino Mega's acts as a main controller and a dedicated controller for the tension mechanism. Arduino shield is an add-on board to Arduino controller that enables easy implementation of motor control without the need for designing a circuit by oneself. The shield used can accommodate up to four stepper drivers at once. Figure 3.11 shows all the electronic components used for the design.

3.3.5 Automation with Arduino Microcontroller

A program to control the flat ironing procedure was developed using an Arduino microcontrollers and accompanying IDE (Integrated Development Environment). This was enabled through I2C and serial communication between the three Arduino boards and a laptop/desktop. The breakdown of its functions is as follows:

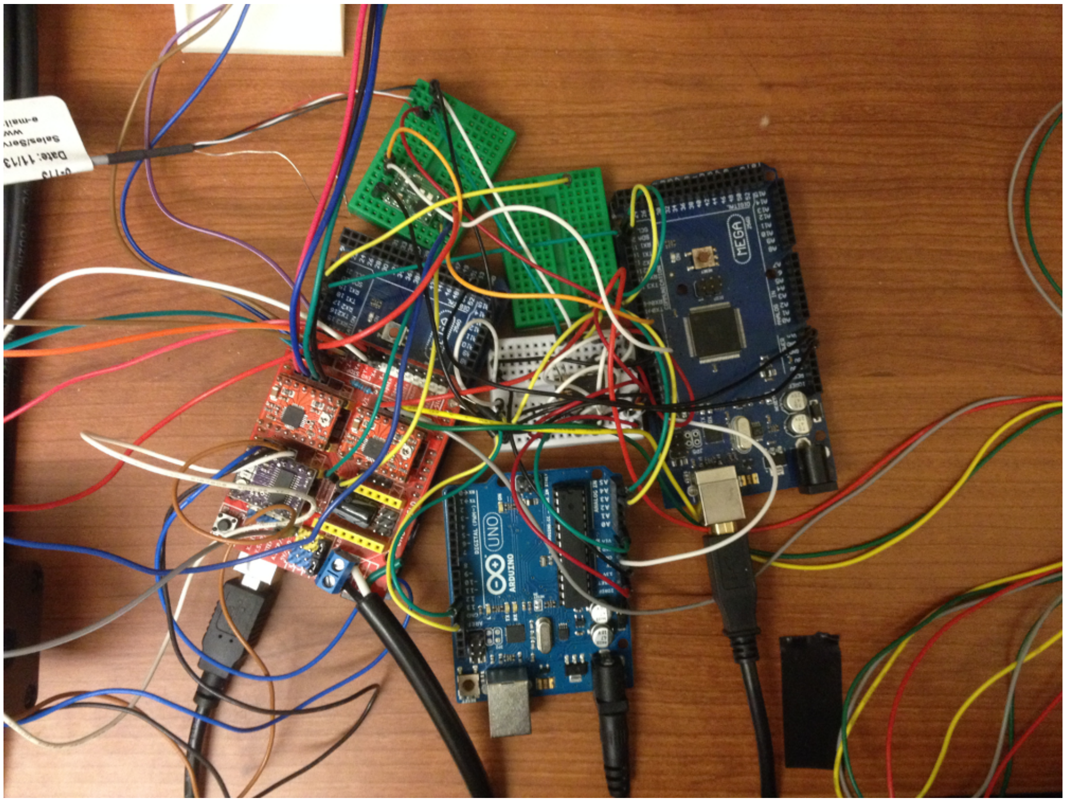

Figure 3.11. Electronic components used for the flat ironing mechanism.

(1) Open, (2) Close, (3) Execution, (4) Calibration, (5) Setting, and (6) Display the setting.

Open function opens up the flat iron to preheat the ceramic plates to a desired temperature before the experiment. Close function closes the flat iron. It enables setting the appropriate pressure prior to the experiment. Execution triggers the simulated heat application procedure. Upon the execution, users will be prompted to input desired tension in hair, a gliding speed of a flat iron and the number of passes. Calibration lets users adjust the position of the sample stage, flat iron, slider of the tension mechanism and flat iron linear stage. Setting allows users to change default parameters such as a maximum sample length, flat iron width, speed of flat iron stepper motor, and the number of steps for Close/Open of the flat iron. Finally, users can see the current parameters using the last function.

3.3.6 Fabrication

To minimize the burden for designing and fabricating every part, most parts were designed using pre-manufactured parts. Some unconventional parts with simple shapes were fabricated using aluminum plates. Parts with complex shapes such as flat iron clamps and a sample holder clamp attached to a load cell were 3D printed. Figure 3.12 shows the completed assembly.

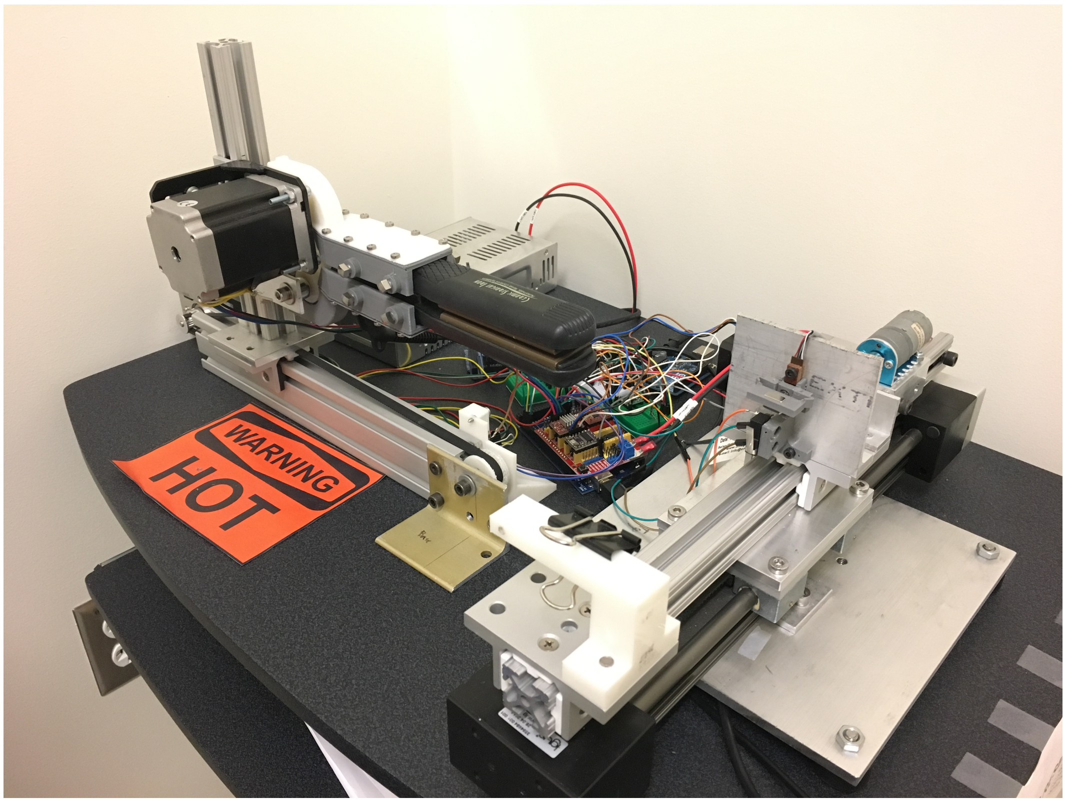

Figure 3.12. Completed assembly of the flat ironing mechanism.

3.3.7 Empirical Analyses and Assessment of Design Requirements

To address issues that could have been overlooked during the design process, empirical analyses are performed. Afterwards, fulfillment of design requirements for the sample stage and clamp mechanism is separately assessed, which is followed by the overall assessment.

Assessment for the Sample Stage: The performance of the final design was assessed for the design criteria. The sample stage was capable of accommodating lengths of hair from 3 in to approximately 7 in. Furthermore, it successfully demonstrated its capacity to hold hair samples securely with the help of an electrical tape. One end of the hair sample was wrapped with the tape to provide a frictional surface which the binder clip can hold onto (Figure 3.13). This additional surface would also serve as a means to label each hair sample (Figure 3.14) and to hang the sample on a string with a binder clip to dry them after each wash. The other end was clamped by a 3D printed clamp (Figure 3.15. This clamp was designed to be detachable from the load cell in order to protect the thin beam from bending while clamping the hair. Figure 3.16 shows the configuration when it is attached. The clamp secures the free hanging end of the hair between the two small magnets for the convenience of mounting and demounting.

The tension mechanism was able to apply tension up to 25 g with the resolution of 0.1 g. Above it, the rate at which hair slips exceeds the rate of tension adjustment, and tension control becomes implausible. Yet, this is well above the target maximum tension of 10 g and satisfies the design requirement. In addition, the feature to apply/cease tension to hair sample was successfully implemented. The linear stage could extend the length of a sample with the resolution of 0.0825 mm.

The sample stage (Figure 3.17) required an empirical test to validate whether it can reach 5 cm/s with the hair fixture mounted on it. The linear stage could move faster than the desired maximum value of 5 cm/s at about 13 cm/s without skipping steps. 1/4 micro stepping was used to reduce the vibration and make the to-and-fro motion smoother. Also, the linear stage had no problem carrying the load back and forth.

Assessment for the Clamp Mechanism: The clamp mechanism successfully secured a commercial ceramic flat iron manufactured by Hairart (Figure 3.18). The

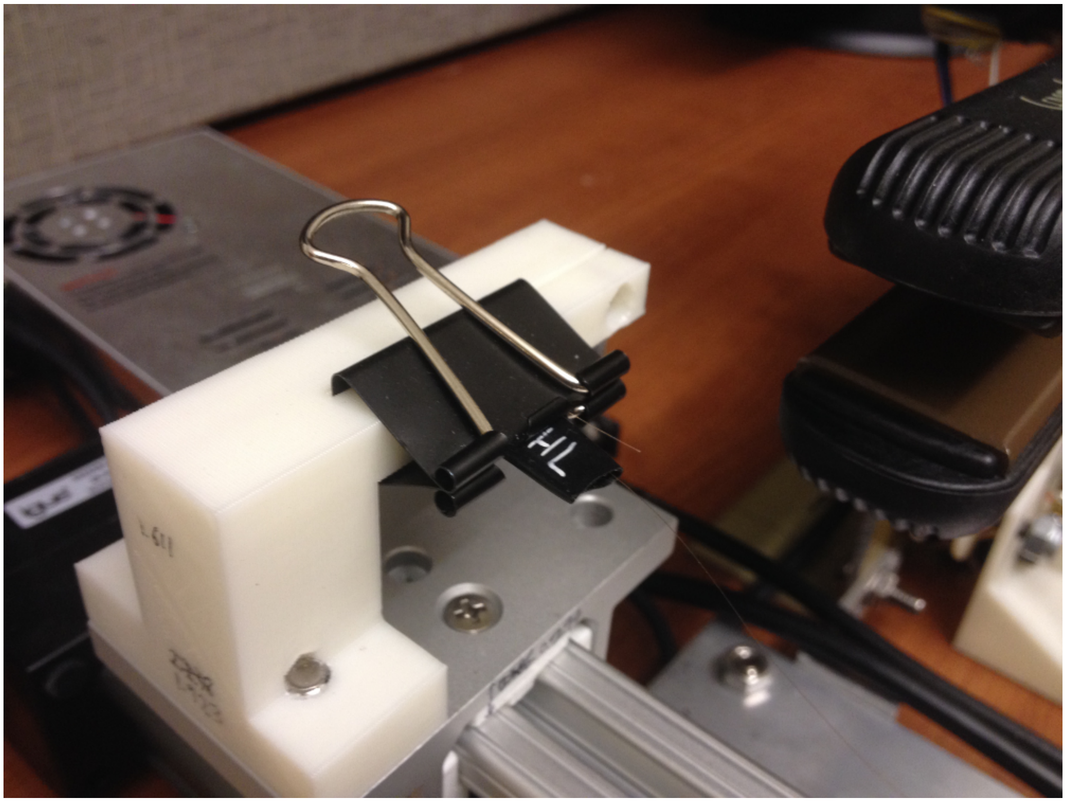

Figure 3.13. A binder clip that clamps on the taped side of hair sample.

stepper motor was able to open and close the flat iron at desired speed by users. Aligning the surfaces of plates perfectly parallel to hair samples was a challenge and was unsuccessful. As a result, when the flat iron clasps on the hair the difference in height introduced additional tension to the hair. This disturbance was managed by dedicating one Arduino microcontroller to continuously adjusting the tension while the flat iron is gliding on the hair sample. The flat iron linear stage could glide at about 10 cm/s without skipping, which is well above the targeted value of 5 cm/s, and successfully carried the load on it. What was unexpected was its generating lots of vibration as it translates towards the hair sample. This was due to a highly concentrated frictional surface caused by asymmetrical distribution of load. A carbon steel block was added to counter-balance it as can be seen in Figure 3.18

Figure 3.14. Electrical tape wrapped around a hair sample to provide a frictional surface and space to label the sample.

Overall Assessment: Overall, the design met all the targeted design criteria and performed as expected. Although there were several unexpected challenges discovered after assembly and test runs, they were all adequately addressed as described in Section 3.3.7.

Despite the satisfactory performance, there is still room for improvements. First is the linear bearing used to translate the slider with a load cell. While being simple and low-cost, it allows enough room for the slider to wiggle as it translates along the frame. Moreover, when the limit switch on the extended arm comes to contact

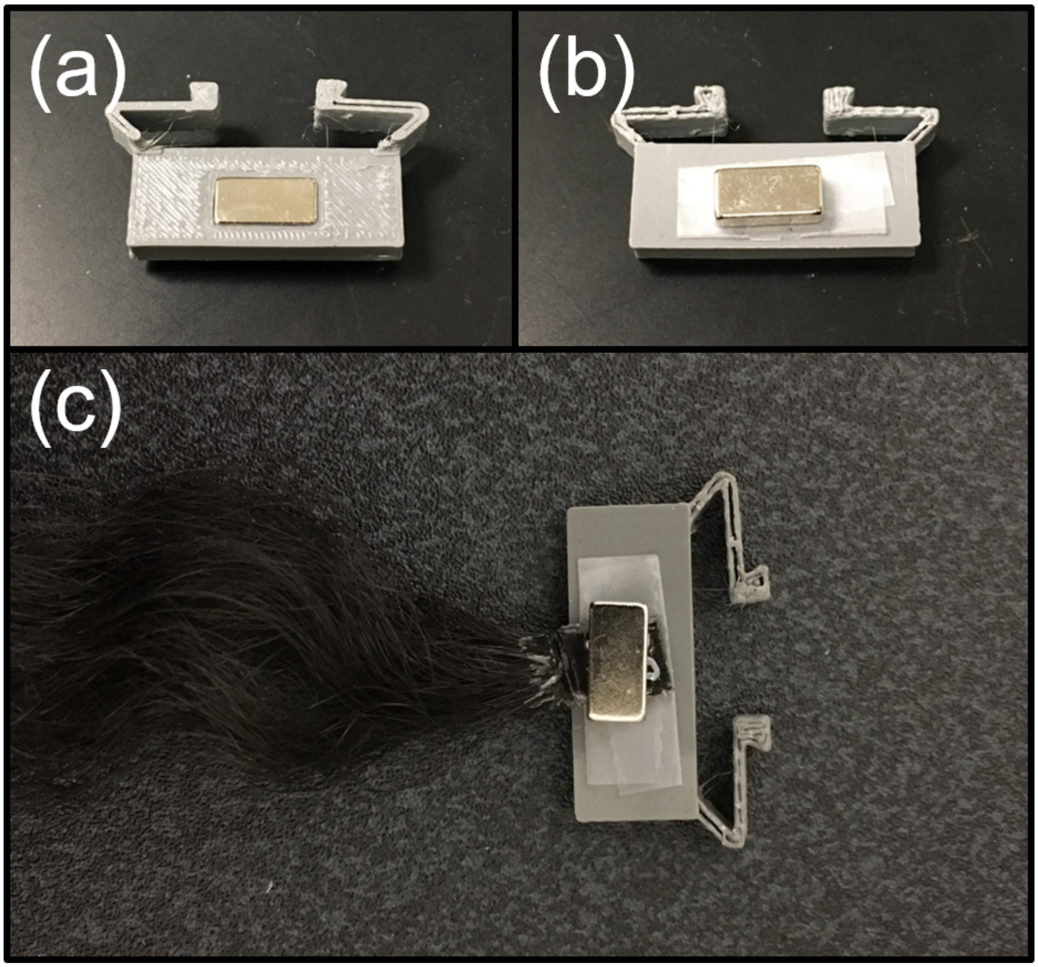

Figure 3.15. (a) A top view of a detachable 3D printed clamp with a magnet in a rectangular hole. (b) A bottom view of the detachable clamp (c) One end of hair sample is place between the two magnets and secured in its place.

with the lower clamp, the slider tends to be pushed back. While this is a subject for improvement, its impact on experiment is deemed negligible.

Second is the flat iron linear stage. It is a simple, low-cost substitute for a proper linear stage; however, due to much room for play as was the case for the load cell slider, it generates a lot of vibration as the linear stage glides towards the hair sample. The problem was addressed by a carbon steel block. Yet, the increased weight hanging in the mid air introduced slight vibration when the linear stage halts abruptly. A

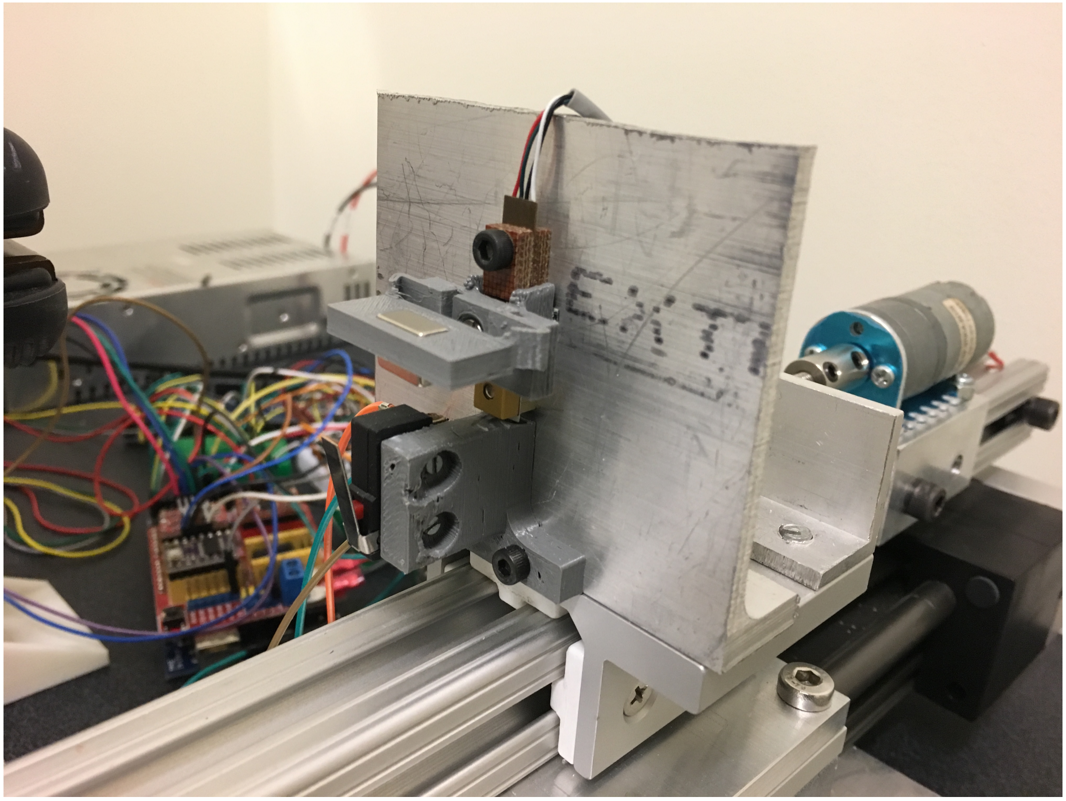

Figure 3.16. The 3D printed clamp attached to a structure to which a load cell is installed. This way, when the hair sample secured to the clamp is pulled the load cell can directly sense the amount of tension being applied to the hair.

better linear stage with tight tolerance between a bearing and rails would solve the problem. However, to reduce the cost, the problem was addressed by implementing deceleration with a microcontroller before the linear stage comes to a halt.

Third is the grip of the sample clamp. While it can apply tension up to 25 g with constant tension adjustment by a dedicated microcontroller, the consistency of the tension applied will increase and the complexity of the system will decrease if the clamp can provide better grip. This may be achieved by further increasing the surface area of the clamp or applying a material with higher friction.

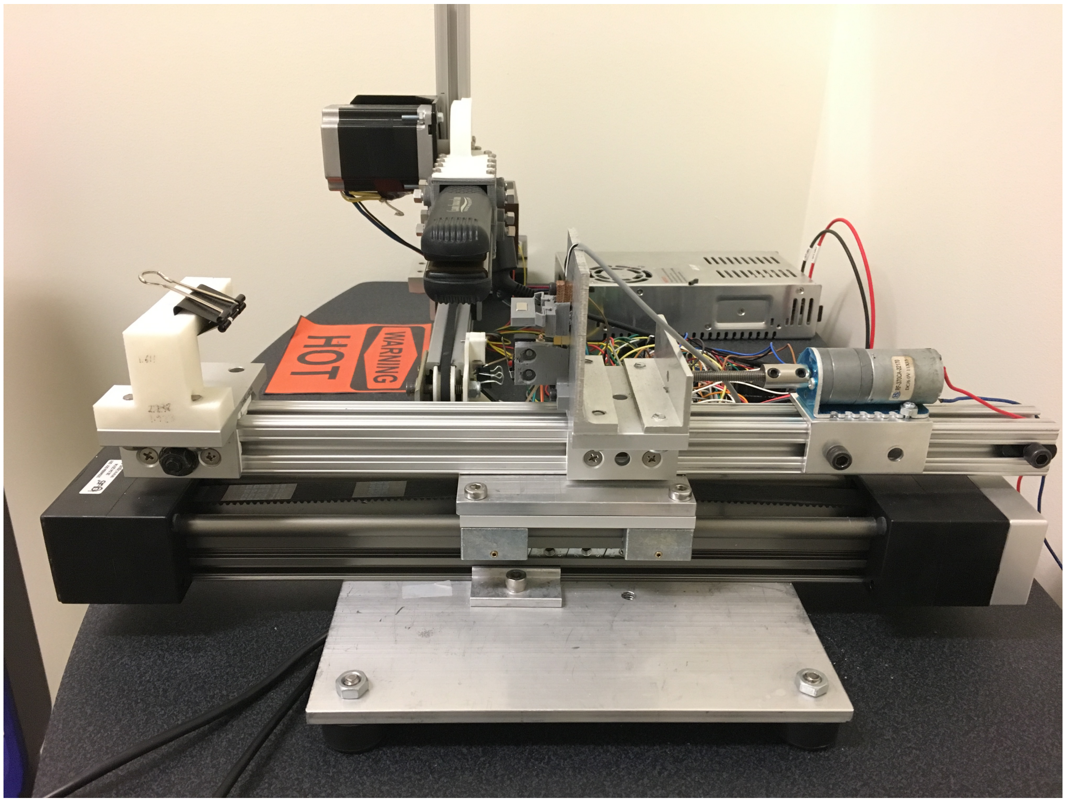

Figure 3.17. Picture of the sample stage.

3.4 Experimental Methods

In this section, sample preparation and experimental procedures are discussed.

3.4.1 Samples

Asian (Type I by STAM) and African hair samples (a mixture of Type V, VI, and VII by STAM) as received from International Hair Importers and Products (IHIP) were used in this study. The samples were collected from multiple subjects and therefore the STAM curl class of African hair was not strictly controlled. Therefore, the results from this study should be considered with respect to the traditional geo-racial hair typing.

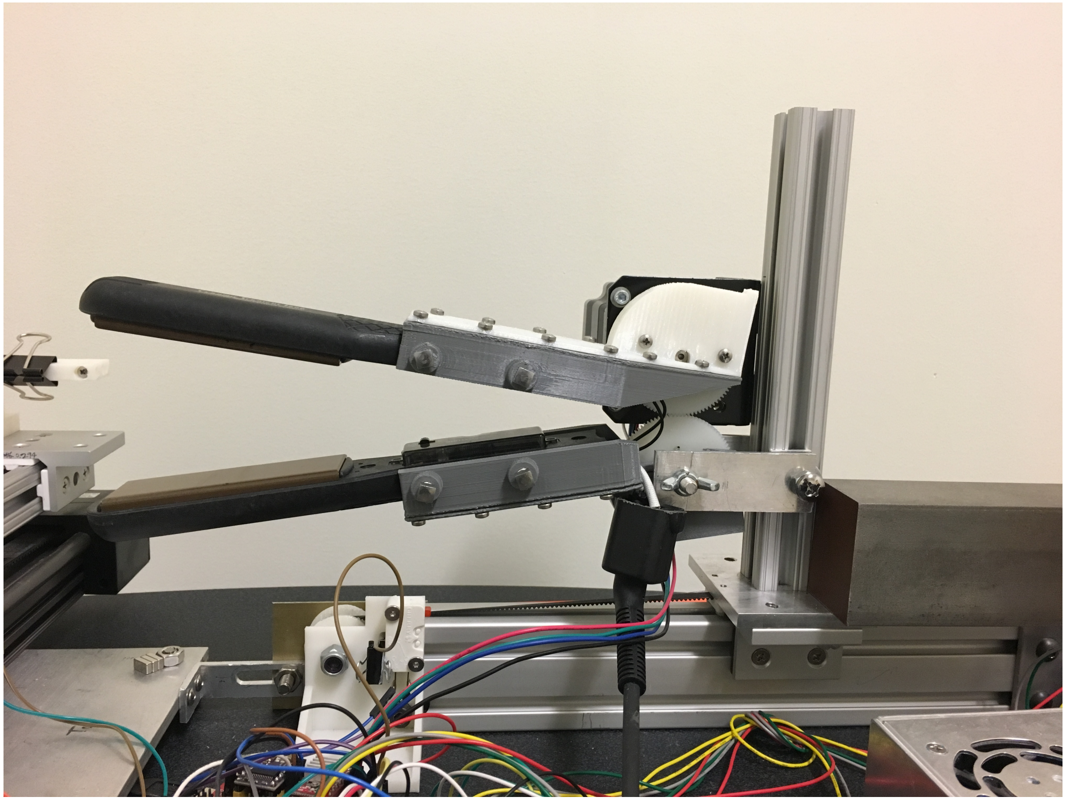

Figure 3.18. Picture of the clamp mechanism.

For the experiments that test the impact of flat ironing on the fatigue strength, bundles of hair were produced. For Asian hair samples, approximately 30 mg of swatches were prepared from the original bundles provided by IHIP (Figure 3.19 (a)). African hair bundles were prepared by IHIP upon request (Figure 3.19 (b)). The cross-sectional dimensions of each bundle were controlled to its best for consistency. Each swatch was soaked in a 1 solution of a clarifying shampoo for 3 minutes before it was equilibrated at 21 °C to 22 °C and 48 %RH to 52 %RH for at least 24 hours.

For the experiments on the straightening efficacy and permanent curl loss, single strands of hair were prepared. They were shampooed and dried overnight following the same protocol as that of the bundles.

Figure 3.19. (a) Representative prepared bundles of Asian hair. Each bundle contains approximately 30 mg of hair, and the thickness and width are approximately 0.22 mm and 10 mm, respectively. (b) Representative prepared bundle of African hair. Each bundle contains approximately 30 mg of hair, and the thickness and width are approximately 0.5 mm and 10 mm, respectively.

3.4.2 Equipment

The flat ironing mechanism introduced in the previous section applied each flat ironing conditions while an infrared camera (A6703sc, FLIR, USA) captures the thermal images to calculate the exposure time discussed in Section 3.2. Figure 3.20 shows the experimental setup comprised of the infrared camera (IR), a laptop for data acquisition, and the flat ironing mechanism. The hair bundle remains fixed while the flat iron moves across the hair, enabling the camera to remain focused on the hair bundles.

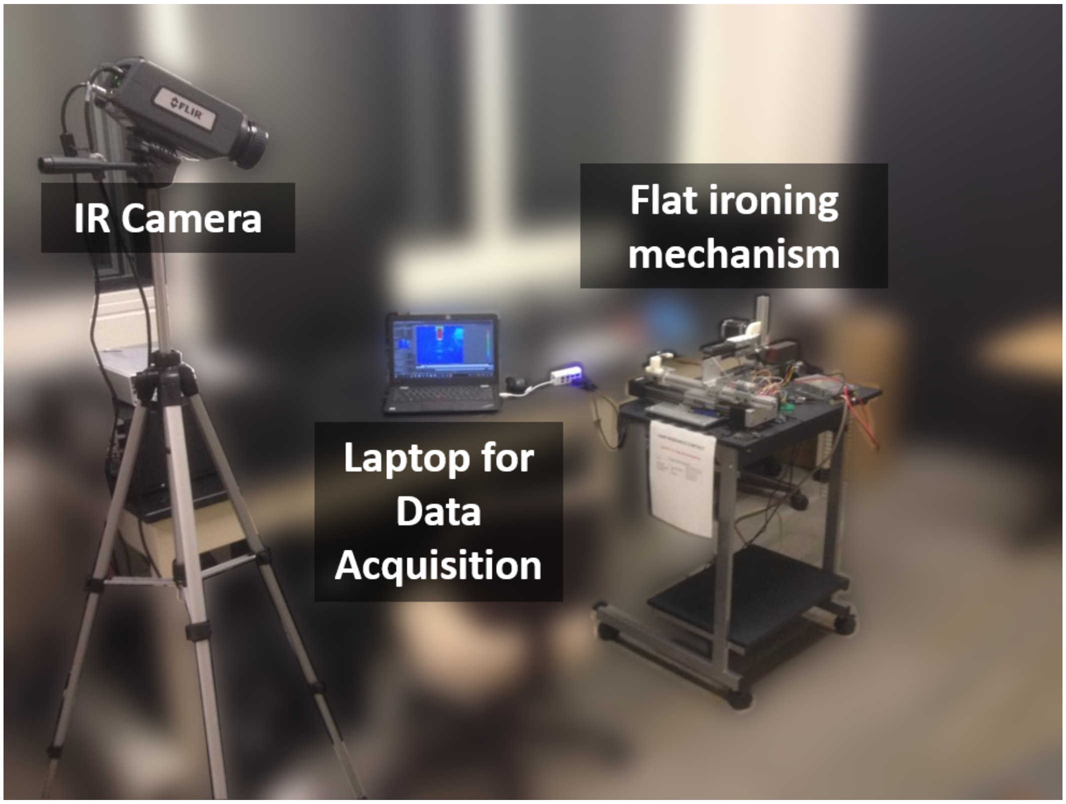

Figure 3.20. An automated flat ironing mechanism to control the gliding speed, the number of passes, and the cooling time between each cycle. The automated control not only enables thermal imaging, but also minimizes experimental variations that would be present with human flat ironing.

3.4.3 Experimental Procedures

The following tables list the flat ironing conditions used to test Asian hair (Table 6.1) and African hair (Table 6.2). Each condition was applied for 40 cycles to Asian hair and 20 cycles to African hair to inflict hair with a sufficient amount of damage to clearly distinguish one condition from another. The lower number of cycles applied to African hair is attributed to inherently low fatigue strength of African hair [65].

Figure 3.21 schematically illustrates an experimental procedure followed to flat iron bundles of hair to assess the reduction in fatigue strength.

Table 3.1. Flat ironing conditions for Asian hair.

Temperature (celsius)	115	164	210
Gliding Speed (cm/s) x Number of Passes	1 x 1	3 x 3	5 x 5

Table 3.2. Flat ironing conditions for African hair.

Temperature (celsius)	115	210
Gliding Speed (cm/s)	1	5
Number of Passes	1	5

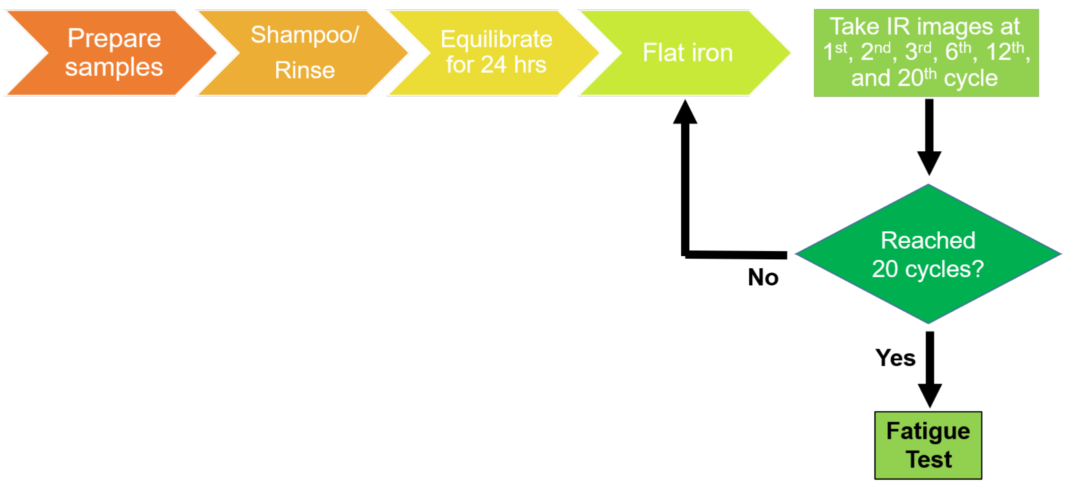

Figure 3.21. Illustration of the entire experimental procedure followed to flat iron a bundle of hair and evaluate the reduction in fatigue strength.

After the sample of bundled hair is prepared as described in the previous section, it is removed from the cardboard box and mounted on the flat ironing mechanism. It is important to ensure that hair is not taut when first mounted as it can cause tension on the sample and disturb zero calibration of the load cell. Next, Open function of the Arduino program introduced in Section 3.3.5 is used to open the flat iron (Figure 3.22). The flat iron will be switched on, and the temperature setting will be adjusted to a desired value (Figure 3.23); five minutes will be allowed to let the flat iron reach the target temperature. Afterwards, Close function will be used to close the flat iron;

one needs to ensure that the two plates are touching each other when the flat iron is closed (Figure (3.24). This is to exert constant pressure on all hair samples and avoid inducing unnecessary tension from increased friction. Then, the experiment is executed. The experimenter will be prompted with a message to input desired tension, number of passes, and gliding speed (Figure 3.25). Note that the feature for active tension control was disable because tension was treated as a fixed parameter as was previously discussed in Section 3.2. After these values are inputted according to the desired condition, the flat ironing process will execute. The IR camera recorded videos during the specified cycles in Figure 3.21 to confirm that the exposure time does not vary in each cycle.

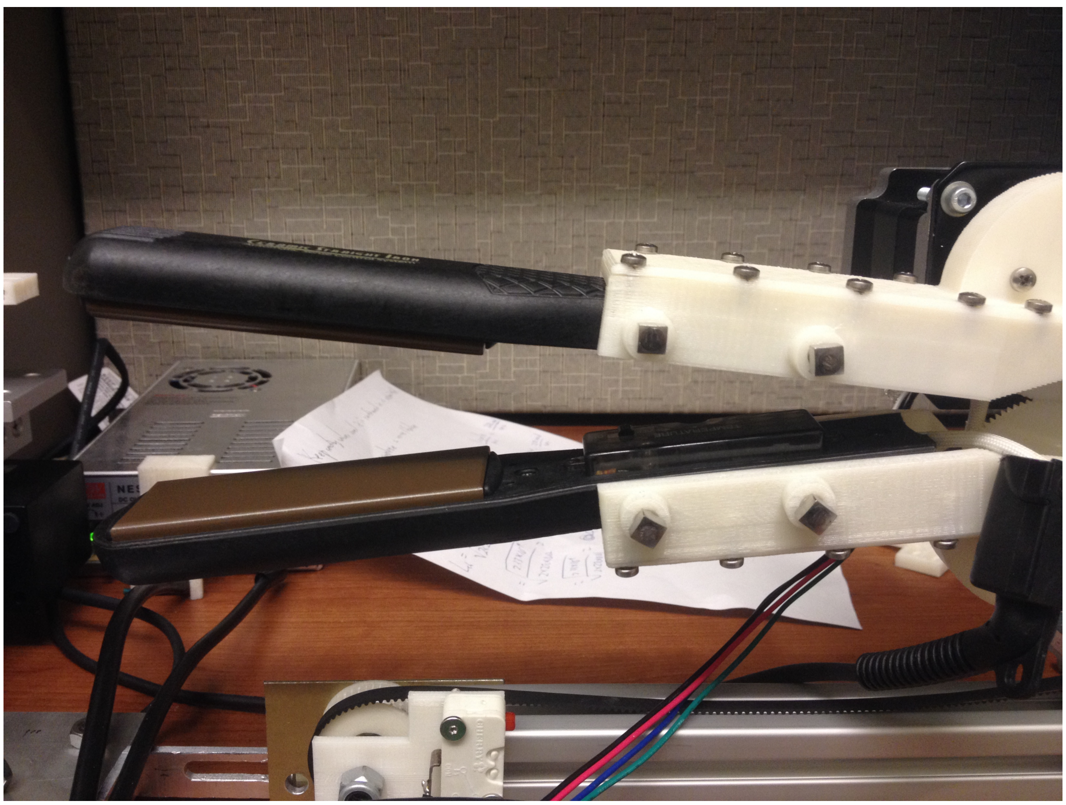

Figure 3.22. With Open function of the Arduino program, the flat iron opens.

After treating all the swatches under all the conditions, reduction in their fatigue strength was measured. Fifty fibers from each swatch were tested to draw statistically

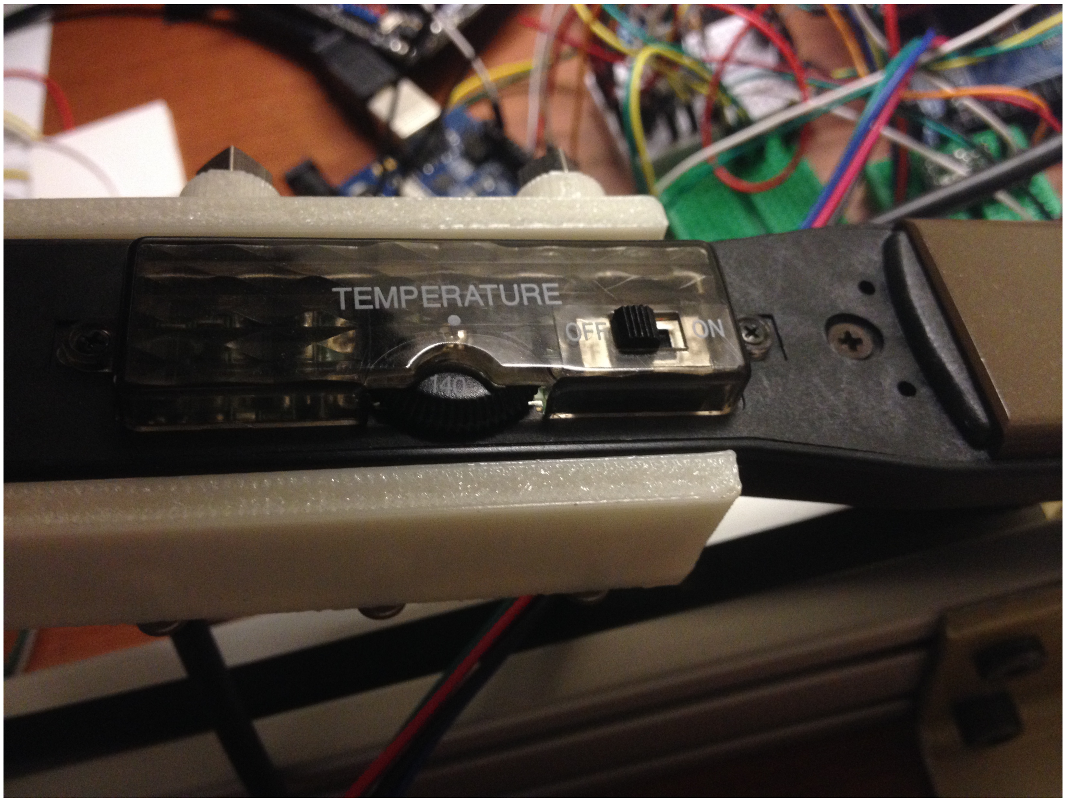

Figure 3.23. An on/off switch and an adjusting knob for temperature. The flat iron is turned on and adjusted for a desired temperature setting while it is open.

sound inferences from the results. All the fibers were selectively chosen from the middle section of the bundle where contact with a flat iron was most direct. Both ends of each fiber was clamped between brass clamps using an automated clamping system (Dia-Stron AAS 1600, Dia-Stron, UK) before they were mounted on a fatigue tester (Dia-Stron CYC801, Dia-Stron, UK). Then, 140 MPa of stress was applied until the fiber finally broke. The particular amount of stress was chosen to stay within the Hookean region while being sufficient to break the fibers within a day to prevent a prolonged experiment time. Throughout the whole testing process, the temperature and relative humidity were maintained at 23 °C and 50 %RH respectively.

Separate sets of experiments were conducted on single strands of hair to assess the effects of flat ironing conditions on hair straightening and curl loss (Figure 3.26.

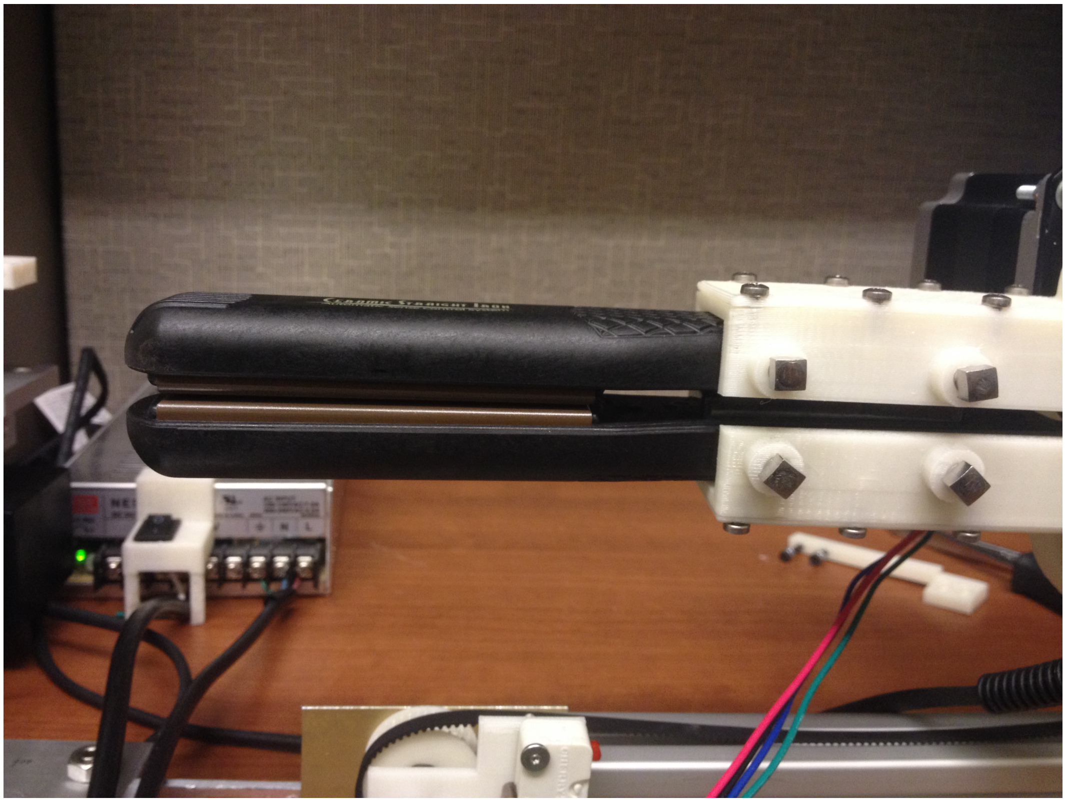

Figure 3.24. Close function closes the flat iron. Note that the Close function is executed multiple times to ensure there is no gap between the plates.

For all the measurement, a single strand of hair was mounted on the flat ironing mechanism and stretched straight with minimal amount of tension (less than 0.1 g) using the embedded load cell to prevent it from affecting the results. The detailed procedure for flat ironing is equivalent as before and is omitted here. To assess each flat ironing metric, L_n, L_e, and CD are measured before the flat ironing. L_n and L_e are measured immediately following the flat ironing to calculate the immediate straightening efficacy as was described in Section 3.1. Then, the hair is equilibrated for 24 hours before L_n and L_e measured again to evaluate the long-term straightening efficacy. After going through one more round of shampooing, rinsing, and equilibrating, CD is measured to calculate the permanent curl loss.

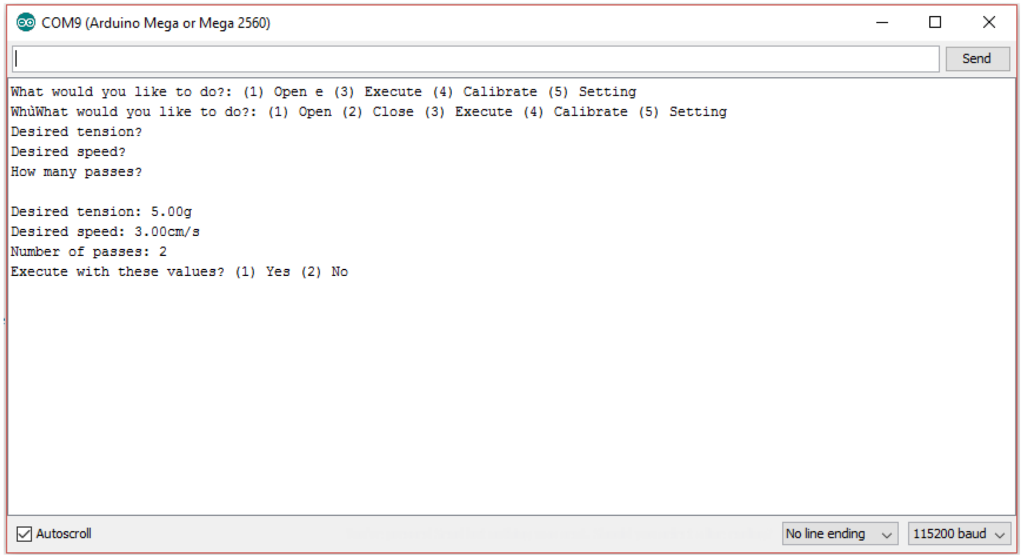

Figure 3.25. A prompt message asking for desired tension, number of passes and gliding speed is printed on a window for serial communication between an Arduino microcontroller and PC. One can open the window from the Arduino IDE.

Figure 3.26. Illustration of the entire experimental procedure followed to flat iron a single strand of hair and evaluate the straightening efficacy and permanent curl loss.

The experiments were conducted on African hair alone as already straight Asian hair would not show any change in shape. Twenty-five (25) fibers were tested for the equivalent flat ironing conditions used in the fatigue experiment for African hair. This allows us to collect meaningful data about the relationships between hair strength, straightening, and curl loss. Unlike the fatigue strength, in the experiments for straightening efficacy and permanent curl loss, flat ironing occurred only for one cycle (not 20 heat cycles as for the bundle experiments). The induced straightening and curl loss effects may differ to a significant degree if administered on a bundle of hair as the interaction between fibers will differentiate the overall heat transfer and the resultant effects of heat.

3.5 Multiple Linear Regression

After running all the experiments, attempts for predictive modeling was conducted by using multiple linear regression. All three flat ironing parameters, gliding speed (V), number of passes (N), and temperature setting (T) were used along with the exposure time (E) as predictors for the four metrics of flat ironing results: fatigue strength (FS), straightening efficacy (SE), long-term straightening efficacy (LTSE), and permanent curl loss by curl index (PCLCI) and by curl diameter (PCLCD).

Throughout all the procedures, the following steps were followed to ensure the best practice. First of all, all datasets were tested for Gaussian distribution necessary to satisfy the basic assumption of regression. For those that did not follow the distribution, Box-Cox transformation was performed as deemed appropriate. If there are data points that are significantly far away from the Q-Q plot, which assesses the Gaussian distribution, the common definition of outlier –any points that lie outside 75^{th} percentile plus 1.5 times the interquartile or 25^{th} percentile minus 1.5 times the interquartile - was applied to eliminate those points as needed. Also, where appropriate, the predictors were used in a higher order of polynomial term to better fit the data. Interaction between the predictors were used to account for the variation in the effect size of a predictor with the presence of the other predictors as well.

For the model selection procedure, Mallows's Cp, adjusted R^2, and the number of predictors were used simultaneously as criteria. The model that minimizes Cp (less bias in the predicted values) and the number of predictors (economic use of predictors) yet maximizes adjusted R^2 (higher explanatory power of the model) was selected as the best model for each response variable.

3.6 Results and Discussion

In this section, the results of experiments and multiple linear regression are presented and discussed. Table 4.3 lists the results from testing the fatigue strength of Asian hair after flat ironing. Some observations were excluded for failing prematurely or being outliers. Nevertheless, the exclusion of observations has no significant impact on conducting the necessary statistical analysis because the remaining number of observations is sufficiently large.

Table 3.3. Results for the fatigue test Asian hair.

Sample	T (C)	V (cm/s)	N	E (sec)	# of Fibers	log(# of cycles to failure)	
						Mean	STD
Control	0	0	0	0	50	3.79	0.61
A1	115	1	1	4.24	48	3.5	0.54
A2	115	3	3	6.17	46	3.51	0.53
A3	115	5	5	10.42	40	3.52	0.53
A4	164	1	1	7.11	47	3.32	0.5
A5	164	3	3	18.38	48	3.27	0.75
A6	164	5	5	22.5	48	3.5	0.59
A7	210	1	1	9.26	44	1.63	0.48
A8	210	3	3	22.88	48	2.24	0.64
A9	210	5	5	33.93	49	2.14	0.56

Box-Cox transformation of the response variables was necessary to impart the Gaussian distribution to the data. Both the data for Asian and African hair went through a log transformation. Henceforth, the transformed form of the response variables is presented. Due to the high volume of data, means and standard deviation are presented instead of providing the whole data.

Multiple linear regression of the fatigue strength of Asian hair indicated that a cubed term of a temperature setting is the single best predictor with the adjusted

R^2 of 0.5282 as shown in Figure 3.27. The best model (adjusted R^2=0.5969) selected following the pre-established criteria is shown below:

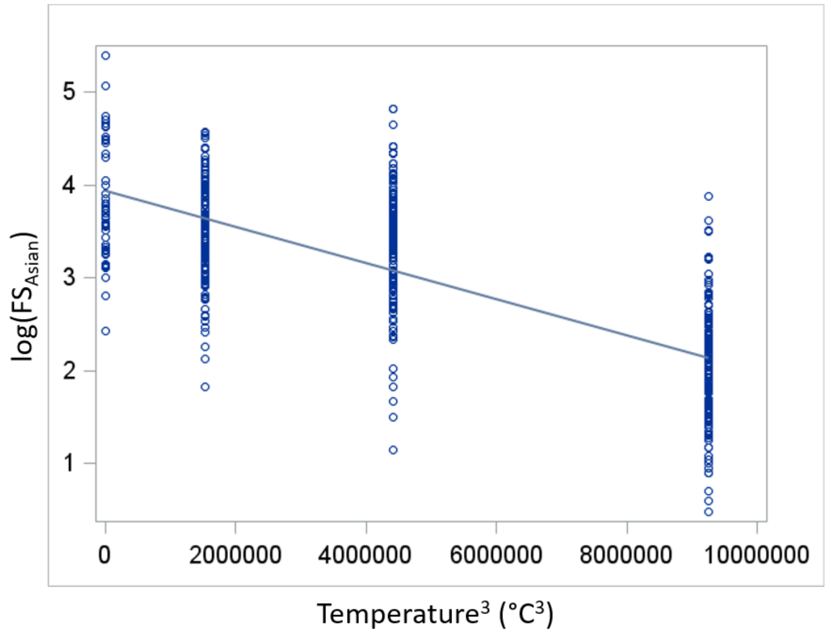

Figure 3.27. $log(FS_{Asian})$ against the single best predictor $Temperature^3$.

$$\log FS_{Asian} = 5.208 \times 10^{-5}T^2 - 8.2 \times 10^{-3}T - 6.713 \times 10^{-10}T^3E^3 + 3.428 \times 10^{-10}T^3E^3N - 4.195 \times 10^{-11}T^3E^3VN + 3.79 \tag{3.8}$$

Including an additional temperature setting term and the interaction terms increase the explanatory power by about 7 %. Even though this may not be an impressive improvement considering the addition of four terms, it greatly reduces the bias in the prediction which is evaluated by Mallowss Cp.

Comparing the residues and the predicted values by the model (Figure 3.28) serves a diagnostic purpose of visualizing how residuals are distributed. One can be assured of the soundness of fit if the residuals are randomly scattered about zero and do not display any signs of pattern. The residuals of the best model for Asian fatigue strength are randomly scattered about zero and therefore satisfies the criterion. The plot indicates that the relatively low R^2 is likely attributed to the inherently large variation in the fatigue strength across the individual strands of hair. The fact that the hair samples were prepared from multiple subjects could further amplify the magnitude of variation. Also, even though only the study on a different growth rate and density (hairs per unit area on a scalp) exists [89], it is well known among people that hair from different areas of scalp behaves differently. Therefore, the model is more suitable for predicting the behavior of the whole population of hair type to which it belongs. The explanatory power of the model is likely to increase if the same experiment is performed with the hair collected from the same area on a scalp of a single subject.

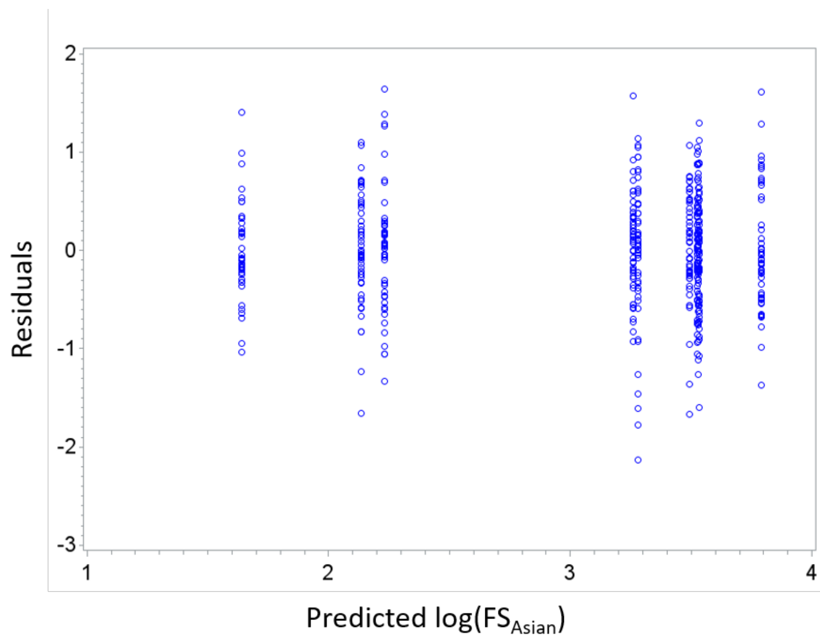

Figure 3.28. Residuals versus predicted values for the fatigue strength of Asian hair.

Next, Table 3.4 lists the results from flat ironing African hair under various conditions. Again, multiple linear regression was performed on the fatigue strength of African hair. It should be noted that the data for African hair had some outliers that were significantly affecting the Gaussian distribution as well as the regression and were eliminated according to the appropriate procedure outlined at the end of

Table 3.4. Results for the fatigue test on African hair.

Sample	T (C)	V (cm/s)	N	E (sec)	# of Fibers	log(# of cycles to failure)	
						Mean	STD
Control	0	0	0	0	47	3.65	0.67
AA1	115	1	1	4.7	39	3.6	0.61
AA2	115	1	5	26.9	47	3.35	0.75
AA3	115	5	1	0.7	45	3.49	0.6
AA4	115	5	5	4.2	49	3.3	0.53
AA5	210	1	1	14.9	46	2.8	0.57
AA6	210	1	5	70.4	47	1.65	0.28
AA7	210	5	1	7	45	3.36	0.67
AA8	210	5	5	42.7	41	3.05	0.68

the previous section. As a result, 13 observations were excluded from the regression process. This is expected for African hair samples as often fail prematurely during mechanical tests due to the inherent defects and inconsistent cross-sectional profiles that introduce weak points [63–65].

In contrast to the experiment with Asian hair, a cubed term of a temperature setting yields a much lower adjusted R^2 of 0.213. For the experiment with African hair, the exposure time is the single best predictor with adjusted R^2 of 0.4166 as shown in Figure 3.29. The best model shown below yields adjusted R^2 of 0.4821.

$$\log \mathrm{FS}_{African} = -4.691 \times 10^{-2} N - 3.042 \times 10^{-11} T^3 E^3 + 5.98 \times 10^{-12} T^3 E^3 N + 3.585 \tag{3.9}$$

In this case, the addition of two terms leads to an increase of R^2 by 7 %. The magnified importance of interaction terms seems to originate from the difference in the flat ironing conditions applied to Asian and African hair. For Asian hair, the gliding speed and number of passes were coupled together (e.g. 1x1, 3x3, and 5x5). This was done to test if a temperature setting would be a dominant factor if the duration for

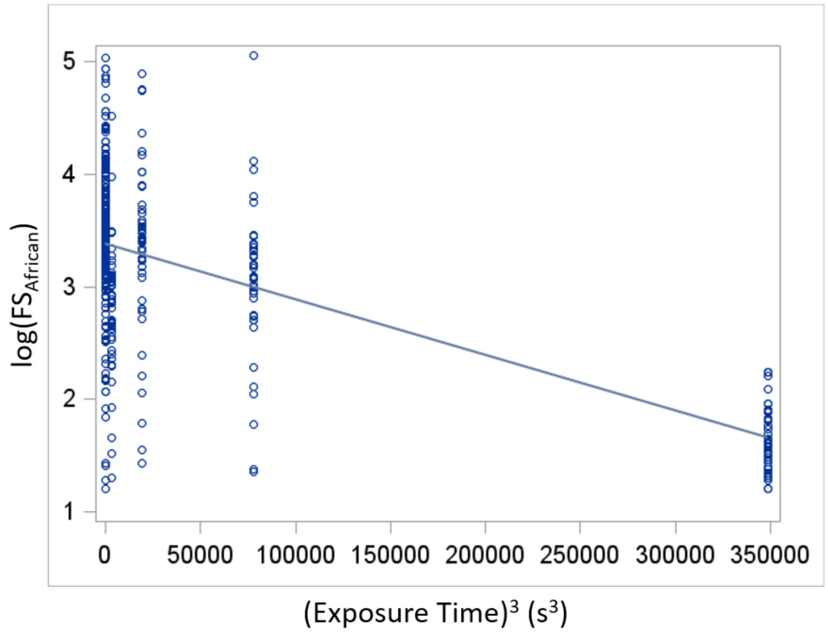

Figure 3.29. $log(FS_{African})$ against the single best predictor $(ExposureTime)^3$.

which a flat iron comes in a direct contact with hair is held constant, which turned out to be the case. Thus, the possible combination between the two variables was limited and their interaction not captured. On the contrary, for African hair, the two variables were decoupled and tested for all possible combinations thereby allowing the interaction between them and with the other variables to be better observed.

The same argument may also explain why the exposure time has become the dominant factor for the case of African hair. The exposure time is the result of the heat transfer which is determined by the effects of other parameters, a temperature setting, the gliding speed and number of passes. Thus, the exposure time seems to largely account for the magnified importance of interaction terms by itself. Based on this reasoning, it may be plausible to expect that by testing all possible combinations of the gliding speed and number of passes, the interaction terms and the exposure time will become significant for Asian hair as well.

The high correlation between the exposure time and the reduction in fatigue strength is consistent with the results of other relevant works. The amount of change in denaturation temperature and enthalpy, which are presumed to be directly related with crystallinity of intermediate filaments in the cortex and the disulfide bonds in the matrix respectively [72, 90], can be described with a first-order kinetic model [21]. Furthermore, the change in the fraction of α-crystalline in the cortex has a direct relationship with the mechanical property of hair such as elastic modulus [9, 91].

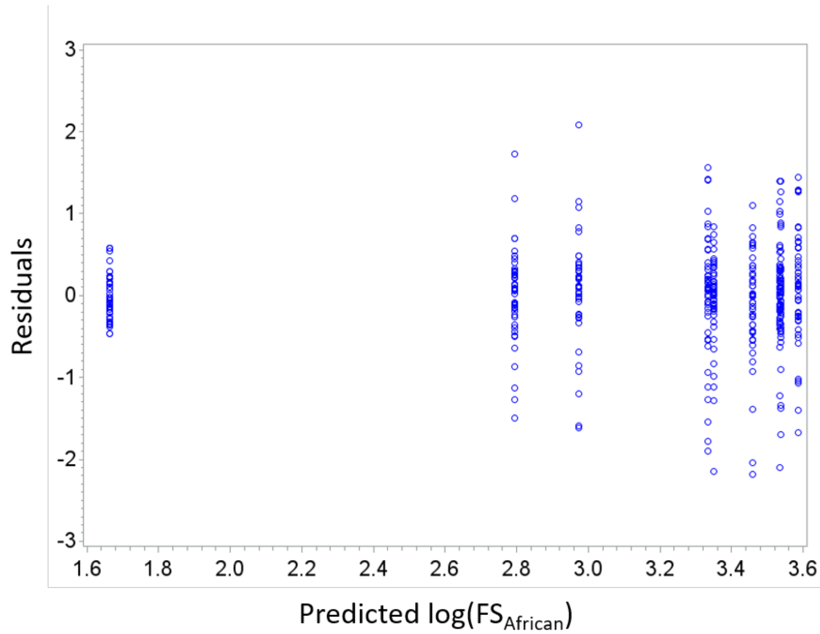

Figure 3.30. Residuals versus predicted values for the fatigue strength of African hair.

Figure 3.30 visually compares residues and predicted values by the best model for the fatigue strength of African hair. As was the case for Asian hair, the inherently high variation across fibers and that hair was from multiple subjects without controlling the area of collection possibly explain the relatively low explanatory power expressed by R^2. Also noteworthy is that there tend to be more influential observations that are scattered farther away from zero, especially toward the lower end, compared with Asian hair. The use of African hair samples where Type V, VI, and VII coexist could mostly explain the higher variability in the fatigue strength of individual strands than Asian hair and the relatively lower R^2 value. Moreover, Porter et al. [67] reported high

Table 3.5. Results for the straightening efficacy experiment on African hair.

Sample	T (C)	V (cm/s)	N	E (sec)	# of Fibers	log(SE+1)		# of Fibers	(LTSE+1)0.2	
						Mean	STD		Mean	STD
AA1	115	1	1	4.7	25	-1	0.46	15	0.87	0.07
AA2	115	1	5	26.9	24	-1.19	0.47	24	0.88	0.08
AA3	115	5	1	0.7	25	-0.87	0.68	25	0.91	0.09
AA4	115	5	5	4.2	25	-0.98	0.5	16	0.92	0.08
AA5	210	1	1	14.9	25	-1.66	0.42	20	0.75	0.07
AA6	210	1	5	70.4	25	-1.53	0.42	25	0.8	0.08
AA7	210	5	1	7	25	-1.48	0.46	25	0.8	0.08
AA8	210	5	5	42.7	25	-1.64	0.36	20	0.76	0.06

variability in the mechanical strength and thermal stability of African hair within the same STAM hair type, which could further amplify the variability. Interestingly, the variability is minimized when the hair is treated by the harshest condition (210 °C, 1cm/s, 5 passes).

Table 3.5 shows the results for straightening efficacy test on single strands of African hair. Response variables of both the straightening efficacy and long-term straightening efficacy were transformed by taking the log and the power of 0.2, respectively. The results for the long-term straightening efficacy are devoid of some observations because the decision to measure it was made after completing several runs of experiments on the straightening efficacy. Nonetheless, the regression analysis is unhampered because of the high volume of data available and the consistency in the ranges of mean and standard deviation.

Figures 3.31 and 3.32 are plots of log(SE+1) and $(LTSE+1)^{0.2}$ against the temperature setting which is the dominant factor in both cases (adjusted $R^2 = 0.2568$ and 0.3674, respectively). Figures 3.33 and 3.34 illustrate the comparisons between residuals and predicted values by each respective best model for the straightening efficacy and long-term straightening efficacy of African hair upon flat ironing. The best models constructed for each metric (adjusted R^2 is 0.277 and 0.3998, respectively) are as follows.

$$\log(SE+1) = -5.08\times 10^{-3}T - 1.58\times 10^{-2}E + 3.977\times 10^{-5}E^2N - 0.317 \quad (3.10)$$

$$(LTSE+1)^{0.2} = -6.032\times 10^{-5}TV - 7.796\times 10^{-4}E^2V + 1.518\times 10^{-4}E^2VN + 0.884 \quad (3.11)$$

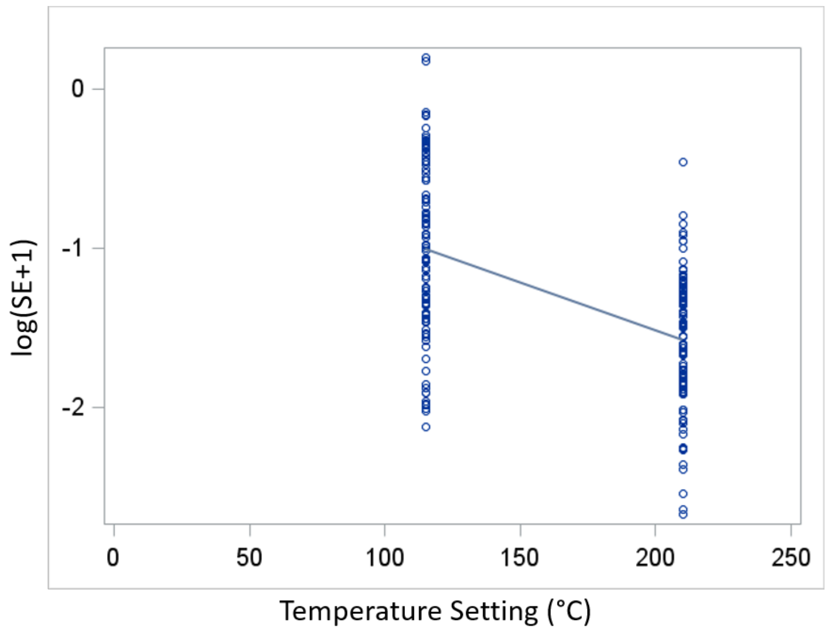

Figure 3.31. $log(SE+1)$ against the single best predictor Temperature Setting.

Similar to the case of fatigue strength, the temperature setting was the most dominant factor for both metrics, and most of the variation could be explained by it alone. However, to minimize the bias in the model, inclusion of extra terms was necessitated by following the Mallows's Cp criterion. As a result, the model for the long-term straightening efficacy now only includes interaction terms.

Note the contrast in the R^2 values between the two metrics. The model for the long-term straightening efficacy is accounting for 12% more variability in the results than the model for the straightening efficacy. It seems that the slight loss of straightening efficacy upon exposure to humidity and stabilization of hair shape

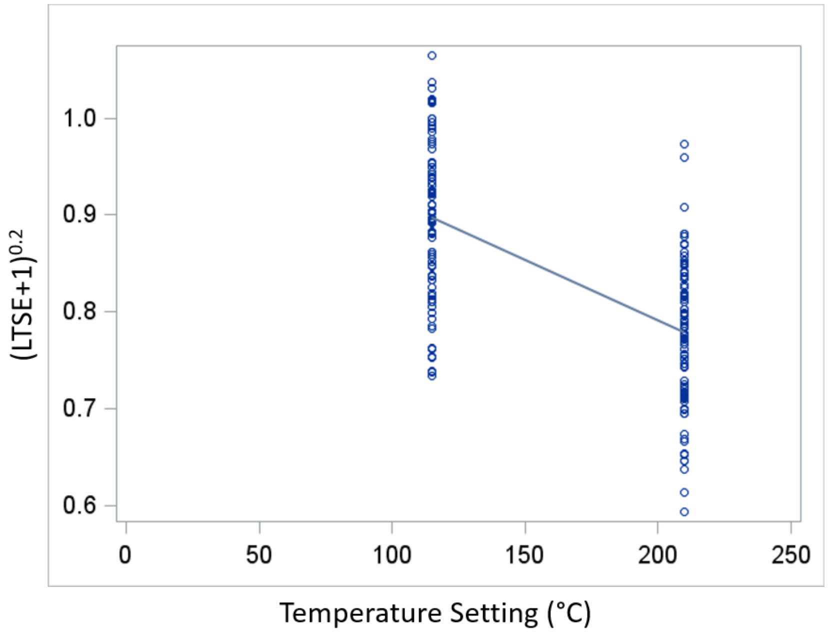

Figure 3.32. $(LTSE + 1)^{0.2}$ against the single best predictor Temperature Setting.

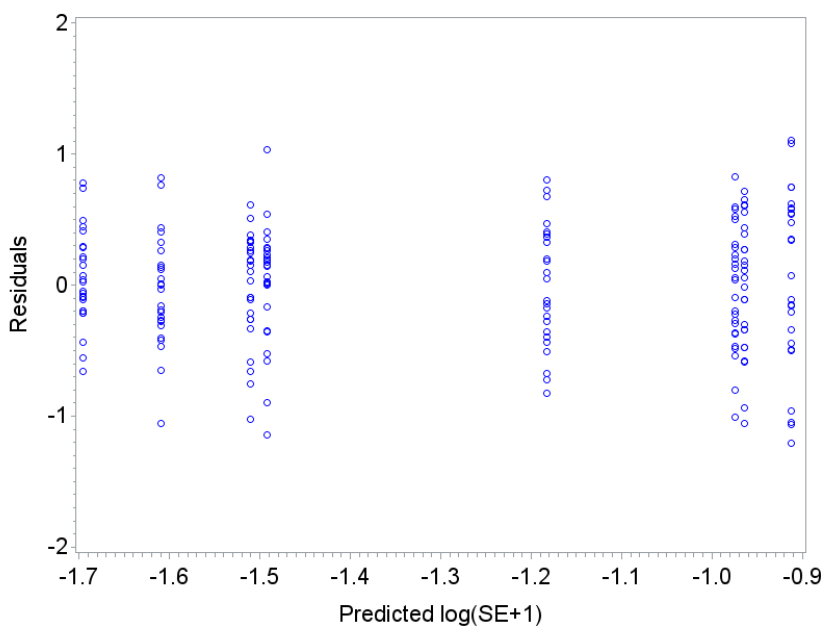

Figure 3.33. Residuals versus predicted values for the straightening efficacy of African hair.

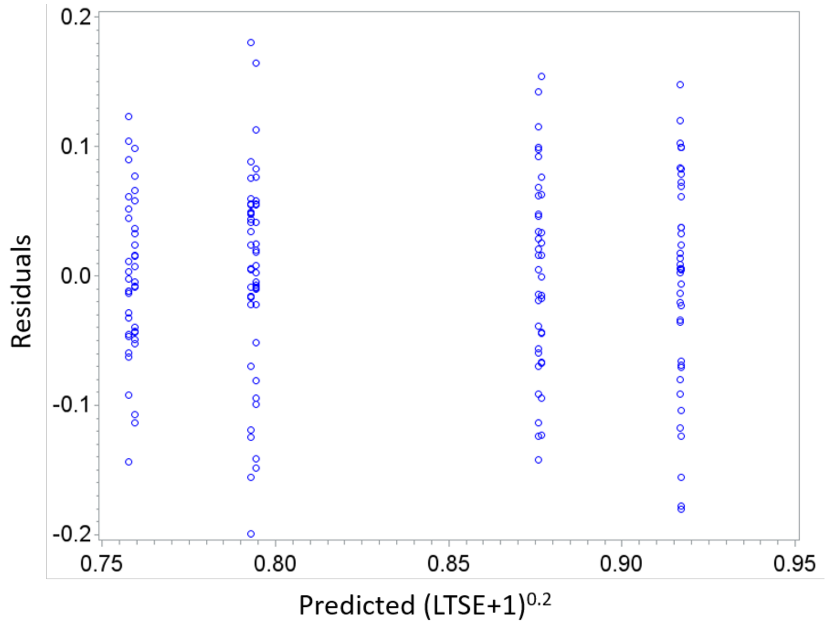

Figure 3.34. Residuals versus predicted values for the long-term straightening efficacy of African hair.

over time reflect the effect of flat ironing more accurately. This could mean that the lost 12% of explanatory power is due to missing predictors that can account for the immediate straightening efficacy.

Tension in hair could be a potential culprit; however, as was previously described, tension in hair was carefully measured and kept to near zero for each heat application. Moreover, calculation for the required tensile force to induce permanent deformation of hair shape based on the wet-state Young's modulus and cross-sectional area of African hair [63] indicates that any tensile force below what is equivalent to approximately 0.9 g would still allow hair to remain within a Hookean region. Therefore, in a dry state hair would be even more resistant against shape change with the presence of such low tension.

This may have more to do with intrinsic variability in each strand of hair such as the ability to absorb moisture or some other morphological factors that respond differently to heat. Again, the hair samples supplied are from multiple subjects without

Table 3.6. Results for the permanent curl loss experiment on African hair.

Sample	T (C)	V (cm/s)	N	E (sec)	# of Fibers	log(PCLCI+1)		log(PCLCD+1)	
						Mean	STD	Mean	STD
AA1	115	1	1	4.7	23	-0.01	0.42	-0.04	0.28
AA2	115	1	5	26.9	24	0.14	0.61	-0.06	0.23
AA3	115	5	1	0.7	25	0.07	0.43	-0.01	0.21
AA4	115	5	5	4.2	25	-0.03	0.56	-0.07	0.26
AA5	210	1	1	14.9	25	-0.45	0.57	0.4	0.29
AA6	210	1	5	70.4	23	-0.24	0.6	0.32	0.23
AA7	210	5	1	7	25	-0.39	0.59	0.14	0.24
AA8	210	5	5	42.7	25	-0.59	0.49	0.24	0.28

controlling its location on the scalp. Furthermore, mechanical strength and thermal stability are reported to vary by ethnicity even if the hair belongs to the same STAM hair type [67]. Therefore, it is highly likely that the difference in response to heat application relates to these factors. Why such variability appears to a lesser degree upon the exposure to humidity requires a separate in-depth study to be answered.

Finally, we evaluate the permanent curl loss for African hair (Table 4.7). The permanent curl loss was assessed by both the change in the curl index and curl diameter. Both metrics were transformed by taking the log to follow the Gaussian distribution. The few missing observations are due to the breakage or loss of fibers that occurred during the experiments.

The best models for each metric is presented below. The adjusted R^2 value of the modeling utilizing the curl index (0.1678) is clearly much lower than that utilizing the curl diameter (0.3178). Thus, we conclude that the change in curl diameter better evaluates the permanent curl loss due to flat ironing. Like the previous models, relatively low R^2 value plausibly originates from the inherently large variability in the samples.

$$Log(PCLCI + 1) = -1.207 \times 10^{-5} TE^2 V + 2.35 \times 10^{-6} TE^2 VN + 6.07 \times 10^{-2} \tag{3.12}$$

$$\log(PCLCD + 1) = 5.393 \times 10^{-8} TE^4 V - 1.077 \times 10^{-8} TE^4 VN - 2.729 \times 10^{-2} \tag{3.13}$$

Figure 3.35 show the plot of log(PCLCD+1) against the dominant factor, temperature setting, with the adjusted R2 value of 0.2706.

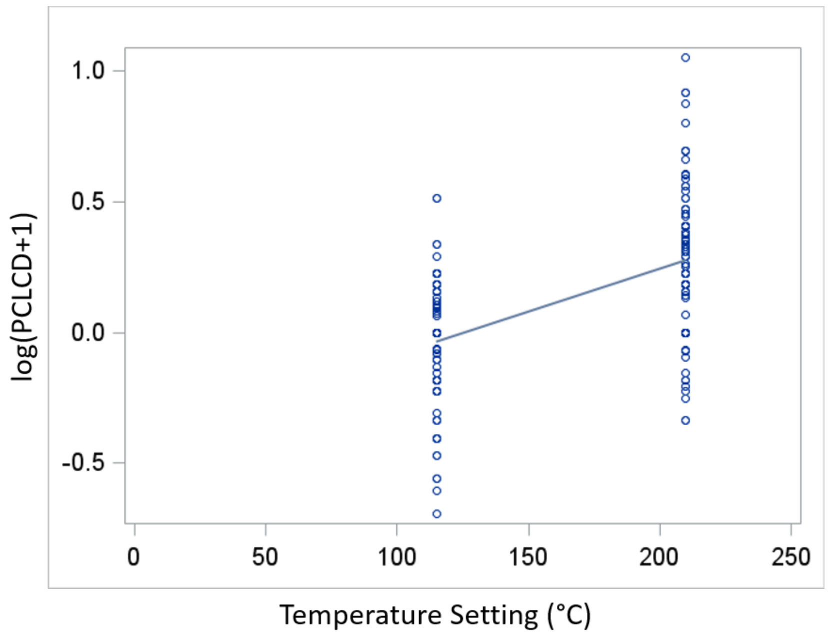

Figure 3.35. log(PCLCD+1) against the single best predictor Temperature Setting.

The residuals versus predicted values again validates random spread of residuals about zero and justifies the soundness of fitting the model (Figure 3.36).

Across all cases, the temperature setting is the most dominant predictor. Thus, the use of temperature setting by manufacturers as the sole criterion was an efficient choice. However, as demonstrated by the model for the fatigue strength of African hair, the interactions between all the participating parameters become far more important than the temperature setting alone when we are dealing with various combinations of gliding speed and number of passes. Furthermore, it is vital to

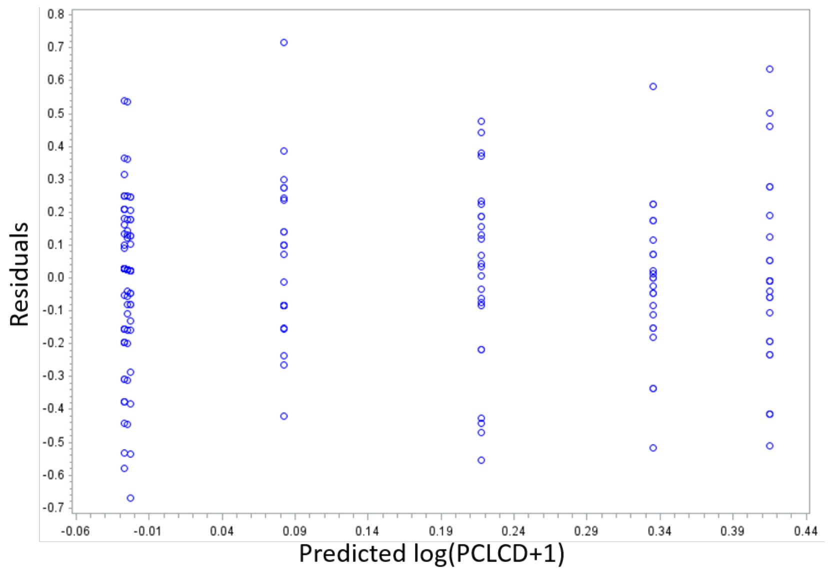

Figure 3.36. Residuals against predicted values for the permanent curl loss of African hair.

consider all participating parameters in order to minimize the bias and maximize the accuracy of the prediction. On the other hand, the single cycle of flat ironing might not have been effective at accurately assessing the effect of prolonged use of a flat iron on the straightening efficacy and permanent curl loss. In fact, the denaturation of α-helices is reported to be closely related with the permanent straightening in African hair [92,93]. Thus, the correlation between the exposure time and the straightening efficacy and permanent curl loss may increase with an increment in the number of flat ironing cycles. To account for all these aspects, construction of predictive models for various flat ironing results is essential for assessing the consequences prior to the use of heat and will prove to be a helpful tool for advising flat iron users on judicious use of the device.

4. EFFECTS OF HEAT PROTECTANTS ON FLAT IRONING

This chapter delves into the actual benefits of heat protectants apart from their market claims about the protection from heat damage. To lay the basis for the inquiry, the know benefits of heat protectants are reviewed. Then, its effects are experimentally validated following the same procedures introduced in the previous chapter except that, this time, analysis of variance (ANOVA) is utilized to specifically evaluate if the effect of the protectants has statistical significance.

4.1 Known Benefits of Heat Protectants

Heat protectants have been widely promoted as a product which protects hair from heat damage caused by heating appliances such as a curling iron and flat iron. The usual explanation for its mechanism commonly involves retarded penetration of heat by a protectant layer that contains silicone. While there are no studies that proved it, a few scientific studies did report the benefits of silicone. Christian et al. [8] observed that use of dimethicone mitigates the reduction in Young's modulus upon heat styling. They also reported improvement in tryptophan preservation even though multiple doses of silicone application were necessary to enable it. They also reported adverse effects of a water-based heat protectant in comparison with a dry protectant; the water-based protectant exacerbated reduction in Young's modulus, break strength, and damages to medulla and cortex.

On the other hand, Dussaud et al. [9] reported that amodimethicone can help preserve hair's thermal stability, which was measured by a mitigated decrease in keratin denaturation temperature and change in denaturation endothermic enthalpy. However, the effect was not distinguishable from that imparted by water. The case was the same for the change in Young's modulus; it decreased by a similar amount with the presence of amodimethicone and water alike. Instead, the silicone provided better fiber alignment, reduced friction, and improved moisture retention.

Despite silicone's proven benefits, one can easily recognize the misalignment between the actual benefits of silicone and what the customers expect. Even though customers expect heat protectants to protect hair from heat as the name suggests, scientifically proven effects for heat protection is tenuous while other benefits for fiber alignment and reduced friction are more prominent. Moreover, considering that heat protectants are promoted as a necessary step in the heat styling process, the evaluations of the product performance conducted by the previous studies seem inadequate for correctly reflecting what customers expect from heat styling. Keratin denaturation or Young's modulus exhibits only partial information about the structural integrity of hair; it is unclear how much of it will translate into a palpable degree of damage customers experience during their daily grooming activities. In particular, when it comes to heat styling that involves flat ironing, the results of straightening and the resultant loss in curls also become the center of concerns. Depending on individual's unique hair care needs, one or both of these concerns may compromise the concern for hair strength to a certain degree. Thus, the performance of heat protectants or any types of products that serve a similar purpose should be evaluated by the metrics that reflect the three main concerns of flat iron users: reduction in hair strength, effectiveness of straightening, and loss of curls as was already introduced in the previous chapter.

In this work, the four metrics of flat ironing results are utilized to evaluate the performance of both a non-silicone containing and silicone containing heat protectant under various flat ironing conditions. Statistical analysis is performed to assess if the presence of the heat protectant makes any statistically significant difference to each metric. Then, a discussion on the overall implications of the results and their utilization for the benefits of flat iron users follow.

4.2 Experimental Methods

The experimental methods and procedures are mostly equivalent to those of the previous chapter. The only difference is the application of a heat protectant for additional conditions that contain them. Then, instead of constructing predictive models, I conducted an analysis of variance (ANOVA) to evaluate if the presence of a heat protectant creates any statistically significant difference to the flat ironing results.

4.2.1 Samples

Asian hair bundles were prepared from the original hair swatches provided by International Hair Importers and Products (IHIP). African hair bundles were prepared by IHIP upon request. Each bundle weighed approximately 30 mg. Both ends were glued to maintain its form and maximize the consistency in the length of each strand when stretched. Each bundle was soaked in a 1 % solution of clarifying shampoo for 5 minutes before being equilibrated at 21 °C to 22 °C and 48 %RH to 52 %RH overnight. Heat protectants were sprayed on two sides of the bundle and spread evenly on the bundle by hand. Then, each bundle was soaked for 5 minutes in the heat protectant before the excess was removed by blotting with a paper towel. In addition, to assess the effect of heat protectant without heat treatment, a sample was prepared by applying the heat protectant following the same protocol but soaking it in the protectant overnight. All bundles were thoroughly washed by manually applying shampoo and rubbed by hand to cleanse the remaining silicone coating that could affect the results of fatigue strength.

The same protocol was followed for preparing single strands of hair samples for the experiments on straightening efficacy and curl loss. Asian hair was treated with a non-silicone containing heat protectant whereas African hair was treated with a silicone-containing heat protectant.

It was assumed that the ingredients of the protectant (except the wet components which rapidly evaporate upon heat application) remain intact on the surface of hair even after multiple heat cycles. The remaining mode by which removal of heat protectant can occur is chaffing on the flat iron surfaces. While this is highly unlikely to happen due to the low friction between the surfaces of hair and flat iron plates, even in the case of removal, only a fraction of protectant in direct contact with the flat iron will be removed. SEM/EDX analysis successfully verified the presence of protectant after 40 cycles of flat ironing.

4.2.2 Procedures

Table 4.1 lists the flat ironing conditions used for Asian hair. The experiments on the Asian hair had an emphasis on investigating the impact of a temperature setting when the combinations of gliding speed and number of passes all yield the consistent dwelling time. The dwelling time is defined as the total amount of time a flat iron is in direct contact with hair. Despite the consistent dwelling time, each combination will produce varying amounts of exposure time because of the difference in heat transfer behavior dependent on the two parameters. The design of experiments compares the effect of a temperature setting and exposure time to determine which is more significant.

Table 4.1. Flat ironing conditions for Asian hair.

Temperature (°C)	115	164	210
Gliding Speed (cm/s) x Number of Passes	1 x 1	3 x 3	5 x 5
Presence of Heat Protectant	Y		N

Table 4.2 shows the flat ironing conditions used for African hair. The experiment now decouples the specific combination of gliding speed and number of passes to test

all possible permutations. The design of experiments concentrates on the effect of interaction between the two parameters.

Table 4.2. Flat ironing conditions for African hair.

Temperature (C)	115	210
Gliding Speed (cm/s)	1	5
Number of Passes	1	5
Presence of Heat Protectant	Y	N

Asian hair went through 40 cycles of each flat ironing condition to damage hair enough to distinguish the difference between the conditions whereas African hair went through only 20 cycles to compensate for its inherently low fatigue strength [65]. All the samples were allowed 1 minute to cool down to an ambient temperature between cycles. This timing minimizes the difference in the potential recovery of mechanical strength through remoisturization reported previously even though a significant improvement required one day [7]. Fifty strands were preferentially selected from the middle section of swatches for the fatigue test by a Diastron (Dia-Stron CYC 801, Dia-Stron, UK) fatigue tester. These strands are more likely to have been in direct contact with a flat iron plate, and this selection minimizes the variation in test results.

The experiments for straightening efficacy and curl loss were performed on 25 single strands of African hair under the conditions listed in Table 4.2. When mounting each hair strand, the tension in it was carefully controlled using a load cell installed with the sample mount. The tension was maintained near zero to avoid the contribution to hair straightening. This set of experiments did not require multiple cycles of heating because there is no need to incur exaggerate degrees of damage for distinction between the results. Each strand went through a single cycle of heating, and the results must not be confused as those of 40 cycles.

4.3 Results and Discussion

Table 4.3 lists the results of the fatigue test and statistical analysis on Asian hair. The two conditions that only differ in the presence of a heat protectant were paired together to assess the effect of the protectant. The parameters are assigned with variables as follows: a temperature setting (T), gliding speed (V), number of passes (N), and the presence of a heat protectant (H). Some observations were omitted due to premature failure during the test. For the fatigue strength of hair, the log of the number of cycles to failure was reported. This was necessary to transform the data in a form that yields a Gaussian distribution to fulfill the basic assumptions of ANOVA. Then, p-values of the two-sample t-test between two conditions in each pair follow. A value of $\alpha = 0.05$ was consistently used as a cut-off for statistical significance; however, if the p-value is sufficiently small and close to 0.05, it was also considered statistically significant. The t-test evaluates if the presence of a heat protectant will yield a statistically significant difference to the metric in interest. The final columns show the results of the Tukey test. The Tukey test identifies statistically significant conditions among the others and group them together according to the given criteria of statistical significance. The conditions that belong to the same group, indicated by the same colored blocks, are statistically equivalent.

The results of the two-sample t-test indicate that the presence of a non-silicone containing heat protectant renders a statistically significant difference only if all the flat ironing parameters are at the highest values (Pair 9). Otherwise, the presence of a heat protectant has no effect on the fatigue strength of hair. The Tukey test indicates that the amounts of reduction in the fatigue strength inflicted by conditions at a high temperature setting of 210°C stand out from the others (Pairs 7, 8, and 9), and even more so by the conditions at a low gliding speed of 1 cm/s (Pair 7).

Table 4.4 shows the results of the fatigue test on African hair. The data are displayed in the same manner as the Asian hair. There are overall less number of observations for each condition because there were more incidents of premature

Table 4.3. Results of two-sample t-test and Tukey test on the fatigue strength of Asian hair to assess the effect of a non-silicone containing heat protectant.

Pair	Condition	T (C)	V (cm/s) x N	H	# of Fibers	log(# of Cycles to Failure)		Two Sample t-test	Tukey Test ($\alpha = 0.05$)						
						Mean	STD		A	B	C	D	E	F	G
1	A1	115	1x40	N	48	3.5	0.54	0.45							
	A10	115	1x40	Y	50	3.59	0.56								
2	A2	115	3x120	N	46	3.51	0.53	0.8							
	A11	115	3x120	Y	49	3.48	0.43								
3	A3	115	5x200	N	40	3.52	0.53	0.57							
	A12	115	5x200	Y	45	3.59	0.62								
4	A4	164	1x40	N	47	3.32	0.5	0.44							
	A13	164	1x40	Y	49	3.21	0.85								
5	A5	164	3x120	N	48	3.27	0.75	0.17							
	A14	164	3x120	Y	43	3.05	0.74								
6	A6	164	5x200	N	48	3.5	0.59	0.45							
	A15	164	5x200	Y	49	3.58	0.45								
7	A7	210	1x40	N	44	1.63	0.48	0.92							
	A16	210	1x40	Y	50	1.61	0.64								
8	A8	210	3x120	N	48	2.24	0.64	0.34							
	A17	210	3x120	Y	48	2.11	0.61								
9	A9	210	5x200	N	49	2.14	0.56	<0.0001							
	A18	210	5x200	Y	49	2.62	0.61								
10	Control	0	0x0	N	50	3.79	0.61	0.12							
	Protect	0	0x0	Y	48	3.6	0.62								

failure. There are also many outliers (38 observations) that seem to be additional premature failure that was not filtered out during the initial censorship. They were removed before the analysis as they seriously affected both the Gaussian distribution and the results of the analysis. However, the preserved number of observations is still abundant, and sound statistical analysis is viable.

The two-sample t-test indicates that the presence of a heat protectant significantly affects the fatigue strength of hair if the number of passes is 5 (Pairs 4, 6, and 8). The p-value of Pair 2 is larger than 0.05 but still quite close to it. Therefore, higher number of passes seems to be a premise for the heat protectant to have any protective effect on the fatigue strength of hair. Even though the exposure time, which is highly correlated with reduction in the fatigue strength (cite predictive modeling paper)

Table 4.4. Results of two-sample t-test and Tukey test on the fatigue strength of African hair to assess the effect of a silicone containing heat protectant.

Pair	Condition	T (C)	V (cm/s)	N	H	# of Fibers	log(SE+1)		Two Sample t-test	Tukey Test (α = 0.05)			
							Mean	STD		A	B	C	D
1	AA1	115	1	1	N	39	3.6	0.61	0.32				
	AA9	115	1	1	Y	44	3.47	0.54					
2	AA2	115	1	5	N	47	3.35	0.75	**0.09**				
	AA10	115	1	5	Y	43	3.58	0.53					
3	AA3	115	5	1	N	45	3.49	0.6	0.95				
	AA11	115	5	1	Y	45	3.5	0.41					
4	AA4	115	5	5	N	48	3.35	0.44	**0.03**				
	AA12	115	5	5	Y	46	3.6	0.65					
5	AA5	210	1	1	N	46	2.8	0.57	0.32				
	AA13	210	1	1	Y	42	2.92	0.46					
6	AA6	210	1	5	N	44	1.68	0.26	**0.001**				
	AA14	210	1	5	Y	44	1.91	0.36					
7	AA7	210	5	1	N	44	3.4	0.59	0.56				
	AA15	210	5	1	Y	41	3.49	0.68					
8	AA8	210	5	5	N	41	3.05	0.68	**0.004**				
	AA16	210	5	5	Y	42	3.43	0.44					
9	Protect	0	0	0	Y	45	3.39	0.61	0.13				
	Control	0	0	0	N	47	3.65	0.67					

According to the Tukey test, the conditions at a high temperature setting (210 °C) and a low gliding speed (1 cm/s) are prominently different from the others (Pairs 5 and 6). Between the two, the higher number of passes reduces the fatigue strength to a larger degree (Pair 6). The results of the Tukey test also indicate that considering the contributions of all the factors to the reduction of the fatigue strength, the presence of heat protectant will lose its significance in preservation of fatigue strength.

Another interesting discovery is the effect of heat protectant on the fatigue strength of hair when no flat ironing has occurred. Tables 3 and 4 present unexpectedly low p-values of 0.12 and 0.13 for the fatigue strength of Asian and African hair respectively. In both cases, remarkable reduction in the fatigue strength has occurred with the presence of heat protectant. This could well be caused by a happenstance and more data are necessary to confirm the phenomenon.

Based on the results of two-sample t-test, the presence of silicone in the formulation may potentially distinguish the effect between the two types of heat protectant because the non-silicone protectant had significant effect at 210 °C and 5 cm/s alone while the silicone protectant had significant effect across all temperatures and gliding speeds as long as the number of passes is high. Nevertheless, it is yet unclear if the reduction in fatigue strength occurred because of the silicone or because of the interaction between other ingredients in the protectant and the type of hair. Either testing the non-silicone protectant on African hair or the silicone protectant on Asian hair should follow to further validate the effect of silicone on the reduction of fatigue strength.

Lastly, even though the Tukey test on all the conditions renders statistically insignificant effect of the heat protectant except the special case of Pair 9 in Asian hair, the paired t-test indicates differences for conditions with a multiple number of passes. Thus, it is hasty to come to any conclusions about the heat protectant's benefits unless its impact on the other two metrics, straightening efficacy and permanent curl loss, is evaluated. The next three tables and their results will provide insights into this holistic approach.

Table 4.5 presents the results of statistical analysis on the straightening efficacy of African hair. The two-sample t-test indicates that the presence of a heat protectant significantly affects the straightening efficacy if flat ironing occurs 5 times at 210 °C and 1 cm/s (Pair 6). The p-value of Pair 5 is only 0.02 larger than 0.05 and can still be regarded quite significant. It is important to note that the direction of improvement is opposite in the two pairs. Lower log(SE+1) means better straightening efficacy. Thus, when flat ironed once, the heat protectant impedes straightening efficacy (Pair 5) whereas when flat ironed five times, the heat protectant improved straightening efficacy (Pair 6). The Tukey test shows that when all the conditions are evaluated simultaneously the presence of heat protectant loses it significance. However, while a temperature setting dominantly divides the straightening efficacy, the straightening efficacy of AA10 clearly stands out and AA2 and AA12 to a little lesser degree from the other conditions at the same temperature.

Table 4.5. Results of two-sample t-test and Tukey test on the straightening efficacy of flat ironing African hair to assess the effect of a silicone-containing heat protectant.

Pair	Condition	T (C)	V (cm/s)	N	H	# of Fibers	log(SE+1)		Two Sample t-test	Tukey Test (α = 0.05)					
							Mean	STD		A	B	C	D	E	F
1	AA1	115	1	1	N	25	-1	0.46	0.8						
	AA9	115	1	1	Y	25	-1.04	0.59							
2	AA2	115	1	5	N	24	-1.19	0.47	0.4						
	AA10	115	1	5	Y	25	-1.31	0.48							
3	AA3	115	5	1	N	25	-0.87	0.68	0.42						
	AA11	115	5	1	Y	25	-0.99	0.32							
4	AA4	115	5	5	N	25	-0.98	0.5	0.25						
	AA12	115	5	5	Y	25	-1.12	0.33							
5	AA5	210	1	1	N	25	-1.66	0.42	0.07						
	AA13	210	1	1	Y	25	-1.46	0.33							
6	AA6	210	1	5	N	25	-1.53	0.42	0.0377						
	AA14	210	1	5	Y	25	-1.78	0.41							
7	AA7	210	5	1	N	25	-1.48	0.46	0.82						
	AA15	210	5	1	Y	25	-1.45	0.33							
8	AA8	210	5	5	N	25	-1.64	0.36	0.4145						
	AA16	210	5	5	Y	25	-1.73	0.37							

Looking at the raw data, there is clear improvement in straightening efficacy, indeed to a larger degree, with the presence of heat protectant even when flat ironing occurs at 115°C (look at Pairs 2, 3, and 4). However, the statistical significance of such improvement is negated by high variability in the straightening results with the absence of heat protectant. This could be due to the varying sensitivity to heat insult that strands from different individuals manifest. Therefore, once controlled for the same subject hair sample, the improvement in straightening efficacy with the heat protectant at a low temperature may indeed be statistically significant.

The results are consistent in the test of the long-term straightening efficacy tabulated in Table 4.6 below. Again, the significance of the heat protectant is present only when the temperature setting is 210 °C and the gliding speed is 1 cm/s (Pairs 5 and 6); the direction of improvement is opposite, impeded when flat ironed once (Pair 5) and improve when flat ironed five times (Pair 6) with the presence of the heat protectant. Also noteworthy is the fewer number of groups and more distinct differentiation between the conditions at two temperature levels by the Tukey test. It is an indication of enhanced uniformity in the straightening effect across conditions after equilibration under constant humidity. AA10 consistently stands out from the other conditions at 115 °C. However, the other two conditions that also stood out to a lesser degree became insignificant. Instead AA1 became another significant condition in the long-term straightening efficacy.

Table 4.6. Results of two-sample t-test and Tukey test on the long-term straightening efficacy of flat ironing African hair to assess the effect of a silicone-containing heat protectant.

Pair	Condition	T (C)	V (cm/s)	N	H	# of Fibers	log(LTSE+1)		Two Sample t-test	Tukey Test ($\alpha = 0.05$)		
							Mean	STD		A	B	C
1	AA1	115	1	1	N	15	-0.71	0.41	0.75			
	AA9	115	1	1	Y	25	-0.65	0.62				
2	AA2	115	1	5	N	24	-0.65	0.46	0.49			
	AA10	115	1	5	Y	24	-0.74	0.45				
3	AA3	115	5	1	N	25	-0.49	0.51	0.3			
	AA11	115	5	1	Y	25	-0.63	0.39				
4	AA4	115	5	5	N	16	-0.41	0.41	0.24			
	AA12	115	5	5	Y	25	-0.57	0.4				
5	AA5	210	1	1	N	20	-1.43	0.45	**0.06**			
	AA13	210	1	1	Y	20	-1.19	0.34				
6	AA6	210	1	5	N	25	-1.16	0.48	**0.0023**			
	AA14	210	1	5	Y	25	-1.56	0.4				
7	AA7	210	5	1	N	25	-1.17	0.55	0.97			
	AA15	210	5	1	Y	25	-1.18	0.44				
8	AA8	210	5	5	N	20	-1.4	0.38	0.8445			
	AA16	210	5	5	Y	25	-1.37	0.53				

Lastly, Table 4.7 lists the results of statistical analysis on the permanent curl loss of African hair after flat ironing. The two-sample t-test indicates that the presence of heat protectant causes a significant difference in permanent curl loss when flat ironing occurs once at 210°C (Pairs 5 and 7). Once again, the opposite direction of influence is observed between the two pairs. The heat protectant preserves curls better if flat ironed at 1 cm/s (Pair 5) but promotes curl loss if flat ironed at 5 cm/s (Pair 7). The Tukey test indicates the grouping is predominantly influenced by a temperature setting. Yet, several conditions stand out. AA11 is relatively inferior in curl preservation compared with other conditions at 115°C. On the other hand, AA7 and AA13 are relatively superior in curl preservation compared with other conditions at 210°C.

Table 4.7. Results of two-sample t-test and Tukey test on the permanent curl loss of African hair due to flat ironing to assess the effect of a silicone-containing heat protectant.

Pair	Condition	T (C)	V (cm/s)	N	H	# of Fibers	log(PCLCD+1)		Two Sample t-test	Tukey Test ($\alpha = 0.05$)						
							F	G		A	B	C	D	E	F	G
1	AA1	115	1	1	N	22	-0.04	0.28	0.64							
	AA9	115	1	1	Y	25	0	0.29								
2	AA2	115	1	5	N	24	-0.06	0.23	0.27							
	AA10	115	1	5	Y	25	0.01	0.23								
3	AA3	115	5	1	N	25	-0.01	0.21	0.21							
	AA11	115	5	1	Y	25	0.07	0.23								
4	AA4	115	5	5	N	25	-0.07	0.26	0.29							
	AA12	115	5	5	Y	25	-0.01	0.15								
5	AA5	210	1	1	N	25	0.4	0.29	0.02							
	AA13	210	1	1	Y	25	0.19	0.33								
6	AA6	210	1	5	N	23	0.32	0.23	0.8207							
	AA14	210	1	5	Y	25	0.34	0.43								
7	AA7	210	5	1	N	25	0.14	0.24	0.08							
	AA15	210	5	1	Y	25	0.26	0.24								
8	AA8	210	5	5	N	25	0.24	0.28	0.954							
	AA16	210	5	5	Y	25	0.24	0.23								

Now that we have finished discussing the results of statistical analysis on all metrics of flat ironing results, the trade-offs between them can be more closely investigated to potentially identify optimal conditions for different hair care goals. To do so, the effect of every condition on the three metrics were carefully compared. In general, hair strength is quite well preserved as long as flat ironing does not occur at 210 °C at 1 cm/s. The trade-off between straightening efficacy and permanent curl loss is conspicuous. Any conditions at 210 °C will have excellent straightening efficacy but induce large permanent curl loss whereas any conditions at 115 °C will be less effective at straightening hair but best at preventing hair from permanent curl loss. It turns out that the straightening efficacy and permanent curl loss are the two most difficult flat ironing effects to reconcile. Introduction of a heat protectant further complicates the situation. While the presence of heat protectant seems to consistently improve the protection of hair strength if multiple strokes of flat ironing occurs, it can have inconsistent effects on straightening efficacy and permanent curl loss. Amid the various conditions, a number of them stand out. Several conditions at 115 °C result in moderate straightening efficacy and excellent preservation of both hair strength and the fatigue strength. These conditions include AA1, AA2, AA9, and AA10 among which AA10 yields the best overall results with the highest fatigue strength and immediate and long-term straightening efficacy with a slightly less curl preservation. It yields a significantly better fatigue strength compared with its pair AA2 which has no heat protectant coating. The next condition of interest is AA7; it yields good straightening efficacy and moderate curl preservation with good preservation of fatigue strength. Compared with its pair AA15 which has protectant coating, it yields significantly better curl preservation with no difference in the fatigue strength. Another condition that stands out is AA16. It yields excellent straightening efficacy, good preservation of the fatigue strength, and moderate preservation of natural curls. Compared with its pair AA8 which has no protectant coating, it yields significantly better fatigue strength according to the t-test. If the straightening efficacy is the absolute goal, one can flat iron under condition AA-14 at the great expense of hair strength and natural curls. Its pair AA6 which has no protectant coating yields significantly lower fatigue strength and straightening efficacy according to the t-test. Based on these findings, we can construct a diagram that reflects the trade-offs between the three metrics. The diagram can be further associated with corresponding hair care goals and act as a guideline for the judicious use of flat irons among the users as shown in Figure 4.1.

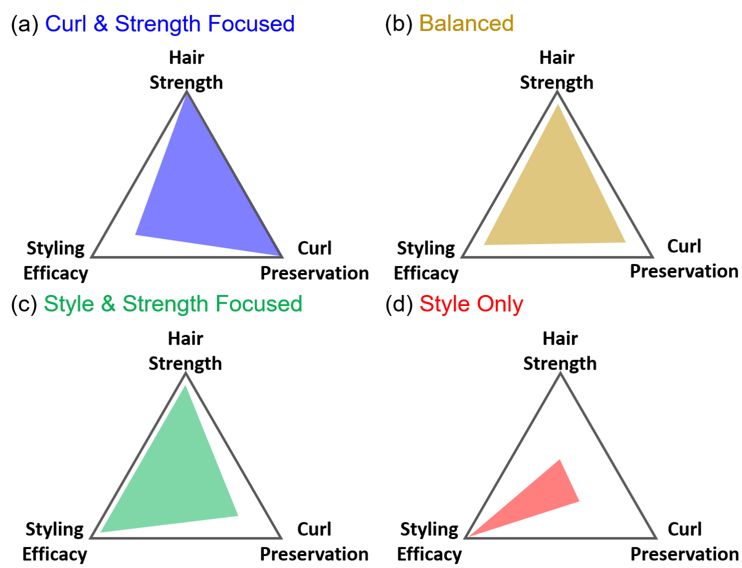

Figure 4.1. Visual representation of tradeoffs between flat ironing effects for different hair styling goals: (a) flat iron at 115 °C at 1 cm/s for moderate straightening and excellent preservation of both hair strength and natural curls; apply a heat protectant and flat iron 5 times for the best result in straightening; (b) flat iron once at 210 °C at 5 cm/s without the heat protectant for good preservation of the fatigue strength and moderate curl preservation and straightening efficacy; (c) flat iron 5 times at 210 °C at 5 cm/s with the heat protectant for slight curl preservation and for both great straightening efficacy and preservation of strength; and (d) flat iron 5 times at 210 °C at 1 cm/s for the best straightening results at the expense of both hair strength and natural curls.

There are caveats to consider when utilizing the guidelines and interpreting the presented data. First, the results of the fatigue strength are based on 20 cycles of flat ironing while those of the straightening efficacy and permanent curl loss are based on only one cycle. Therefore, the results of the straightening efficacy and permanent curl loss may greatly differ from what is presented above. They are expected to be larger in magnitude, and more significant statistical differences may appear between the conditions. Secondly, the effect of the heat protectant assessed in this work is in fact a combined contribution of multiple ingredients that participate simultaneously during the flat ironing process. The study was initially set out with the assumption that the presence of silicone in the formulation would make a difference in how hair responds to heat application, but this may not be the case. For example, PVP and hydrolyzed protein in the formulation of the heat protectant used were reported to have protective effect against heat [4].

Part 2: Thermal Characterization of Hair and Heat Transfer Modeling of Flat Ironing

The high correlation between the exposure time and the reduction in fatigue strength of hair makes the investigation into a technique which can predict the exposure time under flat ironing conditions with high accuracy attractive. In light of this, I propose to construct a heat transfer model between a flat iron and hair to simulate the exposure time. In the first half of Part 2, a discussion on a thermal characterizaion technique is covered to input accurate parameters into the model to be developed. Then, in the second half, a discussion on the modeling technique as well as its experimental validation will follow.

5. THERMAL CHARACTERIZATION OF HAIR

In this chapter, I will introduce Angstrom's method as a means to measure thermal diffusivity of different types of hair to precede a subsequent heat transfer modeling between hair and a flat iron. Theoretical and technical backgrounds of the Angstrom's method will be introduced. Then, detailed descriptions of experimental equipment, procedures, and results will follow.

5.1 Relevant Literature on Thermal Properties of Hair

Studies on thermal properties of hair from a traditional heat transfer perspective are almost non-existent except a few. Pires-Oliveira et al. [94] measured the specific heat capacity of virgin and bleached hair fibers . Liu et al. [95] measured the specific heat of an Asian hair fiber. However, each of them only reported a single data point.

Hou et al. [96] measured thermal diffusivity of human hair by using a technique based on optical heating and electrical thermal sensing (OHETS). The reported values for two samples from a 25-year old male graduate student were 1.94 mm^2/s and 4.13 mm^2/s. 3 years later, Mendioroz et al. [97] developed a measurement technique based on lock-in thermography with laser heating and infrared sensing, finding a diffusivity of 0.14 $mm^2 s^{-1}$. In the following year, Salazar et al. [98] reported a similar result. Most recently, Liu et al. [95] measured the thermal diffusivity to be 0.142 mm^2/s. In summary, the order of magnitude of the thermal diffusivity of human hair is same order or 0.1 mm^2/s, which is the magnitude as a vast majority of polymers.

5.2 Angstrom's Method

To measure thermal diffusivity of hair, we modify a transient method known as Angstrom's method, which was first introduced by a Swedish physicist Anders Jonas Angstrom in 1863 [99], using high-resolution thermal imaging to measure the temperature response to a periodic heat source.

The thermal diffusivity (α) is a parameter which captures the effect of three material properties: thermal conductivity (k), specific heat capacity (c_p), and density (ρ) (Equation (5.1)). In short, the thermal diffusivity indicates how well heat spreads through material.

$$\alpha = \frac{k}{c_p \rho} \tag{5.1}$$

In this method, one end of a sample is periodically heated by a heat source (see Figure 5.1). As the heat propagates from one end to the other, the amplitude of the temperature oscillations diminishes and the phase delay increases. These two parameters are combined to calculate thermal diffusivity as shown in Equation (5.2).

$$\alpha = \frac{\pi f (x_2 - x_1)^2}{(\phi(x_2) - \phi(x_1)) ln \frac{A(x_1)}{A(x_2)}} \tag{5.2}$$

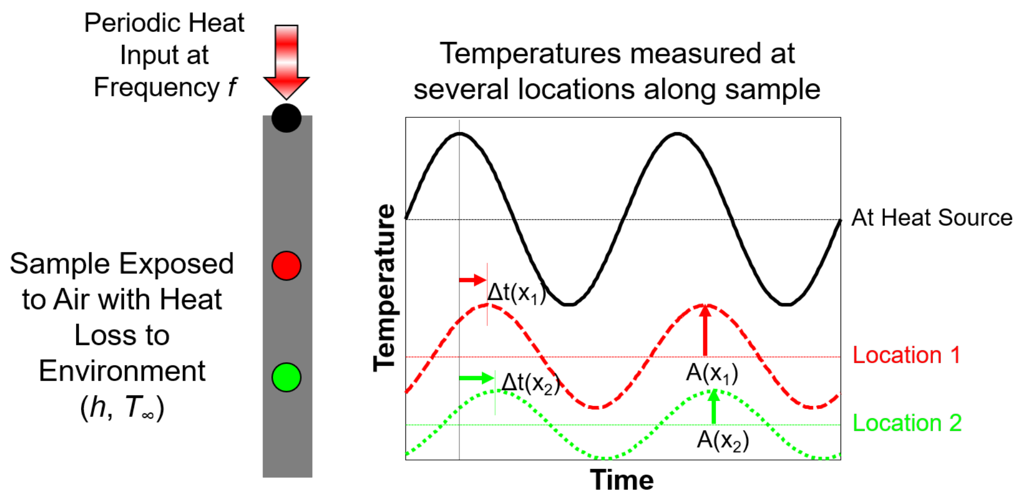

Figure 5.1. Illustration of the basic principle of the Angstroms method. Periodic heating (sinusoidal in the example) is applied to one end of the sample indicated by a block dot. The heat propagates through the red and greed dots, diminishing in its amplitude and lagging in its phase as shown in the graph to the right. These differences are empirically captured to calculate thermal diffusivity of the material in test.

A MATLAB program was written to process the acquired data to calculate the generate plots as shown in Figure 5.2 where the slope is related to the thermal diffusivity of the material. More detailed descriptions of the theory and technical procedures will be covered in the sections to follow.

Angstrom's method is a theoretically robust method widely applied to a variety of materials of various shapes [99–111]. Measurement of highly conductive materials such as copper bar, brass, and quartz repeatedly demonstrated reasonable accuracy [99, 100, 104, 105, 110, 111]. On the other hand, measurement of poorly conducting materials such as a silica rod, polyethylene sheets, and various dental filling materials have also been successfully measured [100, 101, 106]. In particular, past measurements of thermal diffusivity of polymers by Angstrom's method are in good agreement with those measured by a laser flash method and hot wire method [107].

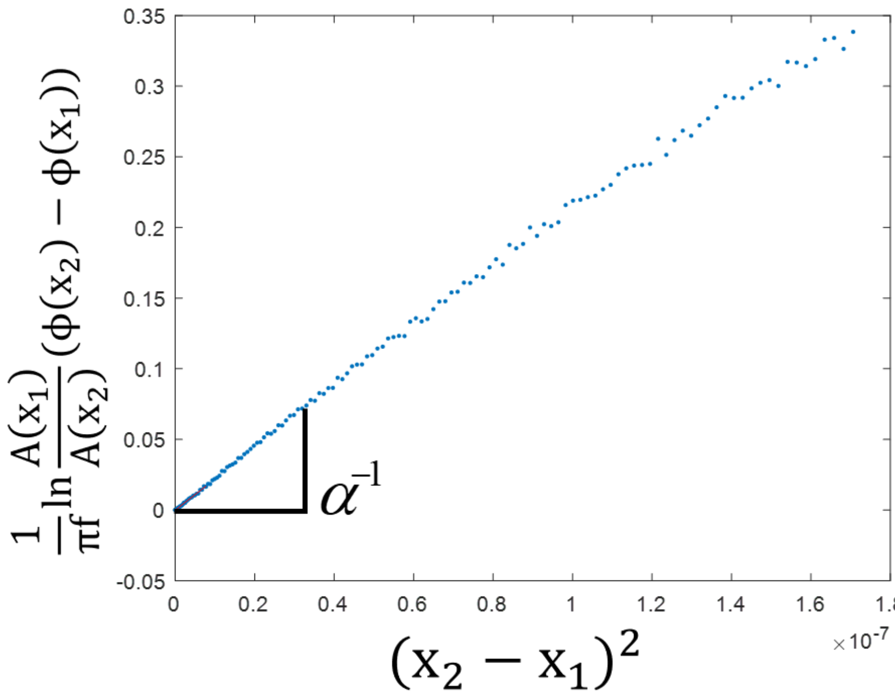

Figure 5.2. A plot generated with a MATLAB program, whose slope represents an inverse of thermal diffusivity of the material.

Angstrom's method was chosen for the following reasons. First, the analysis is simplified by assuming 1D heat transfer. Since the diameter of hair fibers to be measured is in the range of tens of microns, a simple 1D assumption is plausible. Second, the method is robust in measuring thermal diffusivity. The linear heat loss term, which lumps both convection and radiation effects, becomes irrelevant in calculating thermal diffusivity.

A brief overview on the theoretical foundation of Angstrom's method follows in the next section to deepen the understanding of the method.

5.2.1 Theory behind the Angstrom's Method

The following derivation follows that of previous papers [104, 105, 110]. Heat transfer in the system can be modified as 1D conduction with a linear heat loss term:

$$\frac{\partial^2 T}{\partial x^2} - \frac{1}{\alpha}\frac{\partial T}{\partial t} - \frac{PR}{kA}(T - T_0) = 0. \tag{5.3}$$

where T is the temperature [K], x is the location along the length of the hair fiber [m], α is the thermal diffusivity [m^2/s], t is the time [s], P is the perimeter of the fiber [m], R is the heat loss coefficient that combines conduction, convection, and (linearized) radiation losses through a surrounding medium, k is the thermal conductivity [W/(mK)], A is the cross-sectional area of the fiber [m^2], and T_0 is the ambient temperature. We can define $T - T_0$ as τ.

Since a periodic heat wave will be applied to the sample at a fixed frequency $f(=\frac{\omega}{2\pi})$ [Hz], the solution can be expressed as

$$\tau(x,t) = \sum_{n=1}^{\infty} C_n(x)e^{in\omega t} \tag{5.4}$$

where $C_n(x)$ is an expression for the initial temperature profile along the fiber, and $e^{in\omega t}$ describes the development of the temperature profile over time.

Substituting the Equation (5.4) into Equation (5.3) results in the following differential equation:

$$\sum \left(\frac{\partial^2 C_n}{\partial x^2} - C_n\frac{PR}{kA} - C_n\frac{in\omega}{\alpha}) \right) e^{in\omega t} = 0, \tag{5.5}$$

which leads to the following second-order differential equation

$$\frac{\partial^2 C_n}{\partial x^2} - C_n(\frac{PR}{kA} + \frac{in\omega}{\alpha}) = 0. \tag{5.6}$$

The solution of this equation is:

$$C_n(x) = C_{0n}{}^{-\sqrt{\lambda_n}x}, \tag{5.7}$$

where

$$\lambda_n = \frac{R + in\omega}{\alpha}. \tag{5.8}$$

The square root of λ_n is complex because λ_n is a complex number:

$$\sqrt{\lambda_n} = a_n + ib_n. \tag{5.9}$$

Therefore, by equating λ_n (Equation (5.8)) on one side and square of $\sqrt{\lambda_n}$ (Equation (5.9)) on the other, the following equations emerge:

$${a_n}^2 - {b_n}^2 = \frac{R}{\alpha} \tag{5.10}$$

and

$$2a_n b_n = \frac{\omega}{\alpha}. \tag{5.11}$$

Now, the heat loss term R is not present in Equation (5.11), and thus thermal diffusivity α can be calculated by empirically measuring a_n and b_n. Determination of a_n and b_n requires comparing the amplitude and phase difference of temperature at a minimum of two points. Since experimentally, I apply a square heat wave to a heating wire which in turn applies a heat wave to the hair fiber, a Fourier transform is used to decompose the measured temperature wave in each harmonic for the analysis. Thus, the following equations contains subscript n to describe the amplitude and phase change observed at different harmonics. Then, the equation of the temperature response is

$$\tau(x,t) = \sum_{n=1}^{\infty} A_n e^{i(n\omega t - b_n x)}, \tag{5.12}$$

where $A_n = C_{0n} e^{-a_n x}$. By observing the amplitude and phase difference at point 1 and 2, one can deduce the following relationships:

$$\frac{A_n(x_1)}{A_n(x_2)} = e^{-a_n(x_1 - x_2)} \tag{5.13}$$

and

$$\phi_n(x_2) - \phi_n(x_1) = b_n(x_2 - x_1), \tag{5.14}$$

which can be rearranged, respectively, as follows:

$$a_n = \frac{ln(\frac{A_n(x_1)}{A_n(x_2)})}{x_2 - x_1} \tag{5.15}$$

and

$$b_n = \frac{\phi_n(x_2) - \phi_n(x_1)}{x_2 - x_1}. \tag{5.16}$$

Finally, substituting Equations (5.15) and (5.16) into Equation (5.11) and rearranging give the following expression for thermal diffusivity α:

$$\alpha = \frac{n\omega(x_2 - x_1)^2}{2(\phi_n(x_2) - \phi_n(x_1))ln\frac{A_n(x_1)}{A_n(x_2)}}. \tag{5.17}$$

By re-arranging the equations derived above, one can derive the following equation that enables determination of thermal diffusivity:

$$\frac{1}{\pi f}ln\frac{A_n(x_1)}{A_n(x_2)}(\phi_n(x_2) - \phi_n(x_1)) = \frac{1}{\alpha}(x_2 - x_1)^2. \tag{5.18}$$

Experimentally, the amplitude and phase data is extracted from the thermal imaging data and plotted in the form shown in Figure 5.2, where the diffusivity is computed from the slope ($slope = \frac{1}{\alpha}$).

5.2.2 Technical Considerations of the Angstrom's Method

Despite its theoretical robustness against heat loss through to convection and radiation, measurement of a thin wire was found to be largely influenced in a fluid environment [102]. Measurement of carbon fibers [103], thin polymer films [109] and thin copper and graphite sheets [110] was performed in a vacuum to enhance the accuracy except the case of carbon nanotube buckypapers [108]. According to other literature that used the "slope method" which is essentially based on the principle of Angstrom's method, placing samples in a vacuum chamber largely improved the accuracy of measurement [112]. Furthermore, the existing papers on thermal diffusivity of human hair used a vacuum chamber with the aforementioned slope method [97, 98]. Another study on thermal diffusivity of human hair also utilized a vacuum chamber even though it did not use neither the Angstrom's method nor the slope method [95]. Such practices raise questions about theoretical robustness against empirical results. In fact, Angstrom's method is known to account for forced convection and radiation but not natural convection and conduction through fluids [102].

In any measurement of thermal properties of materials, precluding any unnecessary modes of heat transfer is desirable as it minimizes uncertainty in the measurement. Thus, all the measurements were performed in a vacuum environment. In fact, as will be briefly introduced in the chapter, measurement in the air turned out to largely deviate from the vacuum results.

Consideration of diffusion length and ensuing selection of the appropriate frequency and amperage of supplied current deserve a separate and careful examination. It is important because of the theory assumes the sample to be semi-infinitely long to simplify the solution. If the frequency is too low or the amplitude is too high, the heat has insufficient time to dissipate to the enviroment and reaches the boundary, leading to violation of the assumptions. The participation of the boundary conditions lead to inaccurate meausrements as was well demonstrated in the past [100]. Because of this, the length of the sample has to be carefully selected so that the boundary conditions of the sample do not affect the heat transfer. If the length of the sample is limited by the configuration of the experimental setup, the frequency and magnitude of the supplied heating need fine tuning to avoid the interference of the boundaries. In the given context, it directly translates to careful selection of frequency and amperage of a periodic current supplied through the heating wire. The diffusion length is a good estimate to determine the appropriate frequency and power level of periodic heating.

The condition for diffusion length to acheive accruate measurement can be expressed as below [110].

$$L_{sample} \gg \sqrt{\frac{\alpha}{2\omega}} = L_{th} \tag{5.19}$$

Avoiding the violation of 1D assumption is another issue that deserves careful consideration. This has an especially important implication for the experimental setup introduced in this study. As it will be shown later, the periodic heating is applied to a sample by using a resistance heating wire. Both the sample and the heating wire have a cylindrical shape, and the sample is installed perpendicularly on top of the heating wire while maintaining the direct contact with it. Thus, the heat transfer that occurs from the heating wire to the sample is 3 dimensional instead being 1 dimensional. However, since the thickness of the sample is very small that it is safe to assume the heat transfer along the length of the sample past a certain point away from the contacting point is 1 dimensional. This point is also analytically confirmed using a COMSOL simulation of the Angstrom's method. The simulation indicated that the heat transfer along the sample becomes one dimensional within a few hundreds nanometers. This is much smaller than both the length of the sample and the area of view observable by the IR camera used to measure the change in temperature. Also, the amplitude of the temperature in the region near the heating wire exhibits a characteristic peak that rapidly decays. Thus, it is relatively easy to suitable region to select when the calculation of thermal diffusivity is performed using the MATLAB code. This point will be reiterated when the discussion on detailed post-processing appears later in the chapter.

In this work, the Angstrom's method with an infrared (IR) camera as a sensor is introduced as a new measurement technique to measure thermal diffusivity of films and wires with the thickness of a few hundred microns. The proposed method improves the traditional Angstrom's measurement in three aspects. First, the traditional Angstrom's method recorded magnitude and phase change of temperature at two locations [99, 102–105, 107, 109, 110]. This greatly reduces the sight of the phenomenon with limited information of temperature change at two locations. There is no way to detect any anomalies in heat transfer caused by boundary conditions or possible variation in thermal diffusivity along the length of the sample. Use of an IR camera can overcome such limitations by capturing continuous temperature profiles within its area of view. Secondly, the use of an IR camera allows non-contact measurement of temperature. It is required because the microscale samples are sensitive to the heat loss through attached sensors such as thermocouples. It also obviates the need for considering the appropriate spacing between sensors [100]. Lastly, a previous study that utilized IR sensors were limited in reaching a high-level vacuum because of the internal placement of the sensors [110]. However, our method overcomes this limitation by using the external sensor that observes samples through an IR-transparent calcium fluoride (CaF2) window and enables measurement at a higher vacuum level which further minimizes heat loss through convection and increases the measurement accuracy.

5.3 Measurement

In this section, experimental equipment, treatment of samples, and experimental procedures are discussed.

5.3.1 Equipment

The experimental equipment consists of the InfraScope, an IR microscope (MWIR-1024, Quantum Focus Instruments Corporation), a vacuum pump (Turbo-V 81-AG, Varian), a modified sample stage (TS1500, Linkam), a function generator (33120A, Hewlett-Packard), and a power supply (KE2420, Keithley).

The InfraScope measures the change in temperature and records thermal videos. It is an infrared imaging device that offers image resolution of 0.5859 µm/pixel, 2.9297 µm/pixel and 11.7188 µm/pixel depending on the lens configuration (1X, 4X, and 20X magnifications) and 0.1 K temperature resolution (Figure 5.3). The area of view is 144 mm^2, 9 mm^2 and 0.36 mm^2 for 1X, 4X, and 20X magnifications, respectively. For the entire measurements in this work, 4X magnification was used.

Figure 5.3. The InfraScope is an infrared imaging device that offers image resolution ranging from 0.5859 µm/pixel to 11.7188 µm/pixel depending on the lens configuration and 0.1 K temperature resolution.

To conduct the measurement in a vacuum, the TS1500 thermal stage from Linkam was modified to fit a custom-made sample mount. The sample mount is composed of a heating wire, clamps to hold it, and a scaffold to fit it on the existing heating element in the TS1500 (Figure 5.4). As shown in Figure 5.4 (a), a sample is gently pulled taut and placed perpendicularly on top of the heating wire to let heat propagate in both ways from the contact point. The scaffold was 3D printed with the MakerBot's Replicator 2X, using acrylonitrile butadiene styrene (ABS) as a material. The top of the scaffold was oriented downwards and printed without a raft to allow printing of a clean and flat surface. The clamps for holding the heating wire were salvaged from terminal blocks for electrical connection. The sample mount is placed on the esxisting heating element inside the TS1500 stage.

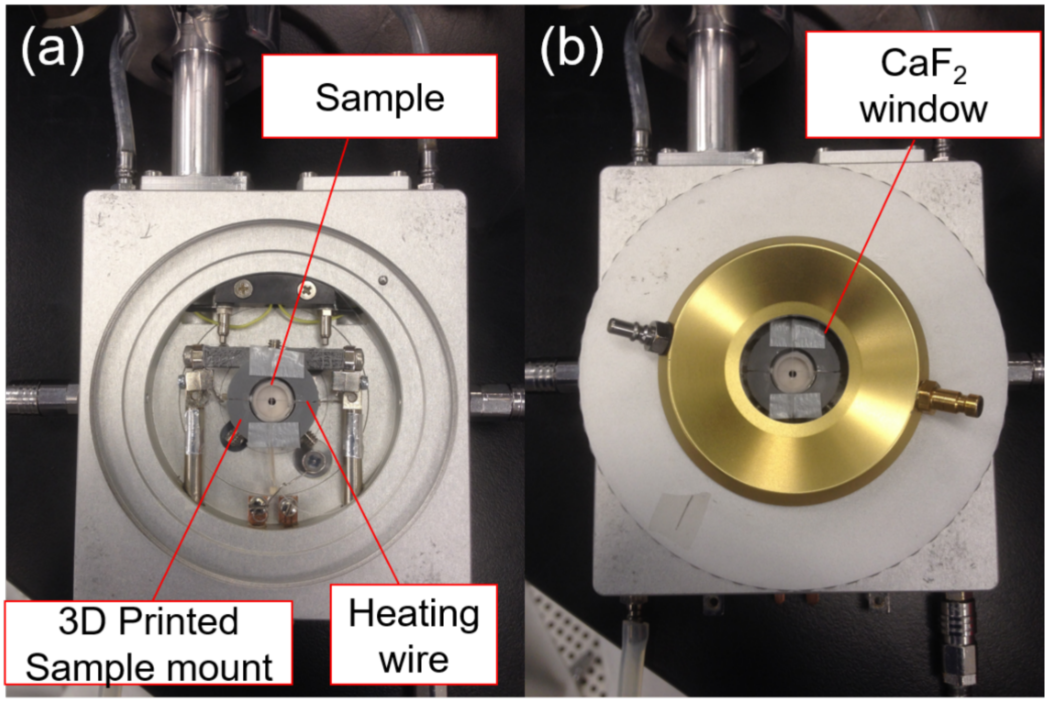

Figure 5.4. (a) A 3D printed sample mount on top of which hair is placed is installed inside a TS1500 vacuum statge. (b) The window is made of calcium fluoride to allow radiation within the necessary wavelengths for the InfraScope to register.

Before taking the measurement, a lid with a small window is placed as shown in Figure 5.4 (b) to seal the environment for vacuum pumping. A calcium fluoride window was used to allow mid-wavelength infrared, which InfraScope utilizes for measurement, to transmit.

Figure 5.5 (a) shows the schematic of the experimental setup. The chromium resistance heating wire (Omega Engineering) on the sample mount (Figure 5.4) applies periodic heating to a sample. The wire is an alloy composed of 80 % nickel and 20 % chromium. Each end of it connects to the two poles inside which extend outside and connect to a power supply. Between one of the poles and the connection from the source meter is a relay (Tyco Electronics) which switches on and off following the

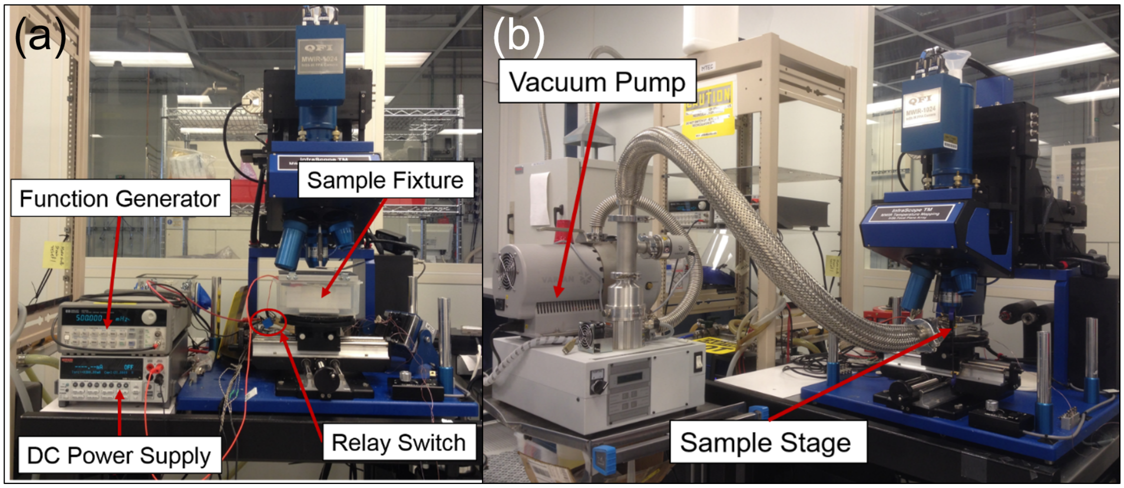

Figure 5.5. (a) The overall experimental setup for air measurement is shown with all equipment labeled. (b) Experimental setup for vacuum measurement.

square wave signal from a function generator. The resultant periodic heating is not of a sinusoidal form by nature of this mechanism, and therefore, is decomposed through Fourier transform for selective analysis on the first harmonic. The vacuum pump (Figure 5.5 (b)) removed the air from the sample stage. The pump can easily achieve a vacuum level of 10^{-5} mbar and can go further down if sufficient time is allowed.

Additionally, to investigate the effect of humidity on hair thermal diffusivity, a humidity chamber with a capacity to maintain a relative humidity level constant was built (Figure 5.6). The chamber consists of two floors. On the lower floor, salt solutions are placed; on the upper floor is a sample mount with hair sample (Figure 5.7). When placed in a sealed space, salt solutions have capacity to maintain a humidity level of the space at a certain level, depending on the type of the salt. To ensure that humidity maintenance is functional, a humidity sensor (OM-THA2, Omega Engineering) was installed. To validate the performance of the chamber, test with four salts was performed, and the results are shown in Table 5.1. Due to the leakage in the chamber, the achievable humidity level ranged from approximately 31 %RH to 83 %RH. 65 %RH is typically considered ambient condition [3, 5, 6, 20] and anywhere below 40 %RH is usually considered dry [6, 20, 113] and above 80 %RH humid. Thus, it is a reasonable range to simulate two extreme cases. With the help of this chamber, one can observe the impact of moisture content in a hair fiber on its measured thermal diffusivity.

Figure 5.6. An image of the humidity chamber constructed to vary the humidity level that the hair is exposed to and observe its effect on thermal diffusivity measurement.

5.3.2 Samples

Samples include several polymer films and monofilaments with relatively well studied properties for validation of measurement accuracy. These include monofilaments of polyether ether ketone (PEEK) and polyvinylidene fluoride (PVDF), films of PEEK,

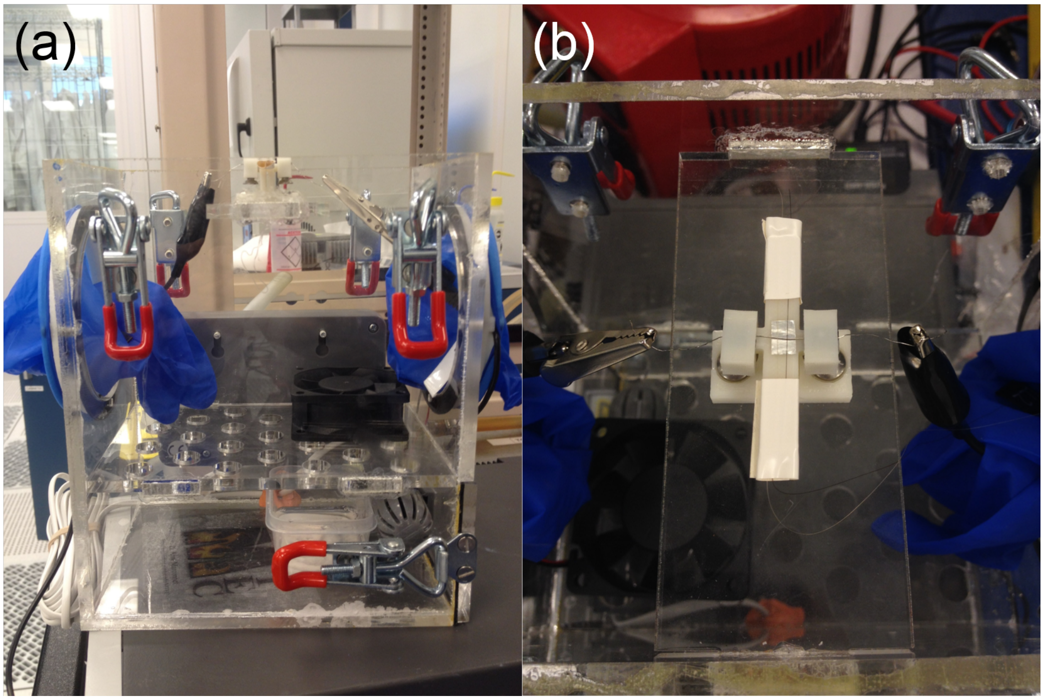

Figure 5.7. (a) The humidity chamber has two floors; on the lower floor is a container with a salt solution; at the bottom of the upper floor is a fan to help evaporate water from the salt solution and at the top is a sample mount. (b) Hair sample is mounted perpendicularly to the heating wire in direct contact beneath it on a sample mount.

Table 5.1. Expected and actual humidity levels achieved by four salts in the humidity chamber.

Salt	Expected Humidity (%RH) [114]	Actual Humidity (%RH)
Lithium Bromide (LiBr)	6.61 ± 0.58	30∼32
Potassium Acetate ($KC_2H_3O_2$)	23.11 ± 0.25	40∼42
Sodium Chloride (NaCl)	75.47 ± 0.14	70∼72
Potassium Chloride (KCl)	85.11 ± 0.29	79∼83

and a gum rubber sheet. After the validation process, three types of human hair (African, Asian, and Caucasian) were measured. All the hair samples were gently washed with tap water using a clarifying shampoo to remove remnant oil and dirt from the surfaces.

5.3.3 Experimental Procedures

The experimental procedures will be elaborated in two parts to facilitate reproduction of the work in the future. The first part provides a detailed, step-by-step measurement procedure. The second part dedicates itself to detailed description of data analysis using the MATLAB program.

Validation of Measurement Accuracy in a Vacuum: Validation of measurement accuracy was performed using the polymer samples in a vacuum environment. To start the measurement, the InfraScope first has to be prepared. It requires liquid nitrogen to maintain the temperature of the camera at around 78 K. While waiting for the camera to reach the desired temperature, the sample stage is placed under the scope, connected to a vacuum pump, and the air is drawn out until the vacuum level reaches approximately 5×10^{-7} bar. Then, the focus of the sample is acquired by adjusting the height of the lens, and a reference image is acquired. The crucial component of infrared imaging is accurate measurement of emissivity. This is usually done by elevating the temperature of the whole sample with precisely controlled thermal stage to eliminate the effects of irradiation from the surroundings reflected by the sample, which may disturb the measurement [115]. However, in this experimental setup the sample cannot be heated since the modified TS1500 replaces the thermal stage. There are two approaches to take care of this problem. One is to measure emissivity of the samples the accurately controlled thermal stage at an elevated temperature before the measurement and apply constant emissivity to the whole observed image. The other is to take the emissivity map of the sample in the TS1500 sample stage at an ambient temperature. Both approaches have their share of uncertainty and were first tried before establishing the final experimental procedure. At the end, the second approach was utilized throughout the whole experiments. Its validity will be justified with both experimental and simulation results in the next section on the results of the measurement.

After the initial setup, the periodic heating is applied to the sample. It requires time for the temperature oscillation to settle at a steady state where gradual increase in the mean temperature disappears. This depends on the size and properties of the sample and has to be established empirically. Once the temperature oscillation reaches a steady sate, the InfraScope can record and save the movie files. Also, note that adequate frequency and amperage levels have to be carefully chosen for accurate measurement using the diffusion depth as was discussed in Section 5.2.2.

Additionally, to calculate the thermal conductivity from the thermal diffusivity, the specific heat capacity is measured using DSC following the procedure specified in ASTM E1269, and the density is measured with a pycnometer.

Measurement of Hair in a Vacuum: After validating the accuracy of the measurement technique, measurement of hair thermal diffusivity followed. The differences in morphology and mechanical properties of hair across types and the individual variability across the fibers of the same type suggest potential difference in thermal diffusivity across these factors as well. Moreover, different locations on an individual fiber possess different levels of mechanical, chemical, and thermal histories. In light of these observations, it is viable to hypothesize that there are three factors that affect thermal diffusivity of hair: hair type, individual fibers of the same hair type, and locations on the same hair fiber (Figure 5.8). To validate this hypotheses, an experiment was designed as shown in the table below. The experimental procedure is equivalent to that introduced in the previous section.

Equation (5.20) illustrates a statistical model used for the ANOVA where the subscripts indicate the level of each factor, and the parentheses indicate which factors are nested in the other factors.

$$T_i + F_{(i)j} + S_{(j)k} + \varepsilon_{(ij)k} \tag{5.20}$$

where

T = Hair type

F = Fiber

S = Section

H = Humidity

i, j, k, l = Level of each factor

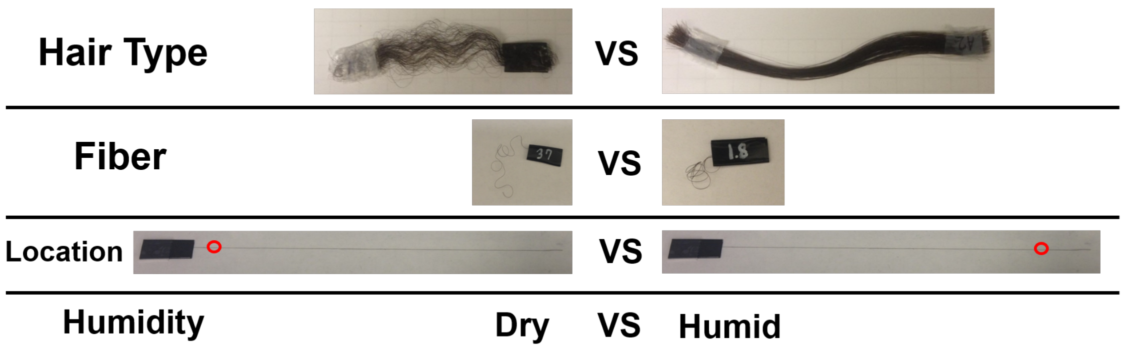

Figure 5.8. Four factors that may influence thermal diffusivity of hair. The first three factors were used to take measurements in a vacuum, and the humidity level included to take the measurement in the humid air.

Table 5.2. Design of experiment for assessing the effect of three factors on thermal diffusivity of hair: hair type, fiber, and section.

Type	Asian		African		Caucasian
Fiber	1	2	3	4	5
Section	Root			Tip	

Since the fiber is nested under hair type, fiber 1 in hair type 1 and fiber 1 in hair type 2 are unrelated, and hence no interaction term exists between fiber and hair type. Likewise, root in fiber 1 and root in fiber 2 are unrelated and no interaction terms exist resulting in leaving only main effects in the model. Fiber is treated as a random factor as a fiber is randomly drawn from numerous fibers of the same hair type.

Measurement in the Humid Air: In addition to the three factors mentioned in the previous section, hair is well-known for its sensitivity to humid environment, which causes frizz on a particularly humid day. Not only does it disrupt the well-groomed hair shape but also its mechanical properties [8, 49, 81]. More importantly, under the ambient condition, hair can absorb about 12 wt% of moisture, which will affect the effective thermal properties of hair. Thus, it is reasonable to hypothesize that the moisture content, in other words, the relative humidity to which hair is exposed, can affect its thermal diffusivity.

Since control of the humidity level is infeasible during the operation of a vacuum pump, the humidity chamber introduced in Section 5.3.1 was used for the measurement. However, due to the participation of the moist air and the natural convection, the measurement accuracy is expected to be unreliable. Thus, the results of the experiment will be used only to evaluate the effect of the humidity and the three previously discussed factors. Table 5.3 shows the design of experiment. After collecting data, a statistical analysis that assumes fiber as a random effect nested under hair type, and section and humidity as fixed effects was performed.

Table 5.3. Design of experiment for testing statistical significance of four factors hair type, fiber, section, and humidity level on Caucasian and African hair.

Type	Caucasian			African
	Virgin	Bleached	Low-Lifted	
Fiber	1		2	
Section	Root		Tip	
Humidity	31%RH		83%RH	

Equation (5.21) illustrates a statistical model used for the ANOVA.

$$T_i + F_{(i)j} + S_{(j)k} + H_l + (T \times H)_{il} + (F \times H)_{jl} + (S \times H)_{kl} + \varepsilon_{(ij)kl} \tag{5.21}$$

where

T = Hair type

F = Fiber

S = Section

H = Humidity

i, j, k, l = Level of each factor

Since fiber is nested under hair type, fiber 1 in hair type 1 and fiber 1 in hair type 2 are unrelated, and hence no interaction term exists between fiber and hair type. Likewise, root in fiber 1 and root in fiber 2 are unrelated and no interaction terms exist. Only interaction terms exist between a humidity level and each of the three factors. Fiber is treated as a random factor as a fiber is randomly drawn from numerous fibers of the same hair type.

Data Analysis: A MATLAB program was developed to process and analyze the movie files. The program reads in the temperature and time data to a matrix and process it through Fourier transform to select the component of the thermal signal at the fundamental frequency (the frequency of the square periodic heating wave generated by the function generator in this case). Then, magnitude and phase difference are then plotted along the length of a fiber. After specifying the reference point to be used as x_o in Equation (5.18), the program calculates thermal diffusivity using the same equation.

As the heat source is located at the center of the sample, thermal diffusivity can be measured in two directions. If the sample is in good contact with the heating wire, the magnitude and phase difference plots show a symmetrical shape as shown in Figure 5.9. The red dashed line indicates the location where the sample is in direct contact with the heating wire. There is a peak at the contacting point, and both magnitude and phase decay exponentially until it reaches the locations indicated by the green dashed lines. Calculation of thermal diffusivity within the region enclosed by the green lines is inaccurate because there is 2D effect which violates the 1D assumption. Thus, the calculation was done outside this region for all the measurements presented in this work.

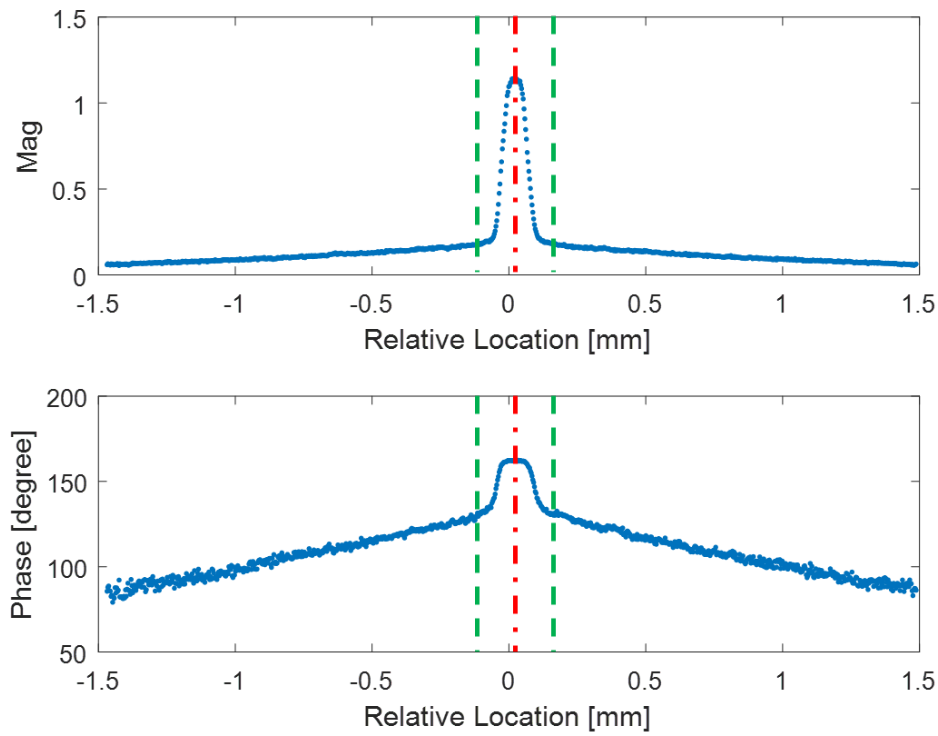

Figure 5.9. Magnitude and phase when good contact between a sample and the heating wire is established. Both plots display excellent symmetry. The red dashed line indicates the location where the sample is in direct contact with the heating wire. There is a peak at the contacting point, and both magnitude and phase decay exponentially until it reaches the locations indicated by the green dashed lines. Calculation of thermal diffusivity within the region enclosed by the green lines is inaccurate because there is 2D effect which violates the 1D assumption. Thus, the calculation was done outside this region for all the measurements presented in this work.

The average of the thermal diffusivities in both directions were obtained. Then, to minimize the inconsistency inherent in manual selection when choosing a region on the sample for diffusivity calculation, the program automatically selects a region of specified number of pixels and sweeps through the whole region by shifting the region by one pixel at a time. This way, one can easily observe any abnormal behavior in thermal diffusivity along the length of the sample and more reliably choose a region for accurate acquisition of a thermal diffusivity value. Figure 5.10 illustrates how the slope of the plot is fitted to calculate thermal diffusivity in different regions at each iteration.

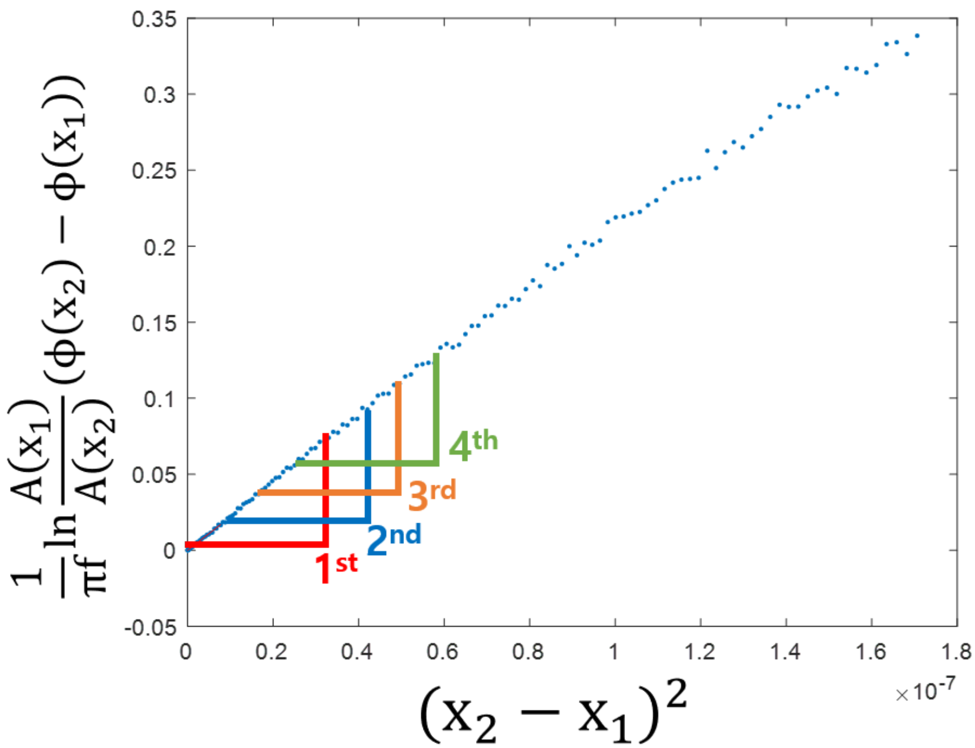

Figure 5.10. The program sweeps the entire length of a fiber with a fixed range of linear region for the calculation of thermal diffusivity by one pixel at a time until the region reaches the end of the sample length.

5.4 Results and Discussion

This section presents the results of the experiments introduced in the previous section and discusses them.

5.4.1 Validation of Measurement Accuracy in a Vacuum

The crucial component of infrared imaging is accurate measurement of emissivity. This is usually done by elevating the temperature of the whole sample with precisely controlled thermal stage to eliminate the effects of irradiation from the surroundings reflected by the sample [115], which may distort the emissivity measurement. However, the custom-made sample fixture which replaces the thermal stage has no capacity for precise temperature control. Therefore, emissivity of the samples had to be measured on the thermal stage before the experiment was performed. The following table provides measured emissivity along with the existing data for comparison.

Table 5.4. Emissivity of the measured samples.

Material	Form	Color	Measured emissivity	Literature value
Fluorocarbon based fishing wire	Monofilament	Clear	0.88	0.81 [116]
PVDF	Monofilament	Clear	0.7	
PEEK	Monofilament	Tan	0.65	0.88–0.894 [117]
	Monofilament	Black	0.83	
	Film	Tan	0.81	
Pure gum rubber	Sheet	Natural	0.85	0.85 [118]
Human hair	Fiber	Light brown and black	0.85	0.91 [119]

Table 5.4 shows the difference in emissivity between the measurement and published data. This seems to be due to the combined effect of material purity, a surface condition and transparency, all of which differ in each study. The measurement also depends on the bandwidth of the detector; the InfraScope utilizes mid-wavelength infrared and does not capture the whole range of radiation. To better understand the

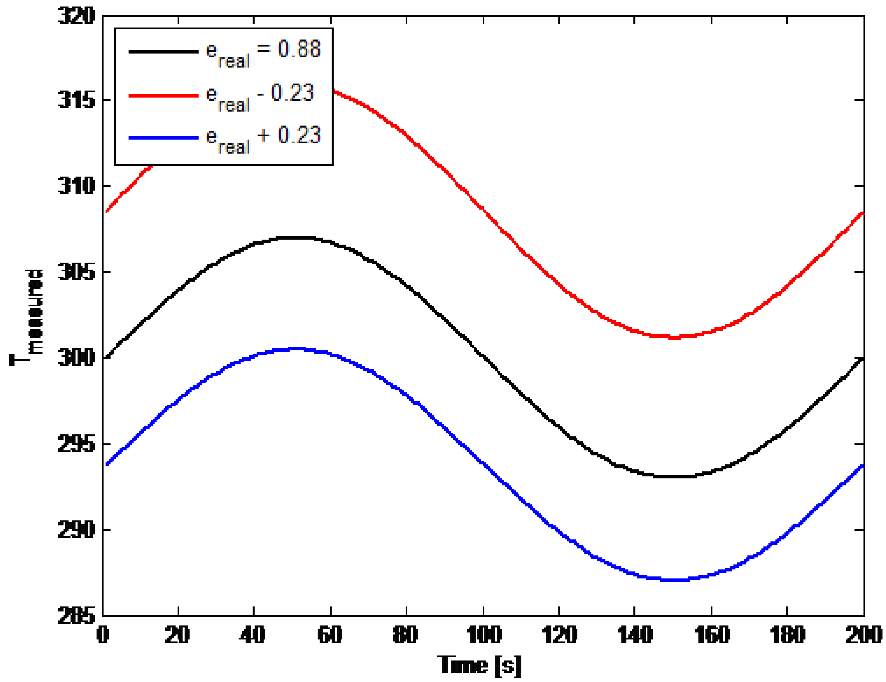

Figure 5.11. Sensitivity of temperature measurement for a thermal wave to uncertainty in emissivity. As is shown, even though the difference in absolute temperature is significant, the amplitude and phase of the oscillations is well preserved.

impact of emissivity, the sensitivity of thermal diffusivity measurement due to error in emissivity was assessed with a MATLAB simulation.

To assume the worst case scenario, the emissivity of tan colored PEEK monofilament, which has the largest discrepancy between a measured value and the literature value, was used for the simulation. Figure 5.11 shows the impact of uncertainty in emissivity on measured temperature. The percent error on the temperature measurement in terms of absolute temperature is small, amounting up to $\pm 2.85\%$, compared to the error in emissivity, which is 26.14%. The error in magnitude is $\pm 4.482\%$. Using propagation of error along with $\pm 1\%$ uncertainty in frequency modulation, the error in measured thermal diffusivity is $\pm 1.08\%$. Thus, the Angstrom's method is robust in the circumstances where large uncertainty in emissivity is present.

Table 5.5. Comparison of thermal diffusivity of PVDF measured using a constant emissivity of 0.7 and emissvitiy mapping whose average emissivity is 1.05.

Frequency	Current	Thermal diffusivity (mm^2/s)		
(mHz)	(mA)	Constant	Mapping	% difference
10	15	0.380	0.37	Constant
50	15	0.357	0.358	10

To further validate the point, I conducted several test cases where I measured thermal diffusivity of the PVDF monofilament in a vacuum, switching between the use of constant emissivity of 0.7 and using the emissivity map acquired by the InfraScope at a room temperature (approximately 18.6 °C) with a mean value of 1.05. Table 5.5 compares the results between the two under different testing conditions.

As predicted by the simulation, the difference between the two results are very small. Also, during the test, we discovered that using the acquired emissivity map at a room temperature provided more consistent thermal diffusivity value along the length of the sample. This seems to be due to the correction in emissivity values according to the surface condition and slight variation in focal depth offered by emissivity mapping, which is lost by applying constant emissivity to the whole area of view. Therefore, I decided to proceed with a emissivity map acquired with the InfraScope for measuring all other samples unless there was a special need for constant emissivity.

Since all the data provided on thermal properties of the measured samples except the PEEK monofilament and hair are in thermal conductivity, separate measurements on specific heat capacity and density accompanies to enable calculation of thermal conductivity from the measured values. Table 5.6 provides an exhaustive list of all relevant properties both measured and acquired from the published data.

Table 5.6. Material properties measured in this work and from published works for comparison.

Material	This Work				Publications				Source
	c_p @ 20°C (J/kgK)	ρ (kg/m^3)	k (W/mK)	α (mm/s^2)	c_p @ 20°C (J/kgK)	ρ (kg/m^3)	k (W/mK)	α (mm/s^2)	
Fluorocarbon fishing line (250µm)	1107	1879	0.72 - 0.84	0.35 - 0.40	1170 - 1900	1690 - 1880	0.11 - 0.3	0.031 - 0.152*	Matweb
PVDF monofilament (406.4µm)	1036	1875	0.69 - 0.78	0.35 - 0.40	960 - 1400	1760 - 1880	0.17 - 0.19	0.065 - 0.112*	Zeus Matbase
PEEK monofilament (101.6µm)	652 - 776	1555	0.38 - 0.42	0.37 - 0.41	1330	1100 - 1480	0.25 - 0.29	0.127 - 0.198*,	Zeus, Mendioroz et al. (2009) [97]
Black PEEK monofilament (203.2µm)	1000	1445	0.59 - 0.61	0.41 - 0.42	1330	1100 - 1480	0.25 - 0.29	0.127 - 0.198*,	Matweb, Salazar et al. (2010) [98]
PEEK film (127µm)	1180	1311	0.30 - 0.36	0.19 - 0.23	1330	1300	0.24	0.139*	Solvay Matweb
PEEK film (254µm)	1184	1313	0.28 - 0.33	0.18 - 0.21	1330	1300	0.24	0.139*	
Gum rubber (400µm)	1715	1157	0.21 - 0.26	0.11 - 0.13	1828 - 1905	940 - 992	0.1496 - 0.25	0.079 - 0.145*	Holding (2008) [120] Sethuraj and Mathew (2012) [121]
Human Hair (100µm)	1040	1523 - 1549	0.22 - 0.26	0.143 - 0.16	1602	1100	0.25	0.14, 0.142	Mendioroz et al. (2009) [97] Salazar et al. (2010) [98] Liu et al. (2014) [95]

*Calculated from published properties

Figure 5.12 compares thermal conductivity of all the samples between the measured values and the published values. There are three remarks to make about the comparison. First, all the values are on the same order of magnitude which typifies thermal conductivity of polymers.

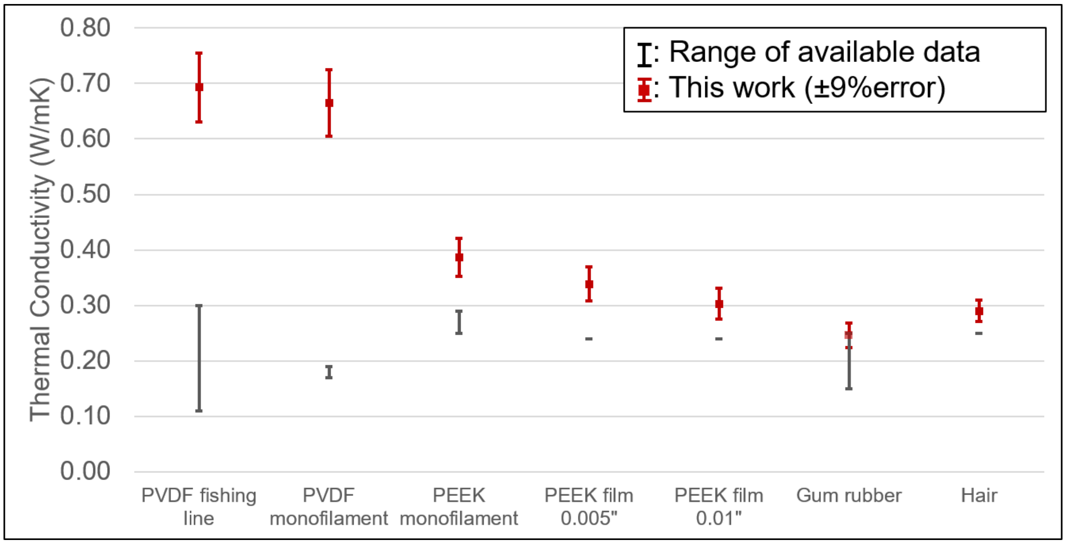

Figure 5.12. Comparison of all the measured and published thermal conductivity of the tested samples.

Second, some of the measured values are reasonably higher than the published values, which is expected because the thermal conductivity increases through a certain manufacturing process that involves drawing. For example, a drawing process typically utilized to manufacture monofilaments can lead to increased crystallinity which in turn increases thermal conductivity of the material [122]. Indeed, the published result on thermal diffusivity of a PEEK monofilament also measured a higher value compared with the other available results [97,98]. Because of this, the measured range of PEEK monofilaments lies well within the published results. The higher measured values found in the PEEK films can partly rely on the same logic as there is a report on the positive correlation between the drawing ratio and thermal conductivity of a polymer film [109]; however, a closer investigation suggests involvement of another factor. The manufacturer of the film specifies ASTM E1530 as a standard for measurement and seems to have made the measurement after the manufacturing process to reflect the change in the property. However, the standard is adequate for measuring cross-plane thermal conductivity of the films while the Angstrom's method in the study has a setup more suitable for measuring in-plane thermal conductivity. A past studies have discovered anisotropy between in-plane and cross-plane thermal conductivities of polymer films where an in-plane value tends to be higher than a cross-plane one [123].

Lastly and most importantly for the objective of this study, the measured thermal conductivity of hair matches extremely well with the existing studies. The publication on the PEEK monofilament and hair both reported thermal diffusivity, which enables direct comparison. Figure 5.13 compares thermal diffusivity of the PEEK monofilament and hair between the measured values and the published values.

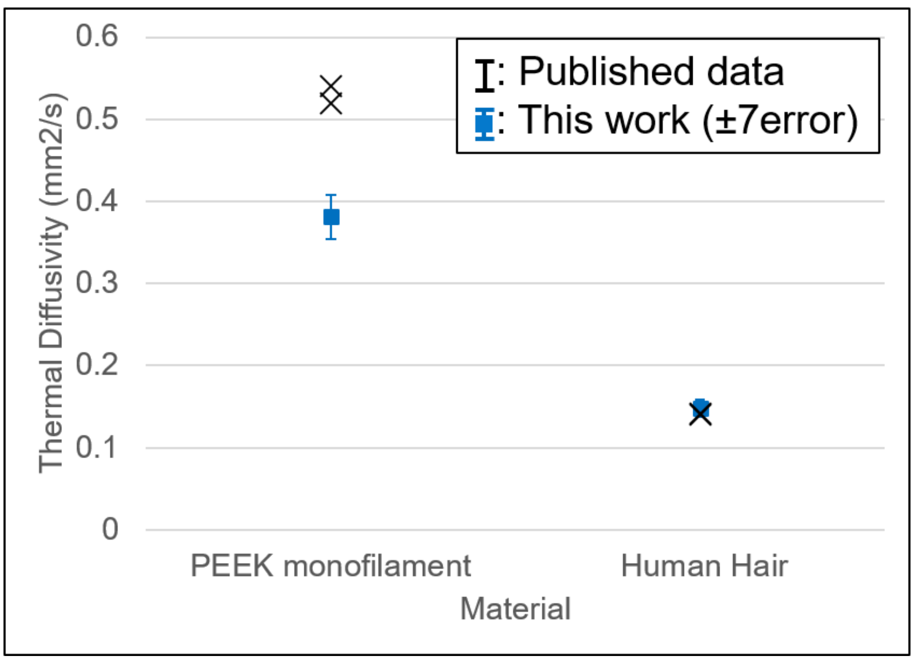

Figure 5.13. Comparison of measured and published thermal diffusivity of the PEEK monofilament and hair.

The results successfully validated the accuracy of the measurement technique by comparing the measured values with the published data and providing compelling reasons for any discrepancy.

5.4.2 Measurement of Hair in a Vacuum

Table 5.7 lists all the measurement results. All measurements were made using the current of 10 mA supplied at 50 mHz, which was found to be most reliable and accurate.

Table 5.8 lists the results of ANOVA ($\alpha = 0.05$) run with SAS. All three factors had statistically insignificant impact on thermal diffusivity of hair. This make the heat transfer modeling process much more convenient because the differences in properties which complicate the modeling process can be safely ignored.

5.4.3 Measurement of Hair in the Humid Air

Results of the experiments to test the statistical significance of the four factors in a humid environment are presented in Table 5.9.

ANOVA was run with $\alpha = 0.05$. The results are shown in Table 5.10. The statistical significant of the factors are consistent with the vacuum results, rejecting the three factors to be insignificant and accepting only one factor, humidity, as significant. Overall, higher humidity depresses thermal diffusivity of hair. Despite the difficulty in accurately measuring thermal diffusivity of hair in the humid air due to the limitations in the theory and the measurement technique, the significant impact of humidity on hair was statistically proven.

Table 5.7. Results of all measured thermal diffusivity under given conditions.

Type	Fiber	Section	Thermal Diffusivity (mm^2/s)
Asian	1	Root	0.142
		Tip	0.141
	2	Root	0.147
		Tip	0.147
	3	Root	0.151
		Tip	0.140
	4	Root	0.154
		Tip	0.145
	5	Root	0.141
		Tip	0.147
African	1	Root	0.145
		Tip	0.143
	2	Root	0.141
		Tip	0.163
	3	Root	0.161
		Tip	0.155
	4	Root	0.158
		Tip	0.156
	5	Root	0.136
		Tip	0.148
Caucasian	1	Root	0.145
		Tip	0.142
	2	Root	0.153
		Tip	0.153
	3	Root	0.157
		Tip	0.140
	4	Root	0.141
		Tip	0.149
	5	Root	0.145
		Tip	0.150

Table 5.8. Results of ANOVA on the three factors.

Factor	p-value (alpha =0.05)
Type	0.2258
Fiber	0.3573
Section	0.0943

Table 5.9. Results of all measured thermal diffusivity under given conditions.

Type	Fiber	Section	Humidity	Thermal Diffusivity (mm^2/s)
African	1	Root	Low	0.470
			High	0.388
		Tip	Low	0.405
			High	0.356
	2	Root	Low	0.473
			High	0.434
		Tip	Low	0.378
			High	0.353
Caucasian	1	Root	Low	0.496
			High	0.443
		Tip	Low	0.479
			High	0.441
	2	Root	Low	0.423
			High	0.352
		Tip	Low	0.381
			High	0.352
Bleached	1	Root	Low	0.384
			High	0.391
		Tip	Low	0.371
			High	0.314
	2	Root	Low	0.379
			High	0.316
		Tip	Low	0.368
			High	0.306
Low Lifted	1	Root	Low	0.455
			High	0.513
		Tip	Low	0.417
			High	0.393
	2	Root	Low	0.395
			High	0.361
		Tip	Low	0.449
			High	0.398

Table 5.10. Results of ANOVA on the four factors.

Factor	p-value ($\alpha = 0.05$)
Type	0.2137
Fiber	0.0733
Section	0.2637
Humidity	0.0047

6. HEAT TRANSFER MODELING OF FLAT IRONING

After successfully measuring all relevant material properties, construction for a heat transfer model begins. The modeling process proceeds in two steps: first, construction of a 2D heat transfer model between a hair bundle and a flat iron utilizing a finite difference method, and secondly, comparison of the model outputs with experimental outputs and adjustment of the fitting parameters to better fit the model.

6.1 2D Heat Transfer Model using the Finite Difference Method

A 2D heat transfer model is constructed using a finite difference method [124]. The finite difference method is type of numerical analysis methods. It utilizes a nodal network in which node resides within a discretized element.

To begin with, a model representation of a hair bundle and a flat iron are laid out as shown in Figure 6.1. In reality, the hair bundle would experience 3D heat transfer through convection and radiation on its sides. However, 2D heat transfer, looking at the hair bundle from the side as in the figure largely simplifies the modeling process and is considered appropriate given the small thickness of the bundle, in which case, heat transfer will dominantly occur through the top and bottom surfaces of the bundle.

To enable the use of the finite difference method, the model geometry was discretized into small rectangular elements of height δy and width δx that enclose nodes (Figure 6.1). In doing so, effective material properties utilizing the rule of mixtures are assumed to account for both air and hair fractions enclosed in each element (Equation (6.1))

$$m_{eff} = F_{hair} m_{hair} + F_{air} m_{air} \tag{6.1}$$

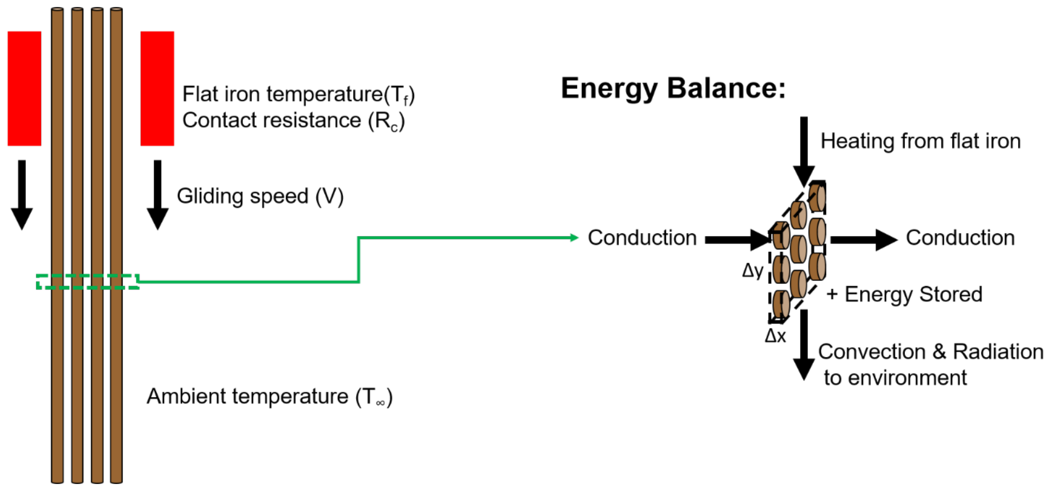

Figure 6.1. A 2D heat transfer model was constructed using the parameters illustrated in the diagram. To apply the finite difference method, the bundle was discretized into small sections of width (Δx) and height (Δy). As shown on the right side, various modes of heat transfer occurs in each section which interacts with one another to manifest the overall heat transfer across the entire bundle.

where

m = Any material property

F = Volume fraction of the material in a bundle

A governing differential equation is a 2D heat diffusion equation shown below (Equation (6.2)).

$$\frac{1}{\alpha} = \frac{\partial^2 T}{\partial x^2} + \frac{\partial^2 T}{\partial y^2} \tag{6.2}$$

α = Thermal diffusivity

T = Temperature

x = location in x-direction

y = location in y-direction

This equation is discretized and modified accordingly with differing boundary conditions. An implicit method with which the temperature of the next time step at the node of interest is calculated by utilizing the temperatures of the current time step at the adjacent nodes. For example, all the nodes inside the hair bundle are subject to heat transfer through conduction only. The equation reduces to:

$$T_{m,n}^{p+1} = F_x(T_{m+1,n}^p + T_{m-1,n}^p) + F_y(T_{m,n+1}^p + T_{m,n-1}^p) + (1 - 2F_x - 2F_y)T_{m,n}^p \qquad (6.3)$$

where

$$F_x = \frac{k_x \Delta t}{\rho c_p \Delta x^2} \qquad (6.4)$$

$$F_y = \frac{k_y \Delta t}{\rho c_p \Delta y^2} \qquad (6.5)$$

and

k_x= thermal conductivity in x-direction

k_y= thermal conductivity in y-direction

Δt = time step

ρ = density

c_p = specific heat capacity

Note the separate notations for thermal conductivity in two directions. This is to flexibly account for the anisotropy in the effective thermal conductivity. The hair and air components in the bundle were assumed to be contributing to thermal conductivity in parallel as shown in the equation below.

$$k_p = F_{hair}k_{hair} + F_{air}k_{air} \qquad (6.6)$$

At the top nodes, heat transfer occurs through convection and radiation to air when a flat iron is not in contact and through conduction and radiation when it is. Both conditions can be described using one equation. The equation below describes the former condition (Equation (6.7)).

$$\begin{aligned} T_{m,n}^{p+1} = {} & F_x(T_{m+1,n}^p + T_{m-1,n}^p) + 2F_y T_{m,n-1}^p + 2B_y F_y T_\infty + 2E_y F_y {T_\infty}^4 \\ & + (1 - 2F_x - 2F_y - 2B_y F_y - 2E_y F_y (T_{m,n}^p)^3) T_{m,n}^p \end{aligned} \tag{6.7}$$

where

$$B_y = \frac{h \Delta y}{k_y} \tag{6.8}$$

$$E_y = \frac{\epsilon \sigma \Delta y}{k_y} \tag{6.9}$$

and

h = coefficient of convection

T_∞ = ambient temperature

ϵ = emissivity

σ = Stefan-Boltzmann constant

T_∞ and h change to T_{flat} (flat iron temperature) and h_e (effective convection coefficient including the contact resistance when flat iron is in contact) when a flat iron is in contact. The equations for the bottom nodes will be the same except the change in the direction of heat flow in one of the terms as follows.

$$\begin{aligned} T_{m,n}^{p+1} = {} & F_x(T_{m+1,n}^p + T_{m-1,n}^p) + 2F_y T_{m,n+1}^p + 2B_y F_y T_\infty + 2E_y F_y {T_\infty}^4 \\ & + (1 - 2F_x - 2F_y - 2B_y F_y - 2E_y F_y (T_{m,n}^p)^3) T_{m,n}^p \end{aligned} \tag{6.10}$$

At the two ends of the bundle, a constant temperature T_∞ is assumed as they are in contact with clamps that can function as heat sinks.

6.2 Experimental Validation of the Model Output

Two types of hair, Asian and African, were tested for the experimental validation. Both samples were prepared from multiple sources by International Hair Importers and Products. Each bundle contained approximately 30mg of hair and the width (approximately 10mm for both Asian and African) and thickness (approximately 0.22mm for Asian and 0.5mm for African) of the bundle were controlled to the best effort as they are parameters that affect the simulation results.

The hair samples were soaked in a 1 % solution of clarifying shampoo for 3 minutes, thoroughly washed with warm water and equilibrated at 21 °C and 48 %RH to 52 %RH for 24 hours before heat application.

Table 6.1 shows the design of experiments for Asian samples and Table 6.2 for African samples. Both include three factors: a temperature setting, gliding speed, and the number of passes. For both cases, data acquired after multiple passes were used for comparison with the simulation results because the results of the initial several passes were significantly impacted by the wet component of the protectant.

Table 6.1. Design of experiments for validation of the heat transfer model with Asian hair samples.

Temperature (celsius)	115	164	210
Gliding Speed (cm/s) x Number of Passes	1 x 1	3 x 3	5 x 5

Table 6.2. Design of experiments for validation of the heat transfer model with African hair samples.

Temperature (celsius)	115	210
Gliding Speed (cm/s)	1	5
Number of Passes	1	5

Experimental equipment and procedures are equivalent to those introduced in Chapter 3. A MATLAB program was developed to post-process the recorded data and output plots and values that can be compared with simulated results. Three types of plots were generated as means of comparison. First of all, the change in temperature along the bundle over time was plotted to confirm accordance in the general behavior of the heat transfer. Next, I compared the amount of time each position in the hair bundle was exposed above a certain temperature as a quantitative comparison that numerically captures any difference between the simulation and experiments.

There are three parameters that are not reliably accounted for despite the best efforts made to estimate them. They include thermal contact resistance between the surfaces of hair bundle and a flat iron, the fractions of hair and air inside a bundle, and the convection coefficient. The thermal contact resistance was found to have relatively little impact on the simulation results while the other two exhibited significant influence. To address this issue, one of the flat ironing conditions was chosen (5 passes at 5 cm/s and 210 °C) and the parameters were adjusted until a satisfactory result was obtained. Then, the rest of the conditions were simulated maintaining the fitting parameters consistent across all of them.

6.3 Results and Discussion

Figure 6.2 shows an example of the comparison between time plots of experimental results and simulation. Throughout all the conditions, the general behavior of heat in hair bundles well matched between the two. The temperature of the hair bundle sharply increases to reach that of a flat iron instantly after coming into contact with the flat iron plates. After the flat iron glides past, the temperature exponentially decays to the ambient temperature.

Figure 6.3 is an example of comparing the change in temperature over time at a specified location on a hair bundle. This profile should essentially look the same across all locations as the only difference will be the delay in the phase contingent on the flat ironing speed. The dips in the experimental plot marked by arrows are produced by the flat iron body's blocking the vision of the IR camera during the measurement when it is in direct contact with the hair bundle.

Figure 6.4 visually illustrates what the exposure time means by utilizing the experimental result shown in Figure 6.3.

Table 6.3 lists the comparison of exposure time above 80 °C, 90 °C, and 100 °C between experimental and model outputs under various flat ironing conditions.

The general trend in the comparison is prominent; the higher all the three flat ironing parameters are, the more accurate the model outputs become except the condition at 164 °C and 3 cm/s for 3 passes. The reason behind this trend becomes clear if the difference instead of % difference is used for comparison. Despite the large variation in the % difference, the difference is relatively constant throughout all conditions. The large variation in the % difference originates from the smaller denominator inevitable for the condition with lower exposure time which is contingent on the lower values of the flat ironing conditions.

Table 6.4 shows the results of the comparison on the African hair.

Again, using the % difference as a metric for the accuracy of the model could be misleading if the exposure time is very small in the first place. For example, when

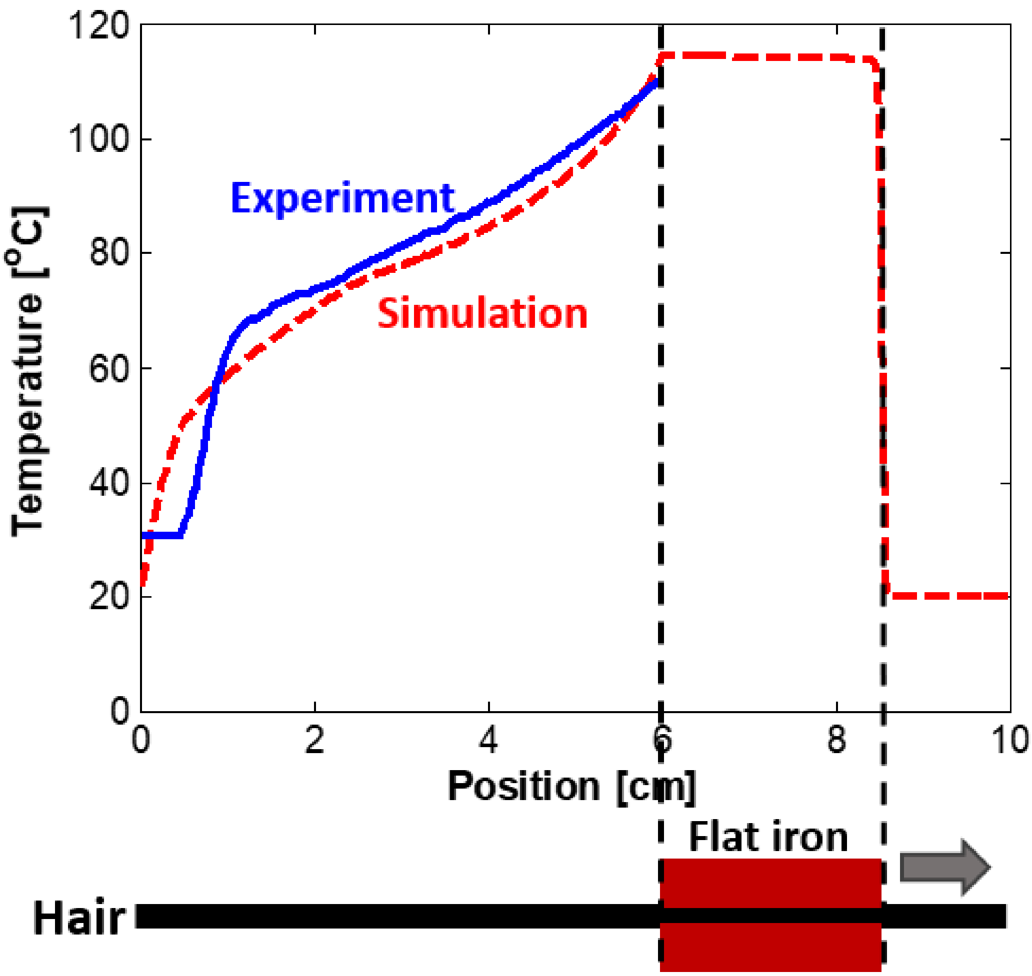

Figure 6.2. Simulation (red) and experimental results (blue) of the temperature profile over the length of a hair bundle are compared when flat ironing occurs at a gliding speed of 1 cm/s at 115 °C. The region marked by black dotted lines illustrates the location of the flat iron moving to the right.

flat ironing happens once at 115 °C and 5 cm/s, the % difference is very large but the numerical difference is very small. By the same token, when flat ironing happens 5 times at 210 °C and 1 cm/s, the % difference is relatively small, but the numerical difference amounts up to 10 seconds. Considering this caveat, the model performs better when the condition involves a single pass of flat ironing. This behavior is different from the case of Asian hair where conditions with higher number of passes

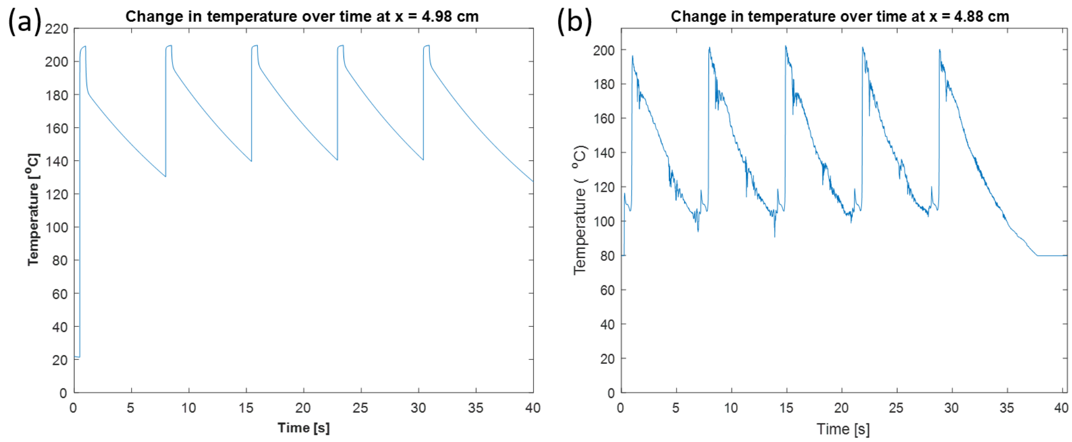

Figure 6.3. Comparison of change in temperature over time at a specified location between the (a) simulation and (b) experimental results. In the experimental results, the dip in temperature before each peak originates from the hindered observation of the temperature of a hair bundle by a flat iron body.

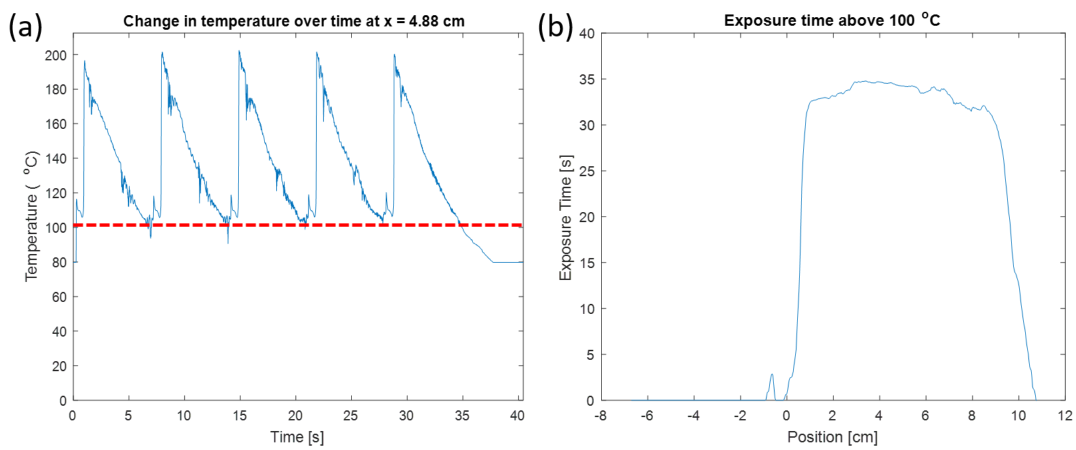

Figure 6.4. Visual illustration of what the exposure time means and how it is calculated. (a) The temperature throughout all location on a hair bundle is monitored, and the duration of time for which each location is above 100 °C is counted. (b) Then, the recorded exposure time at each position is plotted as shown in the right.

performed better. The difference may originate from the better fiber alignment and consistency in cross-sectional dimensions of Asian hair. The Asian hair bundles did

Table 6.3. Comparison of exposure time over 80 °C, 90 °C, and 100 °C between simulation and experimental results under various flat ironing conditions on Asian hair. The last column presents % difference between the two to quantify the accuracy of the model prediction.

Temperature (celsius)	Gliding Speed (cm/s)	Number of Passes	Threshold Temperature (celsius)	Experiment (s)	Simulation (s)	Difference	% Difference
115	1	1	80	6.6	8.5	2.0	30%
			90	5.3	7.4	2.1	39%
			100	4.2	6.3	2.1	49%
	3	3	80	13.9	15.4	1.6	11%
			90	9.7	11.9	2.2	22%
			100	6.2	8.8	2.6	42%
	5	5	80	26.6	21.8	-4.8	-18%
			90	18.4	15.9	-2.5	-14%
			100	10.4	10.7	0.3	3%
164	1	1	80	9.1	11.8	2.7	29%
			90	8.1	10.6	2.5	31%
			100	7.1	9.6	2.4	34%
	3	3	80	25.3	25.1	-0.2	-1%
			90	22.4	21.6	-0.8	-3%
			100	18.4	18.5	0.1	1%
	5	5	80	34.0	38.0	4.0	12%
			90	26.9	32.1	5.2	19%
			100	22.5	26.9	4.4	20%
210	1	1	80	11.6	13.8	2.2	19%
			90	10.3	12.6	2.3	23%
			100	9.3	11.6	2.3	25%
	3	3	80	25.4	29.7	4.4	17%
			90	24.2	27.7	3.6	15%
			100	22.4	24.6	2.2	10%
	5	5	80	37.3	37.6	0.3	1%
			90	35.8	36.4	0.7	2%
			100	33.9	35.4	1.5	4%

not experience change in the cross-sectional dimensions regardless of the number of flat ironing cycles because the fibers are already straight. In contrast, the African hair bundles become more organized and aligned with the increasing number of flat ironing cycles. Therefore, the cross-sectional dimensions which govern the volume fraction of a solid phase (hair) and a gaseous phase (air) in the bundle will change over time, affecting the results of the simulation. Then, it might make more sense to

Table 6.4. Comparison of exposure time over 80 °C, 90 °C, and 100 °C between experimental and simulation results under various flat ironing conditions on African hair.

Temperature (celsius)	Gliding Speed (cm/s)	Number of Passes	Threshold Temperature (celsius)	Experiment (s)	Simulation (s)	Difference	% Difference
115	1	1	80	8.9	9.3	0.4	5%
			90	6.5	6.8	0.3	5%
			100	4.7	4.7	0	0%
		5	80	46.8	46.9	0.1	0%
			90	35.6	34.3	-1.2	-3%
			100	26.9	23.7	-3.2	-12%
	5	1	80	1.2	1.9	0.6	53%
			90	0.8	0.7	-0.1	-17%
			100	0.7	0.6	-0.1	-20%
		5	80	16.4	22.6	6.2	38%
			90	8.2	11.3	3.1	38%
			100	4.2	3.7	-0.5	-12%
210	1	1	80	18.8	19.0	0.2	1%
			90	16.6	16.5	-0.1	0%
			100	14.9	14.4	-0.5	-3%
		5	80	80.6	70.8	-9.8	-12%
			90	78.4	68.3	-10.1	-13%
			100	70.4	66.2	-4.2	-6%
	5	1	80	12.0	12.3	0.4	3%
			90	9.2	9.8	0.6	6%
			100	7.0	7.7	0.7	10%
		5	80	48.2	43.1	-5.1	-11%
			90	45.3	40.6	-5.7	-10%
			100	42.7	38.4	-4.2	-10%

use a different ratio of the volume fraction for the conditions with different number of flat ironing cycles instead of using the fixed ratio for all the conditions.

In addition, including evaporation of moisture from the hair, which alters the effective properties such as thermal conductivity, specific heat capacity and density of the bundle may improve the simulation. The temperature dependence of material properties could influence the simulation results. However, despite these gaps, the simulation results match the experimental results quite closely especially for the case of Asian hair where the cross-sectional dimensions stay constant over multiple cycles of flat ironing. Thus, the presented heat transfer model proves to be a useful tool for simulating heat transfer between hair and a flat iron under various flat ironing conditions. Even without the accurate information about the density of hair bundle, thermal contact resistance, and convection coefficient, the model is still expected to serve as a useful tool for qualitatively differentiating the effect of different flat ironing conditions. Finally, in conjunction with the previously developed predictive model for the fatigue strength, the model will serve as a practical tool for estimating the amount of reduction in hair strength imparted by certain flat ironing conditions and aid flat users in making better informed decisions.

7. CONCLUSIONS

7.1 Summary

Gaps in the current studies regarding the evaluation of flat ironing performance as it relates to relevant concerns of flat iron users such as reduction in hair strength, straightening efficacy, and permanent curl loss were identified. The guidelines provided by flat iron manufacturers on the use of a flat iron demonstrated inconsistencies in their hair classification and a corresponding range of recommended temperature. Meanwhile, observation of an online hair care community revealed flat iron users' dilemma between the needs for temporary hair straightening and the fear of heat damage. I concluded that these gaps originate from the absence of a practical study that offers a decision making tool for flat ironing and proposed to address them by (1) experimentally investigating the effects of flat ironing conditions and (2) create a heat transfer model between hair and a flat iron to simulate the behavior of heat which is highly likely to be a direct indicator of heat damage.

In Part 1, the study on predictive modeling of flat ironing results and the benefits of a heat protectant were presented. It contributes to the community of hair science in several aspects. First, it provides the methods for quantifying the three flat ironing results: reduction in hair strength, straightening efficacy, and permanent curl loss. These metrics better reflect the concerns of flat iron users and offer researchers and product developers in the field a more effective way of communicating their findings to the consumers. Second, it introduced a more scientifically rigorous method of experimenting the effects of flat ironing by building the fully automated flat ironing mechanism which can accurately control the gliding speed and the number of passes. Third, it demonstrated that construction of predictive models for each flat ironing metric is possible with the temperature setting, gliding speed, the number of passes, and the exposure time as parameters. The study suggested multiple linear regression as one way of establishing the models, assuming linear contribution of each parameter to the flat ironing results. Fourth, the study discovered that the temperature setting was the most dominant factor in predicting the impact of flat ironing conditions on the straightening efficacy and permanent curl loss whereas the exposure time was the single best predictor of reduction in fatigue strength. Finally, it discovered that the effect of a silicone-based heat protectant depends on the flat ironing conditions. For instance, if hair is flat ironed at 210 °C and 1cm/s in the presence of the heat protectant, a single pass will impede the straightening efficacy as opposed to five passes that enhance the straightening efficacy in comparison with the identical conditions without the protectant. This is clear evidence of the need for investigating individual flat ironing conditions for the performance of the complementary products in the flat ironing process. Overall, the study proved that the construction of predictive modeling is essential for providing reliable, unbiased, and accurate prediction of the metrics for desirable and undesirable flat ironing results, and that it has a potential to serve as a powerful tool for flat iron users who want to wield the flat iron at hand in a more judicious way. The example of its application was outlined by the simple guidelines that help flat irons users achieve their styling goals with specific flat ironing conditions.

In Part 2, in light of the high correlation between the reduction in the fatigue strength and the exposure time, the heat transfer model between a flat iron and hair was developed. The study demonstrated the heat transfer modeling by utilizing the finite difference method assuming the heat transfer to occur dominantly in 2D and a hair bundle to be a rectangular slab possessing effective material properties contingent on the volume fractions of hair and air. The model exhibited fairly high predictive accuracy across all flat ironing conditions. The study contributes to a scientific community by introducing a modeling technique which is broadly applicable to fabrics and composites. Thermal characterization of human hair preceded to enable the development of the model. In doing so, the novel measurement technique based on Angstrom's method integrated with infrared thermography was developed and proved its accuracy and reliability in measuring the thermal diffusivity of polymer monofilaments and films of a few-hundred-micron thickness. The measurement technique has a potential to measure other materials on a similar scale and in similar forms. Also, the measurement successfully proved that the thermal properties of hair are consistent across hair types even though humidity can significantly influence it, providing new insights to the community of hair scientists.

7.2 Suggestions for Future Work

I have realized both during and after each project, several ways in which I can improve the experimentation and analysis. I would like to share some of them before I conclude the dissertation.

7.2.1 Investigation of Flat Ironing Results and Predictive Modeling

For the experimental investigation of flat ironing results, examination of various intermediate and even more extreme flat ironing conditions are necessary to fully understand the impact of flat ironing. For example, it was found that the gliding speed is negatively correlated with the reduction in the fatigue strength of hair. However, without the information on the effects of the intermediate speeds, the exact relationship between the gliding speed and the fatigue strength cannot be fully understood.

There is much room for improvement in the experimental equipment. It takes a lot of manpower to run the experiment in the current setting. A fully automated process will eliminate the need of manpower and greatly increase the productivity. Especially useful would be automation of CI and CD measurements. Development of image processing algorithm to perform the measurements would greatly reduce the time taken to measure everything manually and make the process more robust by reducing the magnitude of measurement error.

As was discussed, the African hair used for the experiments was a mixture of Type V, VI, and VII. This could have contributed to large variation in the behavior among the individual hair strands and lowered the explanatory power of the predictive models. More rigorous classification and preparation of hair samples may significantly improve the predictability of the models.

Investigation of straightening efficacy and permanent curl loss after multiple flat ironing cycles rather than a single cycle would better capture the effect of repeated flat ironing. Also, this may reveal the unrealized effect of the exposure time further and make the development of the heat transfer model even more attractive for predicting the results of flat ironing.

There are several alternatives to multiple linear regression used in the study. They have a potential to improve the relatively low explanatory power of the present models. For instance, Weighted Least Squares distribute different weights to each observation, which addresses varying degrees of random error at different levels of explanatory variables.

7.2.2 Evaluating the Performance of Heat Protectants

To better understand the effects of heat protectants and especially the effect of particular ingredients, which was silicone in this study, better-controlled formulation of the protectants is required. The study used commercially available protectants, which is inevitably subject to the confounded effect of all the participating ingredients. While it was sufficient to illustrate the usefulness of the proposed flat ironing metrics and the need to closely investigate different conditions because of potentially bidirectional change in the metric depending on the presence of the heat protectant despite the equivalence in the rest of the parameters.

Flat ironing hair with and without heat protectants in the absence of heat would provide insights into the role of reduced friction on hair imparted by heat protectants. Even though the reduction in the stretching force is generally accepted as beneficial for the long-term hair health, a required amount of reduction to be effective in this regard is now known. If the amount of reduction in stretching force does not contribute much to the preservation of hair strength, it obviates the need of heat protectants in that particular aspect.

Equilibrating hair samples for another 24 hours after the application of heat protectants could be a good practice to improve the reliability of the experimental results. When flat ironing occurs for the first few cycles on the sample with heat protectants, the wet component largely decreases the exposure time which is in turn highly correlated with the reduction in fatigue strength. Also, considering the role of water as a plasticizer which promotes denaturation of hair, these two opposing mechanisms could introduce unwanted effect to the flat ironing results. Having stated the increased complexity in flat ironing hair with wet protectants on it, the investigation of the performance of dry protectants would reveal even more insights into the role of protectants in flat ironing as was once studied [8].

Finally, washing and re-applying heat protectants after and before each flat ironing cycle would make the experimental results more realistic. This process was omitted to specifically focus on the effect of the protective coating by excluding the participation of the wet component. Now that it has been investigated, an additional examination that employs new protocols would be helpful in assessing the performance of the heat protectants in the context of current usage pattern.

7.2.3 Thermal Characterization of Hair and Heat Transfer Modeling

The possible improvements in thermal characterization and heat transfer modeling of human hair revolves around the effect of moisture present both inside and outside of hair.

Hair is highly hygroscopic, and it can take up to about 12% of its weight in water in the ambient condition. Thus, the effective thermal properties of hair should highly dependent on the presence of water. The current experimental setup poses a challenge in maintaining the water content because all measurements are taken in a vacuum where evaporation of water happens at a significantly lower temperature. On the other hand, a use of the technique in the ambient condition poses another challenge due possibly to the participation of natural convection. Thus, measurement of thermal diffusivity in the presence of water requires better design of experimental equipment and understanding of participating modes of heat transfer. Alternatively, finding a way to seal moisture inside hair would enable the use of the current experimental setup which is already proven to accurately and reliably measure thermal diffusivity of hair.

The presence of water all introduces challenges to heat transfer modeling. The range of temperature used for flat ironing is well above the boiling temperature of water and removes water from hair. Hair then resorbs water after it is exposed to the ambient condition. Therefore, accurate prediction of heat transfer in hair requires a clear understanding of the rate at which water is removed and resorbed. The presence of water present additional challenge to utilizing the model and its outputs. It was shown that there is a high correlation between the exposure time and the reduction in fatigue strength. The permanent change in hair structure is highly related with denaturation of keratin which in turn is highly related with water content. Therefore, to better utilize the heat transfer model, more accurate understanding of the relationship among all the participating factors.

REFERENCES

REFERENCES

[1] L. Rebenfeld, H. D. Weigmann, and C. Dansizer. Temperature dependence of the mechanical properties of human hair in relation to structure. *Journal of the Society of Cosmetic Chemists*, 17:525–538, 1966.

[2] M. Gamez-Garcia. The cracking of human hair cuticles by cyclical thermal stresses. *Journal of the Society of Cosmetic Chemists*, 49(3):141–153, 1998.

[3] R. McMullen and J. Jachowicz. Thermal degradation of hair. I. Effect of curling irons. *Journal of the Society of Cosmetic Chemists*, 49(4):223–244, 1998.

[4] R. McMullen and J. Jachowicz. Thermal degradation of hair. II. Effect of selected polymers and surfactants. *Journal of the Society of Cosmetic Chemists*, 49(4):245–256, 1998.

[5] S. B. Ruetsch and Y. K. Kamath. Effects of thermal treatments with a curling iron on hair fiber. *International Journal of Cosmetic Science*, 26(4):217–217, 2004.

[6] D. Harper, J. C. Qi, and P. Kaplan. Thermal styling: efficacy, convenience, damage tradeoffs. *Journal of Cosmetic Science*, 62(2):139–147, 2010.

[7] Y. Zhou, R. Rigoletto, D. Koelmel, G. Zhang, T. W. Gillece, L. Foltis, D. J. Moore, X. Qu, and C. Sun. The effect of various cosmetic pretreatments on protecting hair from thermal damage by hot flat ironing. *Journal of Cosmetic Science*, 62(2):265–282, 2010.

[8] P. Christian, N. Winsey, M. Whatmough, and P. A. Cornwell. The effects of water on heat-styling damage. *Journal of Cosmetic Science*, 62(1):15, 2011.

[9] A. Dussaud, B. Rana, and H. T. Lam. Progressive hair straightening using an automated flat iron: function of silicones. *Journal of Cosmetic Science*, 64(2):119, 2013.

[10] J. Hahn, A. Marconnet, and T. Reid. Using DIY practitioners as lead users: a case study on the hair care industry. *Journal of Mechanical Design*, 138(10):101107, Jul 2016.

[11] A. Picot-Lemasson, G. Decocq, F. Aghassian, and J. L. Leveque. Influence of hairdressing on the psychological mood of women. *International Journal of Cosmetic Science*, 23(3):161–164, 2001.

[12] R. R. Hall, S. Francis, M. Whitt-Glover, K. Loftin-Bell, K. Swett, and A. J. McMichael. Hair care practices as a barrier to physical activity in African American women. *JAMA Dermatology*, 149(3):310–314, 2013. 10.1001/jamadermatol.2013.1946.

[13] R. C. Gathers and M. G. Mahan. African American women, hair care, and health barriers. *The Journal of Clinical and Aesthetic Dermatology*, 7(9):26, 2014.

[14] A. J. McMichael. Hair breakage in normal and weathered hair: focus on the Black patient. *The Journal of Investigative Dermatology. Symposium Proceedings*, 12 2:6–9, 2007.

[15] D. Rucker Wright, R. Gathers, A. Kapke, D. Johnson, and C. L. Joseph. Hair care practices and their association with scalp and hair disorders in African American girls. *Journal of the American Academy of Dermatology*, 64(2):253–262, 2011.

[16] A. Salam, S. Aryiku, and O. E. Dadzie. Hair and scalp disorders in women of African descent: an overview. *British Journal of Dermatology*, 169(s3):19–32, 2013.

[17] R. Lewallen, S. Francis, B. Fisher, J. Richards, J. Li, T. Dawson, K. Swett, and A. McMichael. Hair care practices and structural evaluation of scalp and hair shaft parameters in African American and Caucasian women. *Journal of Cosmetic Dermatology*, 14(3):216–223, 2015.

[18] R. Crawford, C. R. Robbins, and K. Chesney. A hysteresis in heat dried hair. *Journal of the Society of Cosmetic Chemists*, 32:27–36, 1981.

[19] Y. Lee, Y.-D. Kim, H.-J. Hyun, L.-Q. Pi, X. Jin, and W.-S. Lee. Hair shaft damage from heat and drying time of hair dryer. *Annals of Dermatology*, 23(4):455–462, 2011.

[20] R. L. Mcmullen, G. Zhang, and T. Gillece. Quantifying hair shape and hair damage induced during reshaping of hair. *Journal of Cosmetic Science*, 66(6):379–409, 2015.

[21] F. J. Wortmann, G. Wortmann, and C. Popescu. Kinetics of the changes imparted to the main structural components of human hair by thermal treatment. *Thermochimica Acta*, 661:78–83, 2018.

[22] R. C. C. Wagner and I. Joekes. Hair protein removal by sodium dodecyl sulfate. *Colloids and Surfaces B: Biointerfaces*, 41(1):7–14, mar 2005.

[23] W. Humphries, D. L. Miller, and R. H. Wildnauer. The thermomechanical analysis of natural and chemically modified human hair. *Journal of the Society of Cosmetic Chemists*, 23(6):359–370, 1972.

[24] P. Milczarek, M. Zielinski, and M. L. Garcia. The mechanism and stability of thermal transitions in hair keratin. *Colloid and Polymer Science*, 270(11):1106–1115, 1992.

[25] J. Cao. Melting study of the α-form crystallites in human hair keratin by DSC. *Thermochimica Acta*, 335(1):5–9, 1999.

[26] Zs. Éhen, Cs. Novák, J. Sztatisz, and O. Bene. Thermal characterization of hair using TG-MS combined thermoanalytical technique. *Journal of Thermal Analysis and Calorimetry*, 78(2):427–440, 2004.

[27] V. F. Monteiro, A. P. Maciel, and E. Longo. Thermal analysis of caucasian human hair. *Journal of Thermal Analysis and Calorimetry*, 79(2):289–293, 2005.

[28] D. V. Istrate. *Heat induced denaturation of fibrous hard alpha-keratins and their reaction with various chemical reagents*. PhD thesis, Universitätsbibliothek, 2011.

[29] F.-J. Wortmann, G. Wortmann, J. Marsh, and K. Meinert. Thermal denaturation and structural changes of α-helical proteins in keratins. *Journal of Structural Biology*, 177(2):553–560, 2012.

[30] D. Istrate, C. Popescu, M. E. Rafik, and M. Möller. The effect of pH on the thermal stability of fibrous hard alpha-keratins. *Polymer Degradation and Stability*, 98(2):542–549, 2013.

[31] S. White and G. J. White. *Stylin': African American Expressive Culture from Its Beginnings to the Zoot Suit*. Cornell University Press, 1999.

[32] A. Davis-Suvasitgy. *The Science of Black Hair: A Comprehensive Guide to Textured Hair*. SAJA Publishing, 2011.

[33] A. Dickey. *Hair Rules!: The Ultimate Guide for Women with Kinky, Curly, or Wavy Hair*. Villard, 2003.

[34] J.Y. Ryu and S.H. Park. Hair drier having a pad for generating far-infrared rays and anions and method for making the pad, September 28 2004. US Patent 6,798,982.

[35] K. Yu. Hair iron with dimpled face plates and method of use in styling hair, February 28 2012. US Patent 8,124,914.

[36] L. J. Wolfram. Human hair: A unique physicochemical composite. *Journal of the American Academy of Dermatology*, 48(6, Supplement):S106–S114, 2003.

[37] C. Popescu and H. Höcker. Hair–the most sophisticated biological composite material. *Chemical Society Reviews*, 36(8):1282–1291, 2007.

[38] T. Takahashi, R. Hayashi, M. Okamoto, and S. Inoue. Morphology and properties of Asian and Caucasian hair. *Journal of Cosmetic Science*, 57:327–338, 2006.

[39] J. A. Swift and B. Bews. The chemistry of human hair cuticle III: The isolation and amino acid analysis of various subfractions of the cuticle obtained by pronase and trypsin digestion. *Journal of the Society of Cosmetic Chemists*, 27:289–300, 1976.

[40] R. Araújo, M. Fernandes, A. Cavaco-Paulo, and A. Gomes. Biology of human hair: know your hair to control it. In *Biofunctionalization of Polymers and their Applications*, pages 121–143. Springer Science + Business Media, 2010.

[41] L. J. Wolfram and M. K. O. Lindemann. Some observations on the hair cuticle. *Journal of the Society of Cosmetic Chemists*, 22:839–850, 1971.

[42] M. Yasuda, A. Sogabe, and A. Noda. Physical properties of human hair. 2. Evaluation of human hair torsional stress, and a mechanism of bending and torsional stress. *Journal of Society of Cosmetic Chemists of Japan*, 36(4):262–272, 2002.

[43] C. R. Robbins and R. J. Crawford. Cuticle damage and the tensile properties of human hair. *Journal of Cosmetic Science*, 42:59–67, 1991.

[44] C. Bolduc and J. Shapiro. Hair care products: waving, straightening, conditioning, and coloring. *Clinics in Dermatology*, 19(4):431–436, 2001.

[45] W. G. Bryson, D. P. Harland, J. P. Caldwell, J. A. Vernon, R. J. Walls, J. L. Woods, S. Nagase, T. Itou, and K. Koike. Cortical cell types and intermediate filament arrangements correlate with fiber curvature in Japanese human hair. *Journal of Structural Biology*, 166(1):46–58, 2009.

[46] M. Feughelman. The change in stress on wetting and drying wool fibers. *Textile Research Journal*, 29(12):967–970, 1959.

[47] D. W. Cannell. Permanent waving and hair straightening. *Clinics in Dermatology*, 6(3):71–82, 1988.

[48] S. V. Kshirsagar, B. Singh, and S. P. Fulari. Comparative study of human and animal hair in relation with diameter and medullary index. *Indian Journal of Forensic Medicine and Pathology*, 2(3):105â, 2009.

[49] C. R. Robbins. *Chemical and Physical Behavior of Human Hair*. Springer Science + Business Media, 2012.

[50] J. Menkart, L. J. Wolfram, and I. Mao. Caucasian hair, Negro hair and wool: similarities and cifferences. *Journal of the Society of Cosmetic Chemists*, 17:769–787, 1966.

[51] B. C. Powell and G. E. Rogers. *Biology of the Integument: 2 Vertebrates*, chapter Hair Keratin: Composition, Structure and Biogenesis, pages 695–721. Springer Berlin Heidelberg, Berlin, Heidelberg, 1986.

[52] J. W. S. Hearle. A total model for the structural mechanics of wool. *Wool Technology and Sheep Breeding*, 51(1), 2003.

[53] E. H. Mercer. The heterogeneity of the keratin fibers. *Textile Research Journal*, 23(6):388–397, jun 1953.

[54] B. Lindelöf, B. Forslind, M.-A. Hedblad, and U. Kaveus. Human hair form. Morphology revealed by light and scanning electron microscopy and computer aided three-dimensional reconstruction. *Archives of Dermatology*, 124(9):1359–1363, 1988.

[55] B. A. Bernard. Hair shape of curly hair. *Journal of the American Academy of Dermatology*, 48(6):S120–S126, 2003.

[56] S. Thibaut, O. Gaillard, P. Bouhanna, D. W. Cannell, and B. A. Bernard. Human hair shape is programmed from the bulb. *British Journal of Dermatology*, 152(4):632–638, 2005.

[57] B. Xu and X. Chen. The role of mechanical stress on the formation of a curly pattern of human hair. *Journal of the Mechanical Behavior of Biomedical Materials*, 4(2):212–221, 2011.

[58] R. D. B. Fraser and G. E. Rogers. The bilateral structure of wool cortex and its relation to crimp. *Australian Journal of Biological Sciences*, 8(2):288–299, 1955.

[59] S. Thibaut, P. Barbarat, F. Leroy, and B. A. Bernard. Human hair keratin network and curvature. *International Journal of Dermatology*, 46(s1):7–10, 2007.

[60] J. A. Swift. Morphology and histochemistry of human hair. *Experientia Supplementum*, 78:149175, 1997.

[61] S. Nagase, M. Tsuchiya, T. Matsui, S. Shibuichi, H. Tsujimura, Y. Masukawa, N. Satoh, T. Itou, K. Koike, and K. Tsujii. Characterization of curved hair of Japanese women with reference to internal structures and amino acid composition. *Journal of Cosmetic Science*, 59(4):317–332, 2007.

[62] S. Dekio and J. Jidoi. Amounts of fibrous proteins and matrix substances in hairs of different races. *The Journal of Dermatology*, 17(1):62–64, 1990.

[63] Y. K. Kamath, S. B. Hornby, and H. D. Weigmann. Mechanical and fractographic behavior of negroid hair. *Journal of the Society of Cosmetic Chemists*, 35:21–43, 1984.

[64] A. N. Syed, A. Kuhajda, H. Ayoub, and K. Ahmad. African-American hair: its physical properties and differences relative to Caucasian hair. *Cosmetics and Toiletries*, 110(10):39–48, 1995.

[65] T. Evans and R. R. Wickett. *Practical Modern Hair Science*. Allured Business Media, 2012.

[66] R. de la Mettrie, D. Saint-Léger, G. Loussouarn, A. Garcel, C. Porter, and A. Langaney. Shape variability and classification of human hair: a worldwide approach. *Human Biology*, 79(3):265–281, 2007.

[67] C. Porter, F. Dixon, C.-C. Khine, B. Pistorio, H. Bryant, and R. de la Mettrie. The behavior of hair from different countries. *Journal of Cosmetic Science*, 60(2):97–109, 2009.

[68] A. J. McMichael. Ethnic hair update: Past and present. *Journal of the American Academy of Dermatology*, 48(6):S127–S133, 2003.

[69] C. R. Quinn, T. M. Quinn, and A. P. Kelly. Hair care practices in African American women. *Cutis*, 72(4):280–2, 285–9, 2003. Quinn, Chemene R Quinn, Timothy M Kelly, A Paul Journal Article Review United States Cutis. 2003 Oct;72(4):280-2, 285-9.

[70] I. E. Roseborough and A. J. McMichael. Hair care practices in African-American patients. *Seminars in Cutaneous Medicine and Surgery*, 28(2):103–108, June 2009.

[71] J. Cao and F. Leroy. Depression of the melting temperature by moisture for α-form crystallites in human fair keratin. *Biopolymers*, 77(1):38–43, 2004.

[72] F.-J. Wortmann and H. Deutz. Characterizing keratins using high-pressure differential scanning calorimetry (HPDSC). *Journal of Applied Polymer Science*, 48(1):137–150, apr 1993.

[73] F.-J. Wortmann, M. Stapels, R. Elliott, and L. Chandra. The effect of water on the glass transition of human hair. *Biopolymers*, 81(5):371–375, 2006.

[74] D. Istrate, C. Popescu, and M. Möller. Non-isothermal kinetics of hard α-keratin thermal denaturation. *Macromolecular Bioscience*, 9(8):805–812, aug 2009.

[75] C. R. Robbins and G. V. Scott. Prediction of hair assembly characteristics from single fiber properties. *Journal of the Society of Cosmetic Chemists*, 29:783–792, 1978.

[76] C. R. Robbins and C. Reich. Prediction of hair assembly characteristics from single fiber properties. Part II. The relationship of fiber curvature, friction, stiffness, and diameter to combing behavior. *Journal of the Society of Cosmetic Chemists*, 37:141–158, 1986.

[77] C. R. Robbins, C. Reich, and J. Clarke. Hair manageability. *Journal of the Society of Cosmetic Chemists*, 37:489–499, 1986.

[78] J. Clarke and C. R. Robbins. Influence of hair volume and texture on hair body. *Journal of the Society of Cosmetic Chemists*, 42:341–350, 1991.

[79] J. H. S. Rennie, S. E. Bedford, and J. D. Hague. A model for the shine of hair arrays. *International Journal of Cosmetic Science*, 19(3):131–140, 1997.

[80] T. A. Evans and K. Park. A statistical analysis of hair breakage. ii. Repeated grooming experiments. *Journal of Cosmetic Science*, 61(6):439455, 2010.

[81] M. M. Breuer. The binding of small molecules to hair - I: The hydration of hair and the effect of water on the mechanical properties of hair. *Journal of the Society of Cosmetic Chemists*, 23:447–470, 1972.

[82] S. P. Detwiler, J. L. Carson, J. T. Woosley, T. M. Gambling, and R. A. Briggaman. Bubble hair. Case caused by an overheating hair dryer and reproducibility in normal hair with heat. *Journal of the Amercian Academy of Dermatology*, 30(1):54–60, 1994.

[83] C. L. Gummer. Bubble hair: a cosmetic abnormality caused by brief, focal heating of damp hair fibres. *British Journal of Dermatology*, 131(6):901–3, 1994. .

[84] J. Hahn, T. Dandridge, P. Seshadri, A. Marconnet, and T. Reid. Integrating design methodology, thermal sciences, and customer needs to address challenges in the hair care industry. In *Volume 7: 27th International Conference on Design Theory and Methodology*. ASME International, aug 2015.

[85] J. H. Ji, T. S. Park, H.-J. Lee, Y.-D. Kim, L.-Q. Pi, X.-H. Jin, and W.-S. Lee. The ethnic differences of the damage of hair and integral hair lipid after ultra violet radiation. *Annals of Dermatology*, 25(1):54–60, 2013.

[86] A. C. S. Nogueira and I. Joekes. Hair color changes and protein damage caused by ultraviolet radiation. *Journal of Photochemistry and Photobiology B: Biology*, 74(2):109–117, 2004.

[87] N. P. Khumalo, R. P. R. Dawber, and D. J. P. Ferguson. Apparent fragility of African hair is unrelated to the cystine-rich protein distribution: a cytochemical electron microscopic study. *Experimental Dermatology*, 14(4):311–314, Apr 2005.

[88] H. Bryant, C. Porter, and G. Yang. Curly hair: measured differences and contributions to breakage. *International Journal of Dermatology*, 51(s1):8–11, 2012.

[89] G. Loussouarn, C. El Rawadi, and G. Genain. Diversity of hair growth profiles. *International Journal of Dermatology*, 44(s1):6–9, 2005.

[90] F.-J. Wortmann, C. Springob, and G. Sendelbach. Investigations of cosmetically treated human hair by differential scanning calorimetry in water. *Journal of Cosmetic Science*, 53(4):219–228, 2002.

[91] F.-J. Wortmann, G. Wortmann, and C. Popescu. Assessing the properties of thermally treated human hair by tensile testing and DSC: Are they complementary or equivalent methods? In *20th International Hair-Science Symposium, Book of Abstracts*, Germany, 9 2017. DWI - Leibniz-Institute for Interactive Materials.

[92] J. M. Quadflieg. *Fundamental properties of Afro-American hair as related to their straightening/relaxing behaviour*. PhD thesis, Bibliothek der RWTH Aachen, 2003.

[93] F.-J. Wortmann, J. M. Quadflieg, and L. J. Wolfram. Mechanistic aspects of African hair relaxation. In *17th International Hair-Science Symposium - HairS'11*, Aachen : DWI at RWTH Aachen, September 2011.

[94] R. Pires-Oliveira, F. G. Oliveira, T. S. Batista, and I. Joekes. Specific heat capacity of cosmetically treated human hair. In *22nd IFSCC Conference 2013*, Windsor Barra Hotel, Rio de Janeiro, Brazil, 2013.

[95] G. Liu, H. Lin, X. Tang, K. Bergler, and X. Wang. Characterization of thermal transport in one-dimensional solid materials. *Journal of Visualized Experiments: JoVE*, (83), 2014.

[96] J. Hou, X. Wang, and J. Guo. Thermal characterization of micro/nanoscale conductive and non-conductive wires based on optical heating and electrical thermal sensing. *Journal of Physics D: Applied Physics*, 39(15):3362, 2006.

[97] A. Mendioroz, R. Fuente-Dacal, E. Apiñaniz, and A. Salazar. Thermal diffusivity measurements of thin plates and filaments using lock-in thermography. *Review of Scientific Instruments*, 80(7):074904, 2009.

[98] A. Salazar, A. Mendioroz, R. Fuente, and R. Celorrio. Accurate measurements of the thermal diffusivity of thin filaments by lock-in thermography. *Journal of Applied Physics*, 107(4):043508, 2010.

[99] A. J. Ångström. XVII. New method of determining the thermal conductibility of bodies. *Philosophical Magazine Series 4*, 25(166):130–142, 1863.

[100] J. W. Vandersande and R. O. Pohl. Simple apparatus for the measurement of thermal diffusivity between 80–500 k using the modified Ångström method. *Review of Scientific Instruments*, 51(12):1694–1699, dec 1980.

[101] J. M. Belling and J. Unsworth. Modified Angström's method for measurement of thermal diffusivity of materials with low conductivity. *Review of Scientific Instruments*, 58(6):997–1002, jun 1987.

[102] B. Sundqvist. Thermal diffusivity measurements by Ångström's method in a fluid environment. *International Journal of Thermophysics*, 12(1):191206, Jan 1991.

[103] G. Wagoner, K. A. Skokova, and C. D. Levan. Angstrom's method for thermal property measurements of carbon fibers and composites. In *The American Carbon Society, CARBON Conference*, 1999.

[104] A. M. Bouchard. Angstrom's method of determining thermal conductivity. Physics Department, The College of Wooster, May 2000.

[105] A. L. Lytle. Ångströms method of measuring thermal conductivity. Physics Department, The College of Wooster, May 2000.

[106] J. Bodzenta, B. Burak, M. Nowak, M. Pyka, M. Szałajko, and M. Tanasiewicz. Measurement of the thermal diffusivity of dental filling materials using modified Ångström's method. *Dental Materials*, 22(7):617–621, July 2006.

[107] W. N. dos Santos, J. N. dos Santos, P. Mummery, and A. Wallwork. Thermal diffusivity of polymers by modified angstrm method. *Polymer Testing*, 29(1):107 – 112, 2010.

[108] G. Zhang, C. Liu, and S. Fan. Directly measuring of thermal pulse transfer in one-dimensional highly aligned carbon nanotubes. *Scientific Reports*, 3:2549, August 2013.

[109] H. Ghasemi, N. Thoppey, X. Huang, J. Loomis, X. Li, J. Tong, J. Wang, and G. Chen. High thermal conductivity ultra-high molecular weight polyethylene (UHMWPE) films. In *Fourteenth Intersociety Conference on Thermal and Thermomechanical Phenomena in Electronic Systems (ITherm)*, pages 235–239, May 2014.

[110] Y. Zhu. Heat-loss modified Angstrom method for simultaneous measurements of thermal diffusivity and conductivity of graphite sheets: The origins of heat loss in Angstrom method. *International Journal of Heat and Mass Transfer*, 92:784791, Jan 2015.

[111] M. Wolff. Measuring thermal conductivity by Ångstrom's method. Physics Department, The College of Wooster, May 2016.

[112] C. Pradère, J. M. Goyhénèche, J. C. Batsale, S. Dilhaire, and R. Pailler. Thermal diffusivity measurements on a single fiber with microscale diameter at very high temperature. *International Journal of Thermal Sciences*, 45(5):443451, May 2006.

[113] S. Pye and P. K. Paul. Trehalose in hair care: heat styling benefits at high humidity. *Journal of Cosmetic Science*, 63(4):233–241, 2011.

[114] L. Greenspan. Humidity fixed points of binary saturated aqueous solutions. *Journal of Research of the National Bureau of Standards*, 81(1):89–96, 1977.

[115] J. McDonald and G. Albright. Microthermal imaging in the infrared. *Electronics Cooling*, 3:27–30, 1997.

[116] J. Knippers, J. Cremers, M. Gabler, and J. Lienhard. *Construction Manual for Polymers + Membranes.* Birkhauser Architecture; Edition Detail, Basel; Munich, 2011.

[117] J. J. Scialdone, United States., National Aeronautics, Space Administration., and Goddard Space Flight Center. *Atomic Oxygen and Space Environment Effects on Aerospace Materials Flown with EOIM-III Experiment.* National Aeronautics and Space Administration, Goddard Space Flight Center, Greenbelt, Md., 1996.

[118] Optotherm Thermal Imaging. Emissivity in the infrared. Available at: http://www.optotherm.com/emiss-table.htm, Retreived on 4/7/2018.

[119] J. A. Preciado, B. Rubinsky, D. Otten, B. Nelson, M. C. Martin, and R. Greif. Radiative properties of polar bear hair. In *ASME 2002 International Mechanical Engineering Congress and Exposition*, pages 57–58. American Society of Mechanical Engineers, 2002.

[120] S. Holding. Polymers: A property database. *Chromatographia*, 72(5):587–587, Sep 2010.

[121] M. R. Sethuraj and N. T. Mathew. *Natural Rubber: Biology, Cultivation and Technology*, volume 23. Elsevier, 2012.

[122] C. L. Choy, Y. W. Wong, G. W. Yang, and T. Kanamoto. Elastic modulus and thermal conductivity of ultradrawn polyethylene. *Journal of Polymer Science Part B: Polymer Physics*, 37(23):33593367, Dec 1999.

[123] K. Kurabayashi. Anisotropic thermal properties of solid polymers. *International Journal of Thermophysics*, 22(1):277–288, 2001.

[124] T. L. Bergman, A. S. Lavine, F. P. Incropera, and D. P. Dewitt. *Fundamentals of Heat and Mass Transfer.* John Wiley & Sons, 2011.

VITA

VITA

Jaesik Hahn received a B.S. in mechanical engineering from Purdue University, West Lafayette in 2013. Co-advised by Dr. Tahira Reid at the REID lab and Dr. Amy Marconnet at the MTEC lab, he received a Ph.D. degree in mechanical engineering at the same university in 2018. The scope of his research ranges across thermal characterization of human hair, modeling of heat transfer through hair during flat ironing, and predictive modeling of styling efficacy and heat damage to hair induced by flat irons. His early work has been featured in the National Geographic magazine, National Public Radio (NPR), Reuters, the Washington Post, Smithsonian Magazine, and many other media outlets.